Summer 8-15-2019

Understanding the Physiology of Extracellular Electron Uptake in Purple Nonsulfur Bacteria

Michael Singh Guzman
Washington University in St. Louis

WASHINGTON UNIVERSITY IN ST. LOUIS

Division of Biology and Biomedical Sciences
Molecular Genetics and Genomics

Dissertation Examination Committee:
Arpita Bose, Chair
Gautam Dantas
Petra Levin
Himadri Pakrasi
Jim Skeath

Understanding the Physiology of Extracellular Electron Uptake in Purple Nonsulfur Bacteria

by
Michael Singh Guzman

A dissertation presented to
The Graduate School
of Washington University in
partial fulfillment of the
requirements for the degree
of Doctor of Philosophy

August 2019
St. Louis, Missouri

Table of Contents

List of Figures

List of Tables

Acknowledgments

This section is an acknowledgement to not only those who helped me achieve a PhD at WashU, but equally to those whom I would not have made it to this point without. Because of this, I have many people to thank.

I would like to express my deepest appreciation to my adviser, Arpita Bose, and the rest of my committee members for their support and encouragement. I am especially grateful to Arpita for her enthusiasm, creativity, and patience as my mentor. I am grateful to each of my committee members for their role in my scientific and professional development. In particular, Himadri Pakrasi for his leadership of my thesis committee; Bob Blankenship for sharing his wealth of knowledge about photosynthesis and evolution; Gautam Dantas for his professional support and technical expertise; Petra Levin for her valuable feedback on my presentations; and lastly, Jim Skeath whom provided an incredible amount of professional and educational support throughout my graduate training.

The completion of my dissertation would not have been possible without the support of many others within the WashU community. Firstly, my labmates: Tahina Ranaivoarisoa, Dinesh Gupta, Wei Bai, Karthikeyan Rengasamy, Rajesh Singh, Emily Davenport, and Eric Conners. Tahina has been an exceptional laboratory technician, who goes above and beyond each day to make our lab a great place to work. Dinesh has been an important colleague in the lab. He has provided me critical, thoughtful, and truthful feedback on my work. I will always value his friendship and honesty. I am grateful to Karthikeyan and Rajesh whom have made invaluable experimental contributions. Secondly, the scientific collaborators I have had the opportunity to

work with. Special thanks to Clive Jones and David Fike whom offered essential expertise and help with Secondary Ion Mass Spectrometry and data analysis; Dianne Duncan for her valuable help with confocal microscopy; and Mark Meacham and Michael Binkley whom were instrumental in our labs work on microfluidic bioelectrochemistry. Lastly, I'm deeply indebted to institutional programs and grants that have supported me at WashU. Specifically, the NIH Initiative for Maximizing Student Development (IMSD) Program run by Jim Skeath, and formerly, Cherilynn Shadding. The network support, career development seminars, and professional training offered by IMSD played an important role in my success at WashU. A very special thanks to the IMSD administrative staff and to all of my fellow IMSD students.

I am extremely grateful to the advisers whose labs I was lucky enough to train in before WashU; my professors at Portland State University; and the fellowships that helped in my transition to graduate school. I would like to express my deepest gratitude to Brad Tebo, and his graduate student Rick Davis, for opening up the world of geomicrobiology to me. As a first-generation college student, I had a really incomplete understanding of what science was, who did science, and what careers in science could entail. My stay in the lab had profound impression on me and my journey in science. I would also like to extend my sincere thanks to Alex Paredez and his lab, whom during my short stay at the University of Washington, introduced me to a variety of molecular microbiological techniques that have proved invaluable. I also wish to thank Gabriele Varani and Carlos Catalano who administered the NIH Postbaccalaureate Research Education Program during my time at the University of Washington. This program broadened my research training and interests, and it was an essential transitionary period that prepared me for graduate school. Lastly, I would like to thank my former professor Deb Duffield at Portland State University. Deb was always encouraging and showed unwavering support of my

undergraduate research. Her enthusiastic teaching and passion for biodiversity is a continued source of inspiration to me.

Lastly, I would like to thank my family and friends. My mom and dad for their unconditional love and support, and for always encouraging me to do my best in everything. My sister SuRekha for being understanding and encouraging (and for coming out to the Midwest to visit me). My wife Ashley for leaving the sanctuary of our friends and family in Portland, and then a year later in Seattle, so that I could pursue a PhD in a place completely foreign to us both. This was a truly selfless act and I will forever be grateful to her for it. I also would like to thank the friends I've made in St. Louis. Yowshien and Alli for making us feel at home here; Ryan for always going to shows with me; and Luis for being a dependable and trustworthy friend.

Michael Guzman

Washington University in St. Louis

August 2019

Dedicated to my parents.

ABSTRACT OF THE DISSERTATION

Understanding the Physiology of Extracellular Electron Uptake in Purple Nonsulfur Bacteria

by

Michael Singh Guzman

Doctor of Philosophy in Biology and Biomedical Sciences

Molecular Genetics and Genomics

Washington University in St. Louis, 2019

Dr. Arpita Bose, Chair

Microbially catalyzed oxidation-reduction reactions drive nutrient cycling and energy flux on Earth. Photoautotrophs, which include the cyanobacteria (oxygenic) and purple and green sulfur bacteria (anoxygenic), transform light energy into chemical energy and are responsible for substantial global primary productivity. Anoxygenic phototrophs, in particular, play a crucial role in biogeochemical cycling in anoxic illuminated environments because of their ability to oxidize an array of inorganic compounds for CO_2 fixation. Electron donors include molecular hydrogen, nitrite, and reduced sulfur compounds. Recent evidence has also suggested that solid-phase conductive substances (SPCSs), including rust (mixed-valent iron minerals) and their proxies (poised electrodes), can serve as electron donors for anoxygenic phototrophs. This phenomenon is called phototrophic extracellular electron uptake (EEU) and is the reverse process of extracellular electron transfer (EET) performed by metal-reducing bacteria. While numerous examples of microbes performing EET to minerals/electrodes exist and the molecular, physiological, and ecological role of this process is well-studied, very little is understood about EEU. The objectives of this research were to use purple nonsulfur bacteria as a model system to

address key knowledge gaps in our understanding of EEU. In Chapter 1, I provide the first experimental evidence that EEU is linked to photosynthetic electron transfer, energy transduction, and the generation of cellular reducing equivalents in the phototrophic Fe(II)-oxidizing bacterium *Rhodopseudomonas palustris* TIE-1. Furthermore, I show that the Calvin-Benson-Bassham (CBB) cycle (the most broadly distributed CO_2 fixation pathway on Earth) is the primary electron sink for phototrophic EEU. In Chapter 2, I expand our understanding of the diversity of organisms known to engage in EEU by isolating and characterizing a new EEU-capable bacterium *Rhodovulum sulfidophilum* AB26. Using whole-genome- and transcriptome-sequencing, and biochemical approaches, I explore the electron-transfer pathways involved in EEU. This work sets the stage for physiological and genetic studies of this organism. Overall, the findings from this thesis advance our understanding of the physiology of microbial EEU, its diversity, and its role in biogeochemical cycling.

Chapter 1: Introduction

Bacteria that donate or accept electrons from solid phase conductive substances (SPCSs), such as iron or sulfide minerals, substantially influence geochemical cycles on a global scale[1-3]. This microbially-mediated phenomenon is broadly termed extracellular electron transfer (EET)[1]. EET-capable microbes transfer electrons out of the cell during respiration (to reduce SPCSs) or can take up electrons from SPCSs (thus oxidizing them). For example, metal-reducing microbes such as *Shewanella* and *Geobacter* can use SPCSs as electron sinks for metabolism in environments devoid of soluble terminal electron acceptors (e.g. molecular oxygen)[4-7]. Genetic and biochemical studies of metal-reducing microbes have revealed the mechanistic underpinnings of EET in detail[3,8]. The role of EET in facilitating microbial extracellular electron uptake (EEU) from solid electron donors, however, is incompletely understood.

Microbe-electrode interactions have been fundamental towards understanding EET in metal-reducing microbes[9,10]. Electrodes mimic microbial interactions with SPCSs, wherein an electrode can operate as an electron sink (anode), or as an electron source (cathode) for microbial metabolism. Inspired by studies of anode-respiring microbes, geomicrobiologists turned to bioelectrochemistry within the last decade to better understand the bioenergetic and molecular underpinnings of EEU[11]. This was a paradigm shift for EEU research because it equipped researchers with controlled systems to cultivate metal-oxidizing microbes and to begin to understand how solid substrate oxidation is linked to cellular metabolism. This work led to the discovery of EEU by iron-reducers[12,13], methanogens[14,15], acetogens[16,17], sulfate-reducers[18,19], neutrophilic iron-oxidizers[20,21], and recently, anoxygenic phototrophs[22-24]. Collectively, these

discoveries link EEU to biogeochemical cycling in aquatic sediments and subsurface environments.

Because of the nascency of microbial EEU research there is limited information on the molecular mechanisms involved and few microbes in pure culture. Subsequently, identifying EEU-potential in environmental microbiological samples using existing genetic biomarkers is challenging. This has hindered our understanding of the role of these microbes in biogeochemical processes. The objectives of this thesis were to use purple nonsulfur bacteria (PNSB) as a model system to understand: (1) the bioenergetic underpinnings of EEU; (2) the relationship between EEU and cellular metabolism; and (3) the ecology and evolution of EEU. These objectives were addressed using a combination of genetic, physiological, biochemical, geochemical, and bioelectrochemical studies in the model phototrophic iron-oxidizing bacterium *Rhodopseudomonas palustris* TIE-1. In addition, this thesis led to the isolation and characterization of a new EEU-capable marine phototrophic sulfur-oxidizing bacterium (*Rhodovulum sulfidophilum* AB26). This is the first phototrophic marine organism capable of EEU thus far characterized. Using whole genome and transcriptome-sequencing I provide the basis for molecular and biochemical studies in this organism. Overall, this work expands our understanding of the physiology and diversity of EEU.

1.1 Reductive extracellular electron transfer

EET is well-studied in microbes that transfer electrons out of the cell to reduce SPCSs (i.e. reductive EET). Metal-reducing bacteria catalyze organic matter oxidation coupled to the reduction of minerals or solid-phase humic substances in the natural environment[3]. Subsequently, metal-reducers play an important role in carbon cycling in anoxic ecosystems,

such as freshwater and marine sediments, replete with iron- or manganese-oxides[25]. Several mechanisms for EET have been described and are summarized in Figure 1.1. The EET pathways of *Geobacter sulfurreducens* and *Shewanella oneidensis* MR-1 are the most well-characterized at the molecular level. These organisms encode periplasmic and outer membrane bound multiheme *c*-type cytochromes that serve as electron conduits to the extracellular environment. In *S. oneidensis* MR-1 a membrane bound decaheme *c*-type cytochrome (MtrC) transports electrons (e.g. derived from acetate or H_2 oxidation) through the periplasmic space via a membrane-spanning complex consisting of a cytochrome electron shuttle (MtrA) ensheathed in a transmembrane β-barrel protein (MtrB) (Figure 1.2a)[8,26]. Homologs of the Mtr system have been identified in Fe(II)-oxidizing bacteria such as *R. palustris* TIE-1[27] and *Sideroxydans lithotrophicus* ES-1[26,28,29]. Multiheme *c*-type cytochromes are a key component of many EET pathways[30].

Long-range EET has been described via several mechanisms (Figure 1.1). Some microbes secrete endogenously-produced, redox-active soluble mediators. For example, *Shewanella* secretes flavins into the extracellular environment to mediate EET between cells and minerals[31], or cells and electrodes[32-35]. So-called bacterial "nanowires" have also been observed to mediate long-range EET[3,36]. This was first characterized in *G. sulfurreducens*[37]. *G. sulfurreducens* encodes conductive type IV pili that are essential for iron reduction[37]. Similarly, *S. oneidensis* MR-1 produces electrically-conductive pilus-like appendages[38,39]. These extensions of the outer membrane contain multiheme *c*-type cytochromes, including MtrC, and facilitate electron transfer to minerals[38,39]. Nanowires have also been proposed to facilitate electron exchange between cells, a process called interspecies electron transfer[40]. Cells of the filamentous sulfur-oxidizing bacterium Desulfobulbaceae extend end-to-end centimeter distances to transport

electrons from sulfide minerals in anoxic sediments to reduce O_2 in overlying oxic seawater[41,42]. Overall, these long-range EET strategies enable microbes to overcome spatial separation between electron-donors and -acceptors.

A recently explored aspect of microbe-electrode interactions is the contribution of extracellular polymeric substances (EPS) to reductive EET[43,44] (Figure 1.1). EPS are biopolymers produced by a variety of biofilm-forming microorganisms when they colonize surfaces[45]. EPS is composed of protein, polysaccharide, nucleic acids, and lipids, among other biologically-produced macromolecules[46]. Thus, the EPS matrix not only provides constructive and protective properties to biofilms, but it can also be utilized by microbes to exchange information (e.g. DNA via horizontal gene transfer) and electrons (e.g. electron-transfer via cytochrome *c* proteins)[43,44,47]. *Shewanella* biofilms produce EPS[48] that has conductive properties and can mediate EET between cells and electrodes[43,44,49] or cells and minerals[50]. It has been proposed that "electron-hopping" mediated by extracellular *c*-type cytochromes and flavins contribute to electron-transfer through the EPS matrix[43]. The precise proteins involved in electron transfer through EPS, however, have not been fully elucidated[51].

1.2 Oxidative extracellular electron transfer

1.2.1 Extracellular electron uptake by iron-reducing bacteria

Oxidative EET (i.e. EEU) allows microorganisms to use SPCSs as electron donors for cellular metabolism. Microbial EEU from electrodes was first described in *Geobacter* species from anoxic sediment enrichments[12]. Pure cultures from these enrichments were capable of accepting electrons from graphite electrodes poised at -500 mV vs. Ag/AgCl (~ -705 mV vs. Standard Hydrogen Electrode (SHE)) to reduce nitrate to nitrite, and to reduce fumarate to

succinate[12]. In these studies, *Geobacter* species formed monolayers on the surface of the electrodes, suggesting direct contact is important for electron uptake[12]. In subsequent studies it has been shown that electrodes can be used to catalyze microbial reductive dechlorination[52] and microbial uranium reduction[53,54]—opening up the possibility for biocathode-driven bioremediation. Studies of biocathode microbial communities have also demonstrated that EEU is linked to O_2 reduction[55], denitrification[56], and CO_2 fixation[11,23,57]. Cathode-driven methanogenesis has also been reported[14,15]. Although EEU appears to be a physiologically diverse process, the molecular and bioenergetic underpinnings of microbial EEU are poorly understood.

One of the first studies to investigate EEU at the molecular level was performed in *S. oneidensis* MR-1[13]. In this study it was shown that the Mtr system could function in reverse to facilitate EEU from poised electrodes. This process was mediated by the cytochrome CymA, the outer membrane protein MtrB, the ubiquinone pool, and led to cathode-driven fumarate reduction via the periplasmic fumarate reductase FccA (Figure 1.2b)[13]. Furthermore, this study demonstrated that deletion of components of the Mtr respiratory pathway, *cymA*, *fccA*, or *menC* (encoding a gene involved in menaquinone biosynthesis) eliminated 80-90% of fumarate reduction[13]. Whether EEU could lead to energy production via the respiratory electron transport chain, however, remained unclear until a 2018 study by Rowe *et al.*[58]. In this study, Rowe *et al.* used electron transport chain (ETC) inhibitor studies, redox-sensitive bioluminescent assays, and genetic mutants of the cellular ETC and EET pathways to demonstrate that a proton gradient is generated during EEU, ATP is synthesized, and that EEU is correlated with an increase in intracellular redox in *S. oneidensis* MR-1[58]. Overall, this work suggested that bacteria can use solid electron donors for energy generation and that EEU may lead to the production of cellular

reducing equivalents for metabolism. It is still unclear, however, if EEU by *S. oneidensis* MR-1 is connected to cellular growth, or if it is a microbial survival strategy utilized to maintain redox balance.

1.2.2 Extracellular electron uptake by iron-oxidizing bacteria

Bioelectrochemical studies have shown that chemoautotrophic iron-oxidizers can be cultivated using poised electrodes as their sole electron donor (Figure 1.3)[20,21]. This was first reported in the chemoautotrophic Fe(II)-oxidizing bacterium *Mariprofundus ferrooxydans* PV-1[21,59]. *M. ferrooxydans* PV-1 is an obligate, neutrophilic iron-oxidizing bacterium that can accept electrons from a graphite electrode poised at -76 mV vs. SHE (a potential low enough to preclude H_2 gas production at the cathode)[21]. *M. ferrooxydans* PV-1 cells formed sparse, monolayer-like biofilms on electrodes and reached current densities of 10 μA cm^{-2} (abiotic O_2 oxidation accounted for nearly ~80% of current consumption)[21]. Interestingly, under Fe(II)-oxidizing conditions *M. ferrooxydans* PV-1 highly expresses a molybdopterin oxidoreductase containing an iron-sulfur cluster domain[59]. Although the involvement of this protein in EEU has not been investigated, it may have a role in electron transfer from Fe(II) and/or electrodes[59]. The electron transfer pathways involved in EEU in *M. ferrooxydans* PV-1 remain poorly understood. This is in part because genetic tools are not available for use in this organism.

To examine how EEU from cathodes is linked to cellular metabolism, Ishii *et al.* performed physiological studies and chemical marking experiments in the chemoautotrophic Fe(II)-oxidizing bacterium *Acidithiobacillus ferrooxidans*[20]. The iron oxidation pathway of *A. ferrooxidans* is well-studied from a molecular[60,61], genomic[62,63], and biochemical perspective[64,65]. Fe(II) is oxidized by an outer membrane *c*-type cytochrome (Cyc 2). Electrons from Fe(II) have

two potential paths in the ETC: (1) the "down-hill" (exergonic) pathway; or the (2) "up-hill" (endergonic) pathway. The periplasmic blue copper protein, rustacyanin (Rus), is thought to be the branch point[20]. The "down-hill" pathway involves a cytochrome aa3 complex which generates a proton gradient. This proton gradient can be utilized by ATP synthase to drive ATP production. The "up-hill" pathway, however, relies upon cytochrome bc_1-mediated reverse electron flow[66]. This pathway dissipates a portion of the proton gradient to push electrons uphill to reduce NAD^+.

Using the Fe(II)-oxidation electron transfer model as a guide for physiological studies, Ishii *et al.* probed the cellular ETC of *A. ferrooxidans* during EEU from electrodes[20]. The authors showed that *A. ferrooxidans* could take up electrons from a cathode poised at +400 mV vs. SHE. The authors detected a single +820 mV redox peak (in the absence of Fe^{2+} ions) using cyclic voltammetry[20]. This data suggested that attached cells likely have an extracellular electron conduit for EEU independent of cathode-driven iron redox cycling. *In vivo* monitoring of the "down-hill" pathway revealed that cytochrome *c* proteins are involved in EEU since CO-inhibition of these proteins caused current uptake to decrease. Furthermore, the authors observed a decrease in current uptake upon treatment of cells with the cytochrome bc_1 inhibitor antimycin A[20]. This decrease was subtle and transient[20]. Therefore, it is unclear how active the reverse electron flow pathway is during EEU, or if this pathway supplies sufficient reducing power for autotrophic CO_2 fixation.

1.3 Extracellular electron uptake by phototrophic purple nonsulfur bacteria

1.3.1 The phototrophic Fe(II)-oxidizing bacterium *Rhodopseudomonas palustris* TIE-1

The innovative bioelectrochemical work on *Shewanella* and *Geobacter* established the basis for other groups to investigate the bioenergetic underpinnings of phototrophic Fe(II)-oxidizing bacteria using electrodes, including the bacterium *R. palustris* TIE-1[22]. This bacterium is the only phototrophic Fe(II)-oxidizer that is genetically tractable, and thus, is a model system for studying this process. *R. palustris* TIE-1 is a freshwater anoxygenic phototroph that was originally isolated from an iron-rich mat from School Street Marsh in Woods Hole, MA[67]. Genetic studies of this organism have revealed the loci involved in phototrophic Fe(II)-oxidation [27], key regulatory elements[68], and biophysical details of the electron transfer process[69].

Phototrophic Fe(II)-oxidation occurs according to the following reaction[70]:

$$4Fe^{2+} + CO_2 + 11H_2O + h\nu \rightarrow [CH_2O] + 4Fe(OH)_3 + 8H^+$$

In *R. palustris* TIE-1, the *pio* (*p*hototrophic *i*ron *o*xidation) operon is essential for phototrophic Fe(II)-oxidation[27]. The *pio* operon encodes three proteins (Figure 1.4). PioA is an MtrA-homolog that encodes a periplasmic decaheme *c*-type cytochrome. PioB is an MtrB-homolog that encodes a putative outer membrane β-barrel protein. PioC encodes a putative high potential iron sulfur protein (HiPIP) that is thought to transport electrons from Fe(II) to the

quinone pool for cyclic photosynthetic electron flow[27,71]. There is also evidence to suggest PioC can directly transfer electrons to the photosystem and physically interacts with the reaction center during photosynthesis[71]. Because of the prevalence of the PioABC system in related anoxygenic phototrophs, including the photoferrotroph *Rhodomicrobium vannielii*[72,73], this module may enable other organisms to perform phototrophic iron-oxidation. However, there are many unknowns surrounding the molecular details of photoferrotrophy, including the molecular mechanism and whether genes involved in phototrophic Fe(II) oxidation also mediate EEU from SPCSs.

R. palustris TIE-1 utilizes a form of phototrophy called anoxygenic (cyclic) photosynthesis (Figure 1.5a)[74]. This means that the photosynthetic ETC is cyclic and does not evolve oxygen (Figure 1.5a). Subsequently, the net output of photosynthesis is the production of a proton motive force (Δp) and the synthesis of ATP via cyclic photophosphorylation (Figure 1.5b, Figure 1.5c). Thus, unlike oxygenic photosynthesis, no reducing power (e.g. NADH) is generated from this process. It is for this reason external electron donors, such as Fe(II), are required (Figure 1.5). Electrons from external electron donors enter the ETC via soluble electron carriers, typically a periplasmic cytochrome c_2 (Figure 1.5). In many PNSB, including within the Rhodospirillaceae, cytochrome c_2 and/or high-potential iron-sulfur proteins (HiPIPs) mediate photosynthetic electron transfer between cytochrome bc_1 and the reaction-center bacteriochlorophyll[75]. From the reaction center, electrons flow cyclically to the ubiquinone pool and can re-oxidize cytochrome bc_1 (Figure 1.5). If an electron donor is available for photosynthesis, electrons can be used to drive NADH production via NADH dehydrogenase (Figure 1.5).

In phototrophic Fe(II)-oxidizers, electrons are thought to enter the photosynthetic ETC at cytochrome c_2 or the ubiquinone pool and then flow in reverse to NADH dehydrogenase to reduce NAD^+[69,71]. Reverse electron flow is thought to occur during growth on certain forms of iron, such as Fe^{2+} at pH 2 (E^o = +770 mV); or Fe(II)-nitrilotriacetic acid (E^o = +372 mV) and Fe(II)-citrate (E^o = +385 mV) at circumneutral pH[69]. This is because these electron donors are more electropositive than the NAD^+/NADH couple (E^o = -320 mV)[76] and thus reverse electron flow is likely required to push electrons "uphill" against their electrochemical gradient. This process is analogous to what is observed in chemoautotrophic Fe(II)-oxidizing bacteria, such as *A. ferrooxidans*. In *A. ferrooxidans* the "uphill" pathway that produces NADH involves the activity of cytochrome bc_1 and NADH dehydrogenase[77].

1.3.2 A potential extracellular electron uptake pathway

In 2014 Bose *et al.* cultivated *R. palustris* TIE-1 in bioelectrochemical systems and tested whether this organism could perform extracellular electron uptake from a cathode poised at +100 mV vs. SHE—the midpoint potential of iron oxides[22]. With a graphite electrode as the sole electron donor, Bose *et al.* observed that *R. palustris* TIE-1 accepted electrons from a cathode with the highest current densities under illuminated conditions[22]. Furthermore, viable and attached cells were observed on the electrodes, suggesting electron uptake may be mediated by a direct EET mechanism[22]. Indeed, the *pio* operon was highly expressed during EEU[22] suggesting that the PioABC may be involved in EEU from electrodes, analogous to the Mtr system in *S. oneidensis* MR-1[13]. To directly examine if the *pio* system also has a role in extracellular electron uptake from electrodes, Bose *et al.* cultivated a *pio* operon deletion mutant on poised electrodes[22]. Deletion of the *pio* operon led to current uptake levels lowering by only ~30%[22].

The authors also noted a defect in cell-attachment to the electrodes that could explain this decrease in current uptake[22].

Because of a lack of a clear phenotype, the precise role of the PioABC system in EEU remains unclear. Whether the PioABC system is the electron conduit for solid minerals and/or poised electrodes, or only soluble forms of iron, should be investigated in future studies. Nonetheless, it is plausible that anoxygenic phototrophs use solid electron donors to generate reducing equivalents (e.g. NADH) for cellular metabolism, and that the PioABC system plays a role in this process. However, the precise pathway electrons take, and the molecular underpinnings of this process are not fully understood. This includes (1) whether electrons from the cathode enter the photosynthetic ETC; (2) which soluble electron carrier is responsible for delivering electrons to the photosynthetic ETC and/or reaction center; (3) and whether electrons are used for NADH production (e.g. via NADH dehydrogenase).

1.3.3 The physiological electron sinks for phototrophic extracellular electron uptake

Aside from the unknowns surrounding the electron transfer pathway during EEU, even less is known about what happens to electrons after their uptake into the cell[78]. One of the critical questions in phototrophic EEU research is whether electrodes can be used by anoxygenic phototrophs for CO_2 fixation. Bioelectrochemical studies of chemoautotrophic bacteria have suggested that cellular growth occurs on cathodes[21,57,63] but whether this growth is linked to *de novo* carbon assimilation via EEU is unclear. CO_2 fixation has been shown in the acetogen *Sporomusa ovata* grown on cathodes. *S. ovata* can accept electrons from electrodes poised at -400 mV vs. SHE for CO_2 reduction to acetate via the Wood-Ljungdahl pathway[17]. Several other

acetogens, including several *Sporomusa* and *Clostridium* species, produce acetate and various other multicarbon compounds via EEU[16,17]. Whether PNSB, which take up electrons at sufficiently more positive electrode potentials, can perform CO_2 fixation via EEU should also be investigated.

In *R. palustris* TIE-1 and many PNSB, CO_2 fixation occurs via the CBB cycle. The CBB cycle is the primary mechanism for CO_2 fixation on Earth and is conserved among photosynthetic plants, algae, and cyanobacteria[79]. Ribulose-1,5-bisphosphate carboxylase/oxygenase (RuBisCO) performs the critical CO_2 reaction, catalyzing the carboxylation of CO_2 and ribulose-1,5-bisphosphate (RuBP), forming glyceraldehyde 3-phosphate (G3P). Some of the G3P formed by the CBB cycle goes to central metabolism, while most is used to regenerate the CO_2 acceptor molecule (RuBP) to sustain the cycle[79]. Many PNSB, including TIE-1, encode two forms of RuBisCO: forms I and II[80]. In *R. palustris* CGA009/10, a bacterium closely related to TIE-1, form I *ruBisCO* is under the regulatory control of a three-protein, two-component system called CbbRRS. This system is composed of two response regulators (CbbRR1 and CbbRR2) and a hybrid sensor kinase (CbbSR). The CbbRRS system has no discernible DNA binding domains and thus indirectly influences form I *ruBisCO* expression through interactions with CbbR[81-84]. CbbR is a LysR family transcriptional regulator[84]. CbbRRS controls form I *ruBisCO* expression via CbbR in response to the redox and energy status of the cell, specifically the NAD(P)H and ATP levels[83].

To examine if electrons were used for CO_2 fixation during phototrophic EEU Bose *et al.* examined the expression of genes encoding the key CO_2 fixation enzyme of RuBisCO. Form I *ruBisCO* was highly upregulated during EEU[22]. However, an increase in cell density was not observed during EEU. This suggests: (1) TIE-1 is unable to use electrons from poised electrodes

to generate reducing equivalents; (2) electrons are being utilized for redox balance; or (3) the detection limit of previous methods used to measure cell growth were not sufficiently sensitive. Nonetheless, this data suggests that the CBB cycle may be an electron sink during EEU. Future studies, however, should investigate if electrons from the electrode enter the photosynthetic electron transport chain for NAD(P)H generation, and whether this NAD(P)H is used for CO_2 fixation.

1.3.4 The ecology and diversity of purple nonsulfur bacteria

PNSB are a phylogenetically diverse and a metabolically versatile group of microbes (Figure 1.6)[85]. PNSB participate in anoxic carbon cycling via primary productivity (i.e. photoautotrophy) and as consumers of organic compounds (photoheterotrophy[85]). PNSB have been isolated from soil, freshwater, and marine environments[85]. In these environments they oxidize a variety of inorganic electron donors during photoautotrophic growth, including reduced sulfur compounds (e.g. sulfide, thiosulfate, elemental sulfur), gaseous-phase compounds (e.g. H_2), and insoluble minerals (e.g. mixed-valent iron minerals)[85]. Many PNSB species are also capable of N_2 fixation and assimilate a variety of nitrogenous compounds[85]. Thus, PNSB play an important role in biogeochemical C, N, S, and Fe cycling.

Aside from *R. palustris* TIE-1, *Rhodobacter* sp. SW2, *Rhodovulum iodosum*, *Rhodovulum robiginosum*, and *Rhodomicrobium vannielii* are the only known PNSB capable of phototrophic iron-oxidization (Figure 1.6). It is currently unknown whether other PNSB, such as *Rhodovulum sulfidophilum* or *Rhodobacter sphaeroides*, can carry out phototrophic iron-oxidation. It is also unknown whether organisms in either of these phylogenetic clades are capable of phototrophic EEU. Thus far, Mtr homologs have only been identified in *R. vannielii*,

Rhodovulum sp. PH10, *Blastochloris viridis*, *R. palustris* TIE-1, and *R. palustris* CGA009 (Figure 1.6). Although the phototrophic iron-oxidation ability of many of these microorganisms is unknown, it is clear that Fe(II)-oxidation mechanisms independent of Mtr exist in other microorganisms (e.g. *R. robiginosum*). Thus, other PNSB should be tested in future studies for Fe(II)-oxidation activity. Independent of their Fe(II)-oxidation ability, these PNSB should also be investigated for EEU-activity. Because of the limited number of organisms investigated for these metabolisms, the prevalence of phototrophic EEU is poorly understood and our understanding of its ecological role is limited, especially in marine ecosystems.

Many marine PNSB, however, such as *R. sulfidophilum* either (a) use elemental sulfur (S^0) as an electron donor, or (b) produce it externally as a byproduct of sulfide oxidation[85]. This is distinct from purple sulfur bacteria (PSB), which store S^0 internally as intracellular sulfur globules[85]. It has been suggested that in chemoautotrophic sulfur-oxidizers, EET mechanisms may exist that allow these organisms to use elemental sulfur, and/or sulfide minerals as electron donors[86-88]. In a recent marine bacterial isolate, *Thioclava electrotropha*, electrodes poised at the potential of elemental sulfur (-400 to +200 mV depending on the environmental conditions)[88] could serve as electron donors[86]. Furthermore, the sulfur-oxidizing bacterium *Desulfuromonas* strain TZ1 can use poised electrodes as electron acceptors for S^0-oxidation to sulfate[89]. Since marine PNSB are also capable of S^0-oxidation, these organisms might also have EET pathways that allow them to use SPCSs as electron donors.

1.4 Perspectives

Examining the bioenergetic underpinnings of EEU is essential for understanding: (1) the ecological role of this process within microbial communities and (2) its biotechnological

applications. Because PNSB are capable of CO_2 fixation and are broadly distributed, the oxidation of SPCSs may have an important yet overlooked contribution to primary productivity in nature. In light of key knowledge gaps in EEU research, this thesis examines how phototrophs use solid substrates for cellular metabolism, first in the freshwater iron-oxidizing bacterium *R. palustris* TIE-1, and then in the marine sulfur-oxidizing phototroph, *Rhodovulum sulfidophilum* AB26.

In Chapter 2, I examine the electron transfer pathways and bioenergetic underpinnings of phototrophic EEU using a multidisciplinary approach that combines physiological studies, biochemical assays, microfluidics, and microscopy. Here I show that EEU is connected to photosynthetic electron transfer in *R. palustris* TIE-1. I investigate the contribution of key ETC proteins to better understand how electrons are used for the generation of reducing equivalents. Secondly, I test whether EEU is connected to CO_2 fixation using molecular genetics, transcriptomics, and geochemical studies. These investigations reveal that EEU is connected to CO_2 fixation and that the CBB cycle is the primary electron sink.

In Chapter 3 I use bioelectrochemical approaches to characterize the electroactivity of a marine phototrophic sulfur-oxidizing bacterium I isolated, AB26. I show that AB26 can take up electrons from a poised electrode over a range of potentials that mimic sulfur-oxidation. I use microscopic approaches to characterize the nature of the microbe-electrode interaction. Next, I examine the metabolic potential of this organism using whole genome sequencing to shed light on its biogeochemical and ecological role in the environment. Lastly, I use whole-genome transcriptome sequencing (RNA-Seq) and biochemical approaches as a first step towards identification of the molecular components important for EEU by this microbe. This work provides the first evidence that marine phototrophic bacteria are capable of EEU.

Overall, this thesis provides new insights into the physiology of microbial EEU in photoautotrophs. This work provides the first direct evidence for microbial CO_2 fixation associated with phototrophic EEU and provides a molecular model for how this feat is accomplished in the model organism *R. palustris* TIE-1 (Chapter 2). Lastly, this thesis uses bioelectrochemical and systems approaches to characterize an EEU-capable isolate related to *R. sulfidophilum*, a bacterium found broadly in marine ecosystems (Chapter 3). This study expands the known diversity of phototrophic EEU-capable microorganisms and provides a new genetically-tractable organism for studying this process in the laboratory.

1.5 Figures

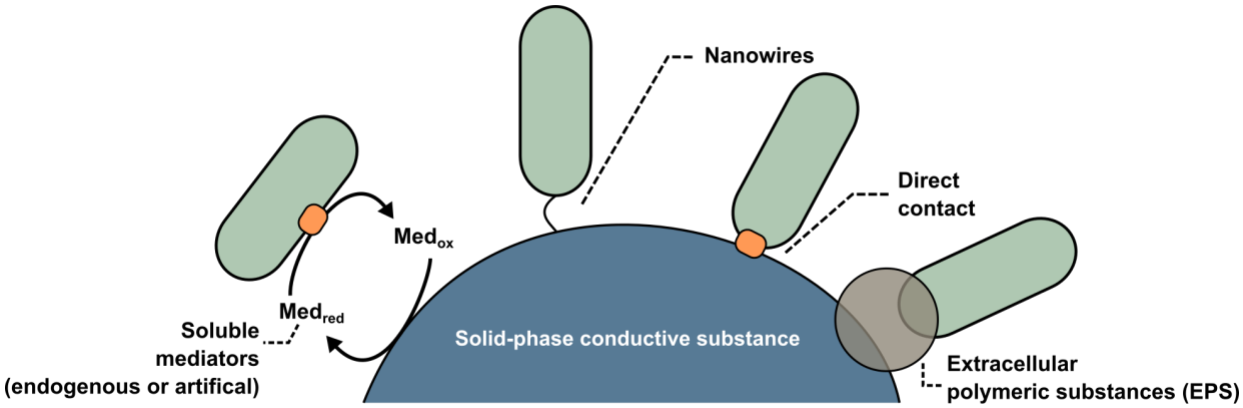

Figure 1.1. Microbial extracellular electron transfer (EET) mechanisms. Indirect and direct EET mechanisms between microorganisms and solid phase conductive substances (e.g. electrodes or metal oxides). Medox: oxidized soluble mediator; Medred: reduced soluble mediator.

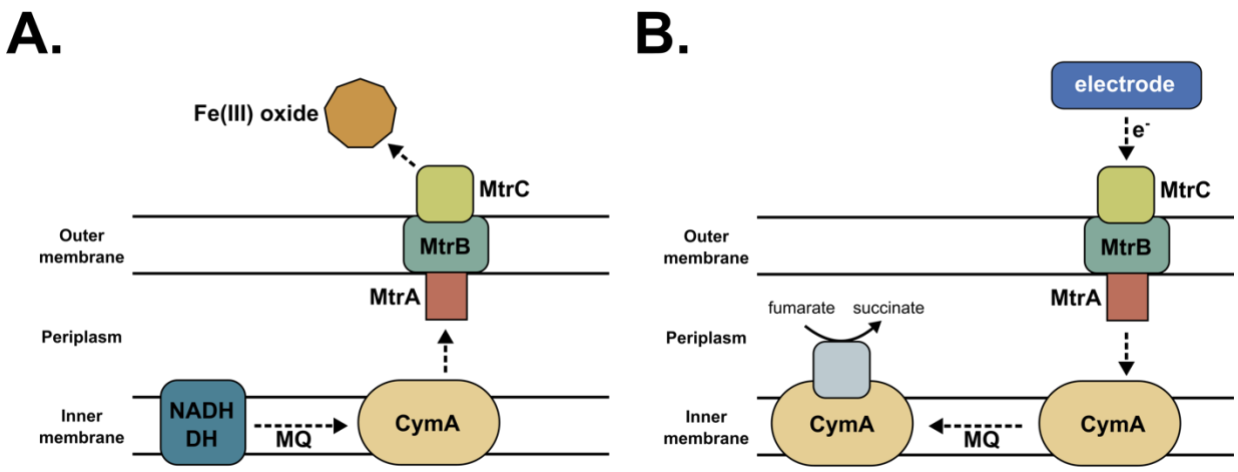

Figure 1.2. EET in *Shewanella oneidensis* MR-1. (a) The Mtr system facilitates EET from metal oxides or electrodes, or it can function in reverse (b) to facilitate extracellular electron uptake (EEU) from electrodes. For details of the stepwise process please see the text. Mtr system (MtrA, MtrB, and MtrC); CymA (tetraheme *c*-type cytochrome); MQ (menaquinone); NADH DH (NADH dehydrogenase).

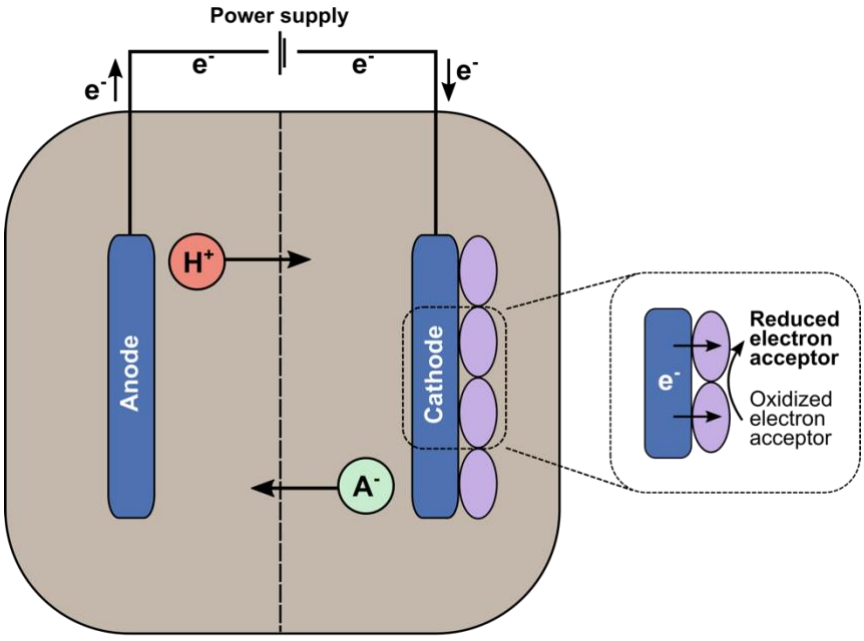

Figure 1.3. Standard bioelectrochemical reactor design. Anodic and cathodic chambers are separated by a membrane to allow ionic flow. Reactors are connected to a power supply (i.e. potentiostat) that controls the set potential of the working electrode (cathode). Microbial cells (purple ovals) in the cathodic chamber accept electrons from the cathode to reduce an intracellular electron acceptor (e.g. CO_2). e^- (electron); A^- (anion); H^+ (proton).

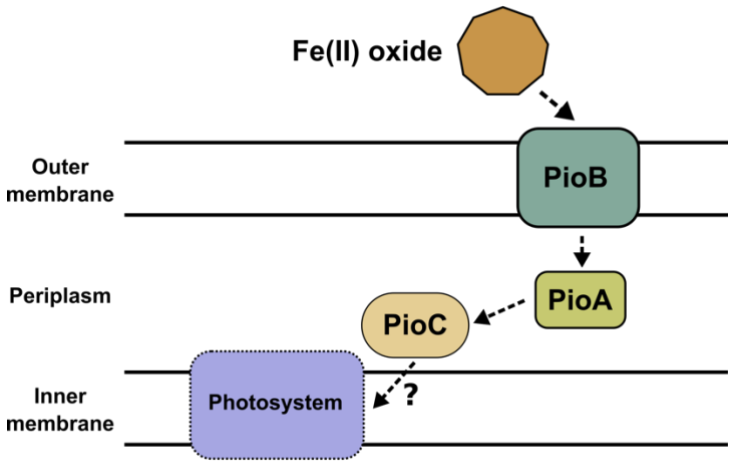

Figure 1.4. Photoferrotrophy via the PioABC system in *R. palustris* TIE-1. The Pio system catalyzes electron transfer from Fe(II) and delivers electrons to the photosystem during phototrophic growth via an unknown mechanism. For details about the electron transfer process please see the text. PioA (periplasmic decaheme *c*-type cytochrome), PioB (outer membrane β-barrel protein), PioC (high-potential iron sulfur protein), ? (electron transfer mechanism unknown).

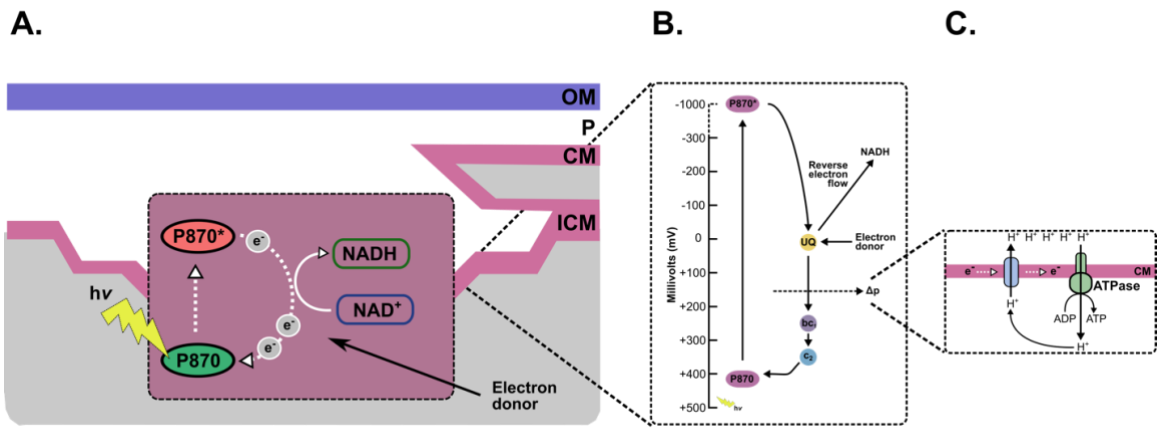

Figure 1.5. Anoxygenic photosynthesis. (a) Conceptual model of electron flow in the photosynthetic ETC. (b) Potential energy diagram of the anoxygenic photosynthetic ETC, including the major protein components. (c) Photophosphorylation. ATP (adenosine triphosphate), ADP (adenosine diphosphate), e^- (electrons), P_{870} (photosystem), P_{870}* (excited photosystem), UQ (ubiquinone), bc_1 (cytochrome bc_1), c_2 (cytochrome c_2), H^+ (protons), *hv* (light), Δp (proton gradient), ATPase (ATP synthase), OM (outer membrane), P (periplasm), CM (cytoplasmic membrane) and ICM (inner cytoplasmic membrane).

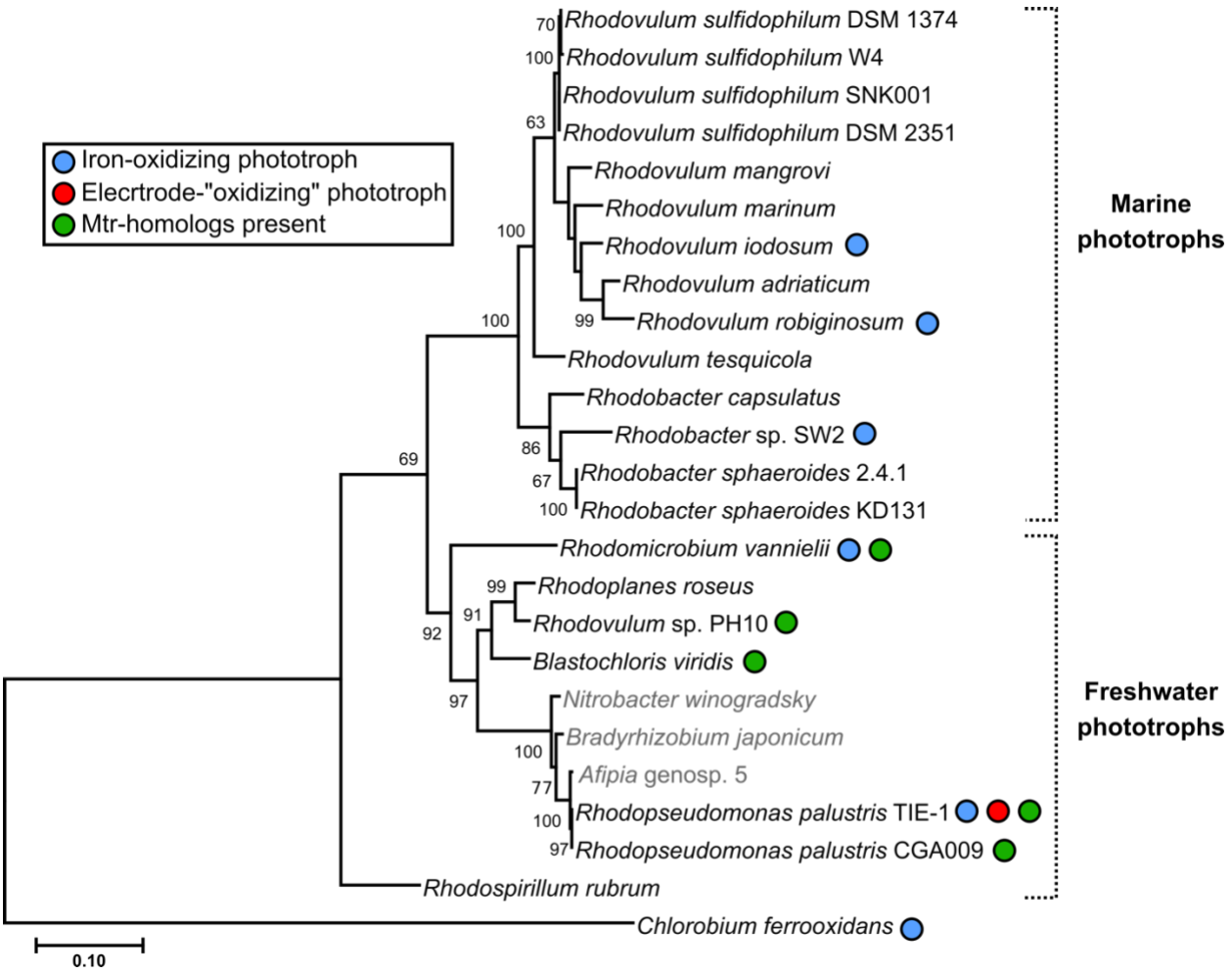

Figure 1.6. Phylogenetic tree of select purple nonsulfur bacteria. Maximum likelihood analysis of the 16S rRNA gene sequences of purple nonsulfur phototrophs and related bacteria from marine and freshwater environments. *C. ferrooxidans* was used as an outgroup. Scale bar represents amino acid substitutions.

1.6 References

1. Hernandez, M. & Newman, D. Extracellular electron transfer. *Cell. Mol. Life Sci.* **58**, 1562-1571 (2001).

2. Lovley, D.R. Dissimilatory Fe(III) and Mn(IV) Reduction. *Microbiol. Rev.* **55**, 259-287 (1991).

3. Shi, L., Dong, H., Reguera, G., Beyenal, H., Lu, A., Liu, J., Yu, H.Q. & Fredrickson, J.K. Extracellular electron transfer mechanisms between microorganisms and minerals. *Nat. Rev. Microbiol.* **14**, 651-662 (2016).

4. Kim, B.H., Kim, H.J., Hyun, M.S. & Park, D.H. Direct electrode reaction of Fe(III)-reducing bacterium, *Shewanella putrefaciens*. *Int. J. Microbiol. Biotechnol.* **9**, 127-131 (1999).

5. Lovley, D.R. & Phillips, E.J. Novel Mode of Microbial Energy Metabolism: Organic Carbon Oxidation Coupled to Dissimilatory Reduction of Iron or Manganese. *Appl. Environ. Microbiol.* **54**, 1472-1480 (1988).

6. Myers, C.R. & Nealson, K.H. Bacterial manganese reduction and growth with manganese oxide as the sole electron acceptor. *Science* **240**, 1319-1321 (1988).

7. Roden, E.E., Kappler, A., Bauer, I., Jiang, J., Paul, A., Stoesser, R., Konishi, H. and Xu, H. Extracellular electron transfer through microbial reduction of solid-phase humic substances. *Nat. Geosci.* **3**, 417 (2010).

8. Hartshorne, R.S., Reardon, C.L., Ross, D., Nuester, J., Clarke, T.A., Gates, A.J., Mills, P.C., Fredrickson, J.K., Zachara, J.M., Shi, L. and Beliaev, A.S. Characterization of an electron conduit between bacteria and the extracellular environment. *Proc. Natl. Acad. Sci. USA* **106**, 22169-22174 (2009).

9. Lovley, D.R. Extracellular electron transfer: wires, capacitors, iron lungs, and more. *Geobiology* **6**, 225-231 (2008).

10. Lovley, D.R. Powering microbes with electricity: direct electron transfer from electrodes to microbes. *Environ. Microbiol. Rep.* **3**, 27-35 (2011).

11. Rosenbaum, M., Aulenta, F., Villano, M. & Angenent, L.T. Cathodes as electron donors for microbial metabolism: Which extracellular electron transfer mechanisms are involved? *Bioresour. Technol.* **102**, 324-333 (2011).

12. Gregory, K.B., Bond, D.R. & Lovley, D.R. Graphite electrodes as electron donors for anaerobic respiration. *Environ. Microbiol.* **6**, 596-604 (2004).

13. Ross, D.E., Flynn, J.M., Baron, D.B., Gralnick, J.A. & Bond, D.R. Towards electrosynthesis in *Shewanella*: energetics of reversing the Mtr pathway for reductive metabolism. *PLoS ONE* **6**, e16649 (2011).

14. Cheng, S., Xing, D., Call, D.F. & Logan, B.E. Direct biological conversion of electrical current into methane by electromethanogenesis. *Environ. Sci. Technol.* **43**, 3953-3958 (2009).

15. Villano, M., Aulenta, F., Ciucci, C., Ferri, T., Giuliano, A. and Majone, M. Bioelectrochemical reduction of CO_2 to CH_4 via direct and indirect extracellular electron transfer by a hydrogenophilic methanogenic culture. *Bioresour. Technol.* **101**, 3085-3090 (2010).

16. Nevin, K.P., Hensley, S.A., Franks, A.E., Summers, Z.M., Ou, J., Woodard, T.L., Snoeyenbos-West, O.L. & Lovley, D.R. Electrosynthesis of organic compounds from carbon dioxide catalyzed by a diversity of acetogenic microorganisms. *Appl. Environ. Microbiol.* **77**, 2882-2886 (2011).

17. Nevin, K.P., Woodard, T.L., Franks, A.E., Summers, Z.M. & Lovley, D. R. Microbial electrosynthesis: feeding microbes electricity to convert carbon dioxide and water to multicarbon extracellular organic compounds. *MBio* **1**, e00103-00110 (2010).

18. Deng, X., Dohmae, N., Nealson, K. H., Hashimoto, K. & Okamoto, A. Multi-heme cytochromes provide a pathway for survival in energy-limited environments. *Sci. Adv.* **4**, eaao5682 (2018).

19. Deng, X. & Okamoto, A. Electrode potential dependency of single-cell activity identifies the energetics of slow microbial electron uptake process. *Front. Microbiol.* **9** (2018).

20. Ishii, T., Kawaichi, S., Nakagawa, H., Hashimoto, K. & Nakamura, R. From chemolithoautotrophs to electrolithoautotrophs: CO_2 fixation by Fe(II)-oxidizing bacteria coupled with direct uptake of electrons from solid electron sources. *Front. Microbiol.* **6**, 994 (2015).

21. Summers, Z.M., Gralnick, J.A. & Bond, D.R. Cultivation of an obligate Fe(II)-oxidizing lithoautotrophic bacterium using electrodes. *mBio* **4**, e00420-00412 (2013).

22. Bose, A., Gardel, E.J., Vidoudez, C., Parra, E.A. & Girguis, P.R. Electron uptake by iron-oxidizing phototrophic bacteria. *Nat. Commun.* **5**, 3391 (2014).

23. Cao, X., Huang, X., Liang, P., Boon, N., Fan, M., Zhang, L. and Zhang, X. A completely anoxic microbial fuel cell using a photo-biocathode for cathodic carbon dioxide reduction. *Energy Environ. Sci.* **2**, 498-501 (2009).

24. Ha, P.T., Lindemann, S.R., Shi, L., Dohnalkova, A.C., Fredrickson, J.K., Madigan, M.T. & Beyenal, H. Syntrophic anaerobic photosynthesis via direct interspecies electron transfer. *Nat. Commun.* **8**, 13924 (2017).

25. Nealson, K.H. & Saffarini, D. Iron and manganese in anaerobic respiration: environmental significance, physiology, and regulation. *Annu. Rev. of Microbiol.* **48**, 311-343 (1994).

26. Shi, L., Rosso, K.M., Zachara, J.M. and Fredrickson, J.K.. Mtr extracellular electron-transfer pathways in Fe(III)-reducing or Fe(II)-oxidizing bacteria: a genomic perspective. *Biochem. Soc. Trans.* **40**, 1261-1267, (2012).

27. Jiao, Y. & Newman, D.K. The *pio* operon is essential for phototrophic Fe(II) oxidation in *Rhodopseudomonas palustris* TIE-1. *J. Bacteriol.* **189**, 1765-1773 (2007).

28. Beckwith, C.R., Edwards, M.J., Lawes, M., Shi, L., Butt, J.N., Richardson, D.J. and Clarke, T.A. Characterization of MtoD from *Sideroxydans lithotrophicus*: a cytochrome *c* electron shuttle used in lithoautotrophic growth. *Front. Microbiol.* **6**, 332 (2015).

29. Liu, J., Wang, Z., Belchik, S.M., Edwards, M.J., Liu, C., Kennedy, D.W., Merkley, E.D., Lipton, M.S., Butt, J.N., Richardson, D.J. and Zachara, J.M. Identification and characterization of MtoA: a decaheme *c*-type cytochrome of the neutrophilic Fe (II)-oxidizing bacterium *Sideroxydans lithotrophicus* ES-1. *Front. Microbiol.* **3**, 37 (2012).

30. Shi, L., Squier, T.C., Zachara, J.M. & Fredrickson, J.K. Respiration of metal (hydr) oxides by *Shewanella* and *Geobacter*: a key role for multihaem c-type cytochromes. *Mol. Microbiol.* **65**, 12-20 (2007).

31. Shi, Z., Zachara, J.M., Shi, L., Wang, Z., Moore, D.A., Kennedy, D.W. and Fredrickson, J.K. Redox reactions of reduced flavin mononucleotide (FMN), riboflavin (RBF), and anthraquinone-2, 6-disulfonate (AQDS) with ferrihydrite and lepidocrocite. *Environ. Sci. Technol.* **46**, 11644-11652 (2012).

32. Coursolle, D., Baron, D.B., Bond, D.R. & Gralnick, J.A. The Mtr respiratory pathway is essential for reducing flavins and electrodes in *Shewanella oneidensis*. *J. Bacteriol.* **192**, 467-474 (2010).

33. Kotloski, N.J. & Gralnick, J.A. Flavin electron shuttles dominate extracellular electron transfer by *Shewanella oneidensis*. *MBio* **4**, e00553-00512 (2013).

34. Marsili, E., Baron, D.B., Shikhare, I.D., Coursolle, D., Gralnick, J.A. and Bond, D.R. *Shewanella* secretes flavins that mediate extracellular electron transfer. *Proc. Natl. Acad. Sci. USA* **105**, 3968-3973 (2008).

35. Von Canstein, H., Ogawa, J., Shimizu, S. & Lloyd, J.R. Secretion of flavins by Shewanella species and their role in extracellular electron transfer. *Appl. Environ. Microbiol.* **74**, 615-623 (2008).

36. Walker, D.J., Adhikari, R.Y., Holmes, D.E., Ward, J.E., Woodard, T.L., Nevin, K.P. and Lovley, D.R. Electrically conductive pili from pilin genes of phylogenetically diverse microorganisms. *ISME J.* **12**, 48 (2018).

37. Reguera, G., McCarthy, K.D., Mehta, T., Nicoll, J.S., Tuominen, M.T. & Lovley, D.R. Extracellular electron transfer via microbial nanowires. *Nature* **435**, 1098 (2005).

38. Gorby, Y.A., Yanina, S., McLean, J.S., Rosso, K.M., Moyles, D., Dohnalkova, A., Beveridge, T.J., Chang, I.S., Kim, B.H., Kim, K.S. and Culley, D.E. Electrically conductive bacterial nanowires produced by *Shewanella oneidensis* strain MR-1 and other microorganisms. *Proc. Natl. Acad. Sci. USA* **103**, 11358-11363 (2006).

39. Pirbadian, S., Barchinger, S.E., Leung, K.M., Byun, H.S., Jangir, Y., Bouhenni, R.A., Reed, S.B., Romine, M.F., Saffarini, D.A., Shi, L. and Gorby, Y.A. *Shewanella oneidensis* MR-1 nanowires are outer membrane and periplasmic extensions of the extracellular electron transport components. *Proc. Natl. Acad. Sci. USA* **111**, 12883-12888 (2014).

40. Shrestha, P.M. & Rotaru, A.E. Plugging in or going wireless: strategies for interspecies electron transfer. *Front. Microbiol.* **5**, 237 (2014).

41. Nielsen, L.P., Risgaard-Petersen, N., Fossing, H., Christensen, P.B. & Sayama, M. Electric currents couple spatially separated biogeochemical processes in marine sediment. *Nature* **463**, 1071 (2010).

42. Pfeffer, C., Larsen, S., Song, J., Dong, M., Besenbacher, F., Meyer, R.L., Kjeldsen, K.U., Schreiber, L., Gorby, Y.A., El-Naggar, M.Y. and Leung, K.M. Filamentous bacteria transport electrons over centimetre distances. *Nature* **491**, 218 (2012).

43. Xiao, Y., Zhang, E., Zhang, J., Dai, Y., Yang, Z., Christensen, H.E., Ulstrup, J. and Zhao, F. Extracellular polymeric substances are transient media for microbial extracellular electron transfer. *Sci. Adv.* **3**, e1700623 (2017).

44. Xiao, Y. & Zhao, F. Electrochemical roles of extracellular polymeric substances in biofilms. *Curr. Opin. Electrochem.* **4**, 206-211 (2017).

45. Flemming, H.C., Neu, T.R. & Wozniak, D.J. The EPS matrix: the "house of biofilm cells". *J. Bacteroil.* **189**, 7945-7947 (2007).

46. Lin, H., Zhang, M., Wang, F., Meng, F., Liao, B.Q., Hong, H., Chen, J. and Gao, W. A critical review of extracellular polymeric substances (EPSs) in membrane bioreactors:

characteristics, roles in membrane fouling and control strategies. *J. Membr. Sci.* **460**, 110-125 (2014).

47. Bond, D.R., Strycharz-Glaven, S.M., Tender, L.M. & Torres, C.I. On electron transport through *Geobacter* biofilms. *ChemSusChem* **5**, 1099-1105 (2012).

48. Cao, B., Shi, L., Brown, R.N., Xiong, Y., Fredrickson, J.K., Romine, M.F., Marshall, M.J., Lipton, M.S. and Beyenal, H. Extracellular polymeric substances from Shewanella sp. HRCR-1 biofilms: characterization by infrared spectroscopy and proteomics. *Environ. Microbiol.* **13**, 1018-1031 (2011).

49. Yang, G., Lin, J., Zeng, E. Y. & Zhuang, L. Extraction and characterization of stratified extracellular polymeric substances in *Geobacter* biofilms. *Bioresour. Technol.* **276**, 119-126 (2019).

50. Gao, L., Lu, X., Liu, H., Li, J., Li, W., Song, Y., Wang, R., Zhang, D. and Zhu, J. Mediation of Extracellular Polymeric Substances in Microbial Reduction of Hematite by *Shewanella oneidensis* MR-1. *Front. Microbiol.* **10**, 575 (2019).

51. Kitayama, M., Koga, R., Kasai, T., Kouzuma, A. & Watanabe, K. Structures, compositions, and activities of live *Shewanella* biofilms formed on graphite electrodes in electrochemical flow cells. *Appl. Environ. Microbiol.* **83**, e00903-00917 (2017).

52. Strycharz, S.M., Woodard, T.L., Johnson, J.P., Nevin, K.P., Sanford, R.A., Löffler, F.E. and Lovley, D.R. Graphite electrode as a sole electron donor for reductive dechlorination of tetrachlorethene by *Geobacter lovleyi*. *Appl. Environ. Microbiol.* **74**, 5943-5947 (2008).

53. Cologgi, D.L., Lampa-Pastirk, S., Speers, A.M., Kelly, S.D. & Reguera, G. Extracellular reduction of uranium via *Geobacter* conductive pili as a protective cellular mechanism. *Proc. Natl. Acad. Sci. USA* **108**, 15248-15252 (2011).

54. Gregory, K. B. & Lovley, D. R. Remediation and recovery of uranium from contaminated subsurface environments with electrodes. *Environ. Sci. Technol.* **39**, 8943-8947 (2005).

55. Rabaey, K., Read, S.T., Clauwaert, P., Freguia, S., Bond, P.L., Blackall, L.L. and Keller, J. Cathodic oxygen reduction catalyzed by bacteria in microbial fuel cells. *ISME J.* **2**, 519 (2008).

56. Clauwaert, P., Rabaey, K., Aelterman, P., De Schamphelaire, L., Pham, T.H., Boeckx, P., Boon, N. and Verstraete, W. Biological denitrification in microbial fuel cells. *Environ. Sci. Technol.* **41**, 3354-3360 (2007).

57. Wang, Z., Leary, D.H., Malanoski, A.P., Li, R.W., Hervey, W.J., Eddie, B.J., Tender, G.S., Yanosky, S.G., Vora, G.J., Tender, L.M., Lin, B., & Strycharz-Glaven, S.M. A

previously uncharacterized, nonphotosynthetic member of the *Chromatiaceae* is the primary CO_2-fixing constituent in a self-regenerating biocathode. *Appl. Environ. Microbiol.* **81**, 699-712 (2015).

58. Rowe, A.R., Rajeev, P., Jain, A., Pirbadian, S., Okamoto, A., Gralnick, J.A., El-Naggar, M.Y. & Nealson, K.H. Tracking electron uptake from a cathode into *Shewanella* cells: implications for energy acquisition from solid-substrate electron donors. *mBio* **9**, e02203-02217 (2018).

59. Singer, E., Emerson, D., Webb, E.A., Barco, R.A., Kuenen, J.G., Nelson, W.C., Chan, C.S., Comolli, L.R., Ferriera, S., Johnson, J. & Heidelberg, J.F. *Mariprofundus ferrooxydans* PV-1 the first genome of a marine Fe (II) oxidizing Zetaproteobacterium. *PloS ONE* **6**, e25386 (2011).

60. Amouric, A., Brochier-Armanet, C., Johnson, D. B., Bonnefoy, V. & Hallberg, K. B. Phylogenetic and genetic variation among Fe (II)-oxidizing acidithiobacilli supports the view that these comprise multiple species with different ferrous iron oxidation pathways. *Microbiology* **157**, 111-122 (2011).

61. Yarzabal, A., Appia-Ayme, C., Ratouchniak, J. & Bonnefoy, V. Regulation of the expression of the *Acidithiobacillus ferrooxidans rus* operon encoding two cytochromes *c*, a cytochrome oxidase and rusticyanin. *Microbiology* **150**, 2113-2123 (2004).

62. Quatrini, R., Appia-Ayme, C., Denis, Y., Jedlicki, E., Holmes, D.S. & Bonnefoy, V. Extending the models for iron and sulfur oxidation in the extreme acidophile *Acidithiobacillus ferrooxidans*. *BMC Genomics* **10**, 394 (2009).

63. Valdés, J., Pedroso, I., Quatrini, R., Dodson, R.J., Tettelin, H., Blake, R., Eisen, J.A. & Holmes, D.S. *Acidithiobacillus ferrooxidans* metabolism: from genome sequence to industrial applications. *BMC Genomics* **9**, 597 (2008).

64. Castelle, C., Guiral, M., Malarte, G., Ledgham, F., Leroy, G., Brugna, M. & Giudici-Orticoni, M.T. A new iron-oxidizing/O_2-reducing supercomplex spanning both inner and outer membranes, isolated from the extreme acidophile *Acidithiobacillus ferrooxidans*. *J Biol. Chem.* **283**, 25803-25811 (2008).

65. Yarzábal, A., Brasseur, G., Ratouchniak, J., Lund, K., Lemesle-Meunier, D., DeMoss, J.A. & Bonnefoy, V. The high-molecular-weight cytochrome *c* Cyc2 of *Acidithiobacillus ferrooxidans* is an outer membrane protein. *J. Bacteriol.* **184**, 313-317 (2002).

66. Chen, Y. & Suzuki, I. Effect of uncouplers on endogenous respiration and ferrous iron oxidation in a chemolithoautotrophic bacterium *Acidithiobacillus* (*Thiobacillus*) *ferrooxidans*. *FEMS Microbiol. Lett.* **237**, 139-145 (2004).

67. Jiao, Y., Kappler, A., Croal, L.R. & Newman, D.K. Isolation and characterization of a genetically tractable photoautotrophic Fe(II)-Oxidizing bacterium, *Rhodopseudomonas palustris* strain TIE-1. *Appl. Environ. Microbiol.* **71**, 4487-4496 (2005).

68. Bose, A. & Newman, D.K. Regulation of the phototrophic iron oxidation (*pio*) genes in *Rhodopseudomonas palustris* TIE-1 is mediated by the global regulator, FixK. *Mol. Microbiol.* **79**, 63-75 (2011).

69. Bird, L.J., Bonnefoy, V. & Newman, D.K. Bioenergetic challenges of microbial iron metabolisms. *Trends Microbiol.* **19**, 330-340 (2011).

70. Widdel, F., Schnell, S., Heising, S., Ehrenreich, A., Assmus, B. & Schink, B. Ferrous iron oxidation by anoxygenic phototrophic bacteria. *Nature* **362**, 834 (1993).

71. Bird, L.J., Saraiva, I.H., Park, S., Calçada, E.O., Salgueiro, C.A., Nitschke, W., Louro, R.O. & Newman, D.K. Nonredundant roles for cytochrome c_2 and two high-potential iron-sulfur proteins in the photoferrotroph *Rhodopseudomonas palustris* TIE-1. *J. Bacteriol.* **196**, 850-858 (2014).

72. Duchow, E. & Douglas, H. *Rhodomicrobium vannielii*, a new photoheterotrophic bacterium. *J. Bacteriol.* **58**, 409 (1949).

73. Heising, S. & Schink, B. Phototrophic oxidation of ferrous iron by a *Rhodomicrobium vannielii* strain. *Microbiology* **144**, 2263-2269 (1998).

74. Imhoff J.F. *Anoxygenic Photosynthetic Bacteria* (eds Blankenship, R.E., Madigan, M.T. & Bauer, C.E.) 1-15 (Kluwer Academic Publishers, 1995).

75. Van Driessche, G., Vandenberghe, I., Devreese, B., Samyn, B., Meyer, T.E., Leigh, R., Cusanovich, M.A., Bartsch, R.G., Fischer, U. and Van Beeumen, J.J. Amino acid sequences and distribution of high-potential iron–sulfur proteins that donate electrons to the photosynthetic reaction center in phototropic proteobacteria. *J. Mol. Evol.* **57**, 181-199 (2003).

76. White, D. *The Physiology and Biochemistry of Prokaryotes* 112-117 (Oxford Press, 2007).

77. Elbehti, A., Brasseur, G. & Lemesle-Meunier, D. First Evidence for Existence of an Uphill Electron Transfer through the bc_1 and NADH-Q Oxidoreductase Complexes of the Acidophilic Obligate Chemolithotrophic Ferrous Ion-Oxidizing Bacterium *Thiobacillus ferrooxidans*. *J. Bacteriol.* **182**, 3602-3606 (2000).

78. Tremblay, P.L., Angenent, L.T. & Zhang, T. Extracellular electron uptake: among autotrophs and mediated by surfaces. *Trends Biotechnol.* **35**, 1-12 (2016).

79. Tang, K.H., Tang, Y.J. & Blankenship, R.E. Carbon metabolic pathways in phototrophic bacteria and their broader evolutionary implications. *Front. Microbiol.* **2**, 165 (2011).

80. Larimer, F.W., Chain, P., Hauser, L., Lamerdin, J., Malfatti, S., Do, L., Land, M.L., Pelletier, D.A., Beatty, J.T., Lang, A.S. & Tabita, F.R. Complete genome sequence of the metabolically versatile photosynthetic bacterium *Rhodopseudomonas palustris*. *Nat. Biotechnol.* **22**, 55-61 (2004).

81. Gibson, J.L. & Tabita, F.R. Nucleotide sequence and functional analysis of *cbbR*, a positive regulator of the Calvin cycle operons of *Rhodobacter sphaeroides*. *J. Bacteriol.* **175**, 5778-5784 (1993).

82. Joshi, G.S., Bobst, C.E. & Tabita, F.R. Unravelling the regulatory twist–regulation of CO_2 fixation in *Rhodopseudomonas palustris* CGA010 mediated by atypical response regulator(s). *Mol. Microbiol.* **80**, 756-771 (2011).

83. Joshi, G.S., Zianni, M., Bobst, C.E. & Tabita, F.R. Further unraveling the regulatory twist by elucidating metabolic coinducer-mediated CbbR-cbb_I promoter interactions in *Rhodopseudomonas palustris* CGA010. *J. Bacteriol.* **194**, 1350-1360 (2012).

84. Van Keulen, G., Girbal, L., Van Den Bergh, E., Dijkhuizen, L. & Meijer, W. The LysR-type transcriptional regulator CbbR controlling autotrophic CO_2 fixation by *Xanthobacter flavus* is an NADPH sensor. *J. Bacteriol.* **180**, 1411-1417 (1998).

85. Hunter, C. N., Daldal, F., Thurnauer, M. C. & Beatty, J. T. *The Purple Phototrophic Bacteria*. Vol. 28 (Springer Science & Business Media, 2008).

86. Chang, R., Bird, L., Barr, C., Osburn, M., Wilbanks, E., Nealson, K. and Rowe, A. *Thioclava electrotropha* sp. nov., a versatile electrode and sulfur-oxidizing bacterium from marine sediments. *Int. J. Syst. Evol. Microbiol.* (2018).

87. Lam, B. R., Rowe, A. R. & Nealson, K. H. Variation in electrode redox potential selects for different microorganisms under cathodic current flow from electrodes in marine sediments. *Environ. Microbiol.* **20**, 2270-2287 (2018).

88. Rowe, A.R., Chellamuthu, P., Lam, B., Okamoto, A. & Nealson, K.H. Marine sediments microbes capable of electrode oxidation as a surrogate for lithotrophic insoluble substrate metabolism. *Front. Microbiol.* **5**, 784 (2014).

89. Zhang, T., Bain, T.S., Barlett, M.A., Dar, S.A., Snoeyenbos-West, O.L., Nevin, K.P. and Lovley, D.R. Sulfur oxidation to sulfate coupled with electron transfer to electrodes by *Desulfuromonas* strain TZ1. *Microbiology* **160**, 123-129 (2014).

Chapter 2: Phototrophic extracellular electron uptake is linked to carbon dioxide fixation in the bacterium *Rhodopseudomonas palustris*

Preface

The following authors contributed to the work in this chapter. Michael Singh Guzman, Arpita Bose, Karthikeyan Rengasamy, David Fike, and J. Mark Meacham designed the research. Michael Singh Guzman, Karthikeyan Rengasamy, Tahina Onina Ranaivoarisoa, Michael M. Binkley, Clive Jones, and Rajesh Singh collected the data. Michael Singh Guzman, Karthikeyan Rengasamy, Clive Jones, Tahina Onina Ranaivoarisoa, and Arpita Bose analyzed and interpreted the data. Michael Singh Guzman and Arpita Bose wrote the manuscript. All authors reviewed, revised, and approved the final manuscript.

This chapter is published in its entirety [Guzman, Michael S., et al. Phototrophic extracellular electron uptake is linked to carbon dioxide fixation in the bacterium Rhodopseudomonas palustris. Nat. Commun. 10, 1355 (2019)] and is available at https://www.nature.com/articles/s41467-019-09377-6.

We thank the following members of the Washington University community: Marta Wegorzewska for her careful reading of the manuscript; Dianne Duncan for her help with confocal microscopy; and Himadri Pakrasi, Robert Blankenship, Gautam Dantas, Joshua Blodgett, Wei Bai, Dinesh Gupta, and Yunci Qi for their helpful comments during the preparation of this manuscript. M.S.G. was supported by the Initiative for Maximizing Student Development (IMSD) training grant from the U.S. National Institutes of Health (grant number R25-GM103757). This work was supported by the following grants to A.B.: The David and Lucile Packard Foundation Fellowship (grant no. 201563111), the U.S. Department of Energy (grant no. DESC0014613; also to D.A.F.), and the U.S. Department of Defense, Army Research Office (grant no. W911NF-18-1-0037). This work was also funded by a Collaboration Initiation Grant, an Office of the Vice Chancellor of Research Grant, and an International Center for Energy, Environment and Sustainability Grant from Washington University in St. Louis.

2.1 Abstract

Extracellular electron uptake (EEU) is the ability of microbes to take up electrons from solid-phase conductive substances such as metal oxides. EEU is performed by prevalent phototrophic bacterial genera, but the electron transfer pathways and the physiological electron sinks are poorly understood. Here we show that electrons enter the photosynthetic electron transport chain during EEU in the phototrophic bacterium *Rhodopseudomonas palustris* TIE-1. Cathodic electron flow is also correlated with a highly reducing intracellular redox environment. We show that reducing equivalents are used for carbon dioxide (CO_2) fixation, which is the primary electron sink. Deletion of the genes encoding *ruBisCO* (the CO_2-fixing enzyme of the Calvin-Benson-Bassham cycle) leads to a 90% reduction in EEU. This work shows that

phototrophs can directly use solid phase conductive substances for electron transfer, energy transduction, and CO_2 fixation.

2.2 Introduction

Microbial phototrophic carbon dioxide (CO_2) fixation accounts for substantial primary productivity on Earth[1]. Anoxygenic phototrophs, which include the green and purple sulfur bacteria, are metabolically versatile microbes that oxidize an array of inorganic compounds[2]. These include H_2S, H_2, Fe^{2+}, and intriguingly, solid phase conductive substances (SPCSs) via a process called extracellular electron uptake (EEU)[3-5]. Microbial oxidation-reduction reactions with SPCSs play an important role in soil, marine sediments, and deep subsurface microbial communities[6]. The cellular electron transfer and metabolic pathways that allow photoautotrophs to utilize SPCSs via EEU, however, are largely unknown. It remains elusive whether electron uptake from SPCSs is connected to cyclic photosynthetic electron transfer and/or the generation of reducing equivalents for CO_2 fixation. Subsequently, the ecological and evolutionary role of phototrophic EEU remains poorly understood.

Poised electrodes in bioelectrochemical systems (BESs) have been used as proxies of microbial interactions with natural SPCSs, such as metal oxides[5,7]. Studies using BESs have led to fundamental insights into the molecular underpinnings of extracellular electron transfer in mineral respiring microbes[4,8]. These studies have revealed extracellular electron transfer is a widespread process in nature[4,5,8]. Furthermore, microbe-electrode interactions have been leveraged for biotechnological applications such as microbial electrosynthesis[9]. Our laboratory[3,10], and others[11,12], have recently applied BESs to better understand the molecular details of microbial phototrophic EEU. This has led to the discovery of at least two pure cultures

capable of EEU from electrodes, the anoxygenic phototrophs *Rhodopseudomonas palustris* TIE-1[3] and *Prosthecochloris aestuarii*[12]. Thus far, only *R. palustris* TIE-1 is genetically tractable[13], and as such is a model system for studying EEU.

Here, we use an interdisciplinary approach combining bioelectrochemistry, molecular biology, isotope-based geochemistry, nanotechnology and microfluidics, to examine the bioenergetic pathways and physiological electron sinks that allow photoautotrophs to use SPCSs as electron donors. Using TIE-1 as a model system we show that EEU is linked to the photosynthetic electron transport chain (pETC), and that this process leads to cells becoming highly reduced with respect to both the intracellular nicotinamide adenine dinucleotide [NAD(H)] and nicotinamide adenine dinucleotide phosphate [NAD(P)(H)] pools. We also test the ability of TIE-1 to fix CO_2 during EEU using labeling studies. These data show that EEU results in CO_2 fixation to biomass via the Calvin-Benson-Bassham (CBB) cycle. Furthermore, using mutant analysis we observe that the CBB cycle is the primary electron sink. Overall, our results trace the path of electrons following EEU through the electron transport chain and cellular metabolism.

2.3 Results

2.3.1 EEU is linked to photosynthetic electron transfer

EEU from metal oxides or poised electrodes into bacterial cells has been observed in pure cultures[3-6,12,14-20], and mixed microbial communities[4,5,21-23]. However, the electron transfer pathways that underlie EEU have only been probed in chemotrophic microbes[14,15,18,24]. In phototrophic microbes, it is unknown if electrons from a cathode enter the pETC and if this activity is important for the establishment of a proton motive force (PMF), ATP synthesis, or the

generation of reducing equivalents. Bioelectrochemical studies traditionally rely upon macroscale (>500 mL) or mesoscale (0.2 mL to 500 mL) BESs that are scaled for biomass production[25]. In such BESs it is difficult to isolate the response of surface-attached cells. This is because other factors like the influence of planktonic cells[3,10], extracellular enzymes[26], and abiotic reactions confound the interpretation of electrochemical data[3,10]. Being able to collect electrochemical data from surface-attached cells exclusively would shed light on whether EEU leads to electron transfer into the pETC.

To achieve this, we designed and constructed a microfluidic bioelectrochemical cell (µ-BEC) (Figure 2-1a, Supplementary Figure 2-1). The µ-BEC is a four-chamber, three-electrode, small-volume (1.6 µL per well) BES that is compatible with confocal microscopy (Figure 2-1a) (see methods for a complete description of the µ-BEC design and assembly). Its major advantage is that it allows us to study surface-attached cells exclusively as planktonic cells can be washed out with microfluidic control (Figure 2-1b). Appropriately grown microbial cells were incubated in µ-BECs for ~120 h at +100 mV vs. Standard Hydrogen Electrode (SHE) under continuous illumination. Once we obtained stable current densities under illuminated conditions (~-100 nA cm^{-2}), planktonic cells were washed out of the system with microfluidic control. Medium flow was turned off following this wash because constant flow led to excessive noise in the electrochemical data. To determine that we only had surface-attached cells and no plankton, we performed confocal fluorescence microscopy with LIVE/DEAD® staining in the intact µ-BEC. We observed surface-attached cells in single-layer biofilms (Figure 2-1c and Supplementary Figure 2-2a). Previous studies have shown that EEU-capable microbes, including TIE-1, make single-layer biofilms on electrodes[3,9,27-29]. Furthermore, we were unable to detect the presence of any motile planktonic cells in the µ-BEC.

We used the above approach to obtain surface-attached cells in the µ-BEC and used these biofilms to study the influence of light and chemical inhibitors on EEU. Confocal imaging using LIVE/DEAD® staining was performed in the intact µ-BEC after these tests that typically lasted for a few minutes (see methods for details). We observed light-stimulated EEU by pre-established wild-type (WT) TIE-1 biofilms (Figure 2-1d). Upon illumination, biofilms reached stable current densities within ~1-2 seconds and typically reached a maximum of ~ -100 nA cm^{-2} (Supplementary Table 2-1,2-2,2-3). Overall, the µ-BEC replicates the biofilm architecture reported in bulkier systems and permits reproducible measurements of EEU by surface-attached cells.

To better understand electron flow during EEU we pursued a chemical probe-based approach to selectively inhibit key proteins involved in cyclic pETC. TIE-1 and related anoxygenic phototrophs use cyclic photosynthesis[30] to generate energy (Figure 2-2). The photosystem (P_{870}) is reported to be at the potential of +450 mV[30]. Quinones reduced by the photosynthetic reaction center (P_{870}*) donate electrons to the proton-translocating cytochrome bc_1[31]. Electrons are then transferred to cytochrome c_2, and cycled back to the reaction center[30]. To test whether cytochrome bc_1 is involved in EEU, we used antimycin A, a specific inhibitor of cytochrome bc_1[32] to block cyclic pETC (Figure 2-2a). Antimycin A is a quinone analog that blocks the Q_i site of cytochrome bc_1, inhibiting electron transfer from ubiquinol to cytochrome *b*, thus disrupting the proton motive Q cycle[31,32]. We observed a decrease in current uptake with antimycin A treatment (Figure 2-2a, Supplementary Table 2-1). Current density became anodic (positive current) under phototrophic conditions (12.46 ± 1.34 nA cm^{-2}; $P < 0.0001$, one-way ANOVA) relative to untreated controls (-85.5 ± 5.42 nA cm^{-2}) but reverted to cathodic (negative current) densities under dark conditions (-3.46 ± 1.80 nA cm^{-2}; $P = 0.0006$, one-way ANOVA)

(Figure 2-2a). Importantly, we did not observe a difference in the number of live/dead cells attached to electrodes in inhibitor treated vs. untreated control reactors (Supplementary Figure 2-2). These data suggest that electrons enter the pETC and that cytochrome bc_1 is involved in electron flow during EEU.

Cyclic electron flow by the pETC is important for the establishment of a proton motive force (PMF) that drives ATP production[30]. To investigate whether a proton gradient is important for EEU, we exposed TIE-1 biofilms to the protonophore carbonyl cyanide *m*-chlorophenyl hydrazone (CCCP) (Figure 2-2b). CCCP is a lipid-soluble molecule that dissipates the PMF such that electron transfer is uncoupled from ATP synthesis[30,33]. We observed a decrease in current uptake heading toward anodic current under illuminated conditions upon CCCP treatment (21.2 ± 9.13 nA cm^{-2}; $P < 0.0001$, one-way ANOVA) compared to untreated controls (-113.5 ± 21.7 nA cm^{-2}) (Figure 2-2b, Supplementary Table 2-2). Current uptake was not different between CCCP (-18.4 ± 14.0 nA cm^{-2}; $P = 0.8666$, one-way ANOVA) and untreated controls (-17.52 ± 3.41 nA cm^{-2}) under dark conditions (Figure 2-2b). These results demonstrate that a PMF is required for EEU. Furthermore, dark EEU is not PMF-dependent as EEU can occur in the presence of CCCP.

The proton-translocating NADH dehydrogenase oxidizes NADH to generate a PMF for ATP production[30]. NADH dehydrogenase can also function in reverse to catalyze uphill electron transport from the ubiquinone pool to reduce NAD^+ in the anoxygenic phototrophs *Rhodobacter capsulatus*[34] and *R. sphaeroides*[35]. Its activity is linked to redox homeostasis and carbon metabolism in these organisms[36]. To investigate whether NADH dehydrogenase has a role in EEU in TIE-1, we treated cells with the NADH dehydrogenase inhibitor rotenone[37]. Rotenone blocks electron transfer from the iron sulfur clusters in NADH dehydrogenase to ubiquinone[38]

(Figure 2-2c). In illuminated biofilms, we observed a ~20% decrease in current uptake with low rotenone concentrations (25 µM; -71.8 ± 2.02 nA cm^{-2}; $P < 0.0001$, one-way ANOVA) compared to untreated controls (-94.7 ± 3.61 nA cm^{-2}), and up to a ~50% decrease with exposure to high rotenone concentrations (100 µM; -41.6 ± 4.55 nA cm^{-2}; $P < 0.0001$, one-way ANOVA) (Figure 2-2c, Supplementary Table 2-3). The current uptake maxima were markedly lower under these conditions (Supplementary Table 2-3). After initial current uptake, we observed that rotenone-treated cells showed lowered current uptake post light exposure (Figure 2-2c). It is unclear if this reduction is solely due to lowered current uptake or a combination of both lowered current uptake and increased electron donation to the electrode. The reduction in current uptake could also be a consequence of overreduction of the ubiquinone pool as has been observed in *R. sphaeroides* NADH dehydrogenase mutants[38,39]. Because we observe only a partial lowering of current uptake with NADH dehydrogenase inhibition (Figure 2-2c), the cell likely has additional sinks for using reduced ubiquinone.

CCCP and antimycin A treatment both resulted in anodic current generation under illuminated conditions. Although the magnitude of the electrochemical response was different in the two cases, these data suggest that when the pETC is inhibited, TIE-1 cells likely transfer electrons to the poised electrodes by using them as an electron sink. Overall, our inhibitor studies show that (1) electrons enter the pETC of TIE-1 following EEU; (2) PMF is required for light-dependent EEU; (3) cytochrome bc_1 is involved in electron flow; and that (4) NADH dehydrogenase plays an important role in EEU.

2.3.2 EEU leads to an imbalance in intracellular redox

Nicotinamide adenine dinucleotide (NAD) and its reduced state NADH are essential cofactors for microbes[30]. NADH can be converted to NAD(P)H via $NAD(P)^+$ transhydrogenase[40] (Rpal_4660-4662). NADH and NAD(P)H are key electron donors for biosynthetic reactions, including CO_2 fixation. To better understand how the intracellular redox pool is affected by EEU, we examined the $NADH/NAD^+$ and $NAD(P)H/NAD(P)^+$ ratios in planktonic cells[41]. We compared these ratios to aerobic chemoheterotrophy (i.e. the inoculum) and phototrophic conditions where other electron donors were provided. We observed that the $NADH/NAD^+$ ratio in the WT during EEU was higher than aerobic chemoheterotrophic growth (Figure 2-3a). The $NADH/NAD^+$ ratio was also higher than phototrophic growth on hydrogen (H_2) or photoheterotrophic growth on acetate or butyrate ($P < 0.0001$; Figure 2-3a, one-way ANOVA). The $NAD(P)H/NAD(P)^+$ ratio was also highest during EEU compared to other conditions ($P < 0.01$, one-way ANOVA; Figure 2-3b).

Analysis of intracellular redox suggests that EEU may lead to a highly-reduced environment in the cell. The lack of NAD^+ or $NAD(P)^+$ might require *de novo* NAD synthesis for cellular survival. Therefore, NAD biosynthesis might increase during EEU. We analyzed the expression of the *de novo* (aspartate-dependent) NAD biosynthesis pathway[42] in the WT transcriptome encoded by *nadABCDE*. This pathway was not differentially expressed under any phototrophic condition, including EEU (Figure 2-3c). NAD kinase which converts NAD^+ to $NAD(P)^+$ was also not differentially expressed under the conditions tested (Figure 2-3c). These data suggest NAD biosynthesis does not increase at the level of gene expression during EEU despite a highly reduced redox pool.

We reasoned that $NAD(P)^+$ consuming and/or producing reactions might be upregulated during EEU to maintain redox balance. Therefore, we assessed the expression of $NAD(P)^+$/H-requiring reactions across the TIE-1 genome. We observed that the majority of $NAD(P)^+$/H-requiring reactions were downregulated under phototrophic conditions (Figure 2-3d). Interestingly, an NADP-dependent FMN-binding flavin reductase-like protein (*fre*) was upregulated during photoautotrophic growth, increasing ~4-fold during EEU (Figure 2-3d). A pair of $NAD(P)^+$/H-dependent oxidoreductases (*akr3* and *akr4*) were also differentially expressed (Figure 2-3d). *Akr3* was upregulated under all phototrophic conditions whereas *akr4* was specifically upregulated during phototrophic H_2 oxidation and EEU. These data suggest that under EEU the cells are highly reduced and that the lack of oxidized NAD^+ and/or $NAD(P)^+$ is not relieved by *de novo* NAD biosynthesis. However, several $NAD(P)^+$/H-dependent reactions are upregulated.

2.3.3 EEU is linked to CO_2 fixation via the CBB cycle

Our data shows that EEU results in electron transfer to the pETC (Figure 2-2), eventually producing NADH and NAD(P)H (Figure 2-3). In anoxygenic phototrophs CO_2 fixation is a major sink for NAD(P)H[30]. In our initial study on EEU by TIE-1, we observed that mRNA transcripts for genes encoding form I ribulose-1,5-bisphosphate carboxylase/oxygenase (RuBisCO) increased during EEU[3]. RuBisCO catalyzes CO_2 fixation in many autotrophic organisms as part of the Calvin-Benson-Bassham (CBB) cycle[30]. Therefore, we asked whether CO_2 fixation occurs during EEU via RuBisCO. TIE-1 encodes two forms of RuBisCO: forms I (*cbbLS*) and II (*cbbM*)[43]. Using transcriptomic analysis, we analyzed the expression of the CBB cycle in TIE-1 and observed that form I *ruBisCO* was upregulated under all phototrophic conditions, but its expression was highest during EEU (~6-fold, $P < 0.0001$, one-way ANOVA)

and phototrophic iron oxidation (~7-fold, $P < 0.0001$, one-way ANOVA) (Figure 2-4a). Form II *ruBisCO* was expressed at similar levels across all phototrophic conditions (Figure 2-4a). The other enzyme unique to the CBB cycle, phosphoribulokinase (Prk), was also upregulated during EEU ($P < 0.0001$, one-way ANOVA; Figure 2-4a). Prk catalyzes the synthesis of the CO_2 acceptor molecule, ribulose 1,5-bisphosphate (RuBP)[30].

The expression of genes encoding CBB cycle-specific enzymes, including form I *ruBisCO*, suggests that CO_2 fixation occurs during EEU. There are established methods for answering whether CO_2 fixation is occurring in planktonic cells that can be grown in bulk[44,45]. However, in the case of EEU the cells attach to electrodes, which precludes us from using standard methodology. To overcome this, we employed secondary ion mass spectrometry (SIMS), and traced $^{13}CO_2$ assimilation in TIE-1. The WT and a *ruBisCO* double mutant (Δ*cbbLS* Δ*cbbM*) (Supplementary Table 2-4) were subjected to four treatments in BESs as follows: (1) poised electrodes with $^{12}CO_2$; (2) poised electrodes with $^{12}CO_2$ supplemented with 10% $^{13}CO_2$ (poised + $^{13}CO_2$); (3) electrodes at open circuit with $^{12}CO_2$ (passing no current; control); and (4) electrodes at open circuit with $^{12}CO_2$ supplemented with 10% $^{13}CO_2$ (control + $^{13}CO_2$) (Supplementary Figure 2-3). We chose to pre-grow cells under aerobic chemoheterotrophic conditions because the *ruBisCO* double mutant did not have a growth defect here compared to the WT (Supplementary Table 2-5). We used bulk BESs (~70 mL) here because they are closed systems, and do not lose CO_2, unlike the μ-BEC, which is an anoxic microfluidic system under intermittent microfluidic flow.

Cells were cultivated for ~60 hours, and planktonic and surface-attached cells (biofilms) were harvested for SIMS analysis. WT cells under poised conditions were enriched in ^{13}C relative to the nonamended cells, indicating the assimilation of $^{13}CO_2$ by both surface-attached

and planktonic cells (Figure 2-4b, Supplementary Table 2-6). The WT also increased in biomass above open circuit (Supplementary Figure 2-4). In contrast, the *ruBisCO* double mutant had a 96% reduction in $^{13}CO_2$ assimilation compared to WT (Figure 2-4b, Supplementary Table 2-7), a reduced capacity to take up electrons (Supplementary Figure 2-3) and no biomass increase (Supplementary Figure 2-4). These data demonstrate that EEU and CO_2 assimilation are connected, and that RuBisCO catalyzes the major CO_2 assimilation reaction in this system.

The planktonic and the surface-attached cells show the same level of ^{13}C assimilation. This might be due to surface-attached cells and the plankton interacting dynamically with the electrode. To address this, we devised an experiment where pre-established biofilms (from 48-hour bioreactor runs) on poised electrodes (biocathodes) were transferred into "plankton-free" bioreactors with fresh medium (Supplementary Figures 5). We observed that after 48-hours current densities in "plankton-free" bioreactors were ~70% lower than the plankton-containing bioreactors ($P < 0.05$, one-way ANOVA; Supplementary Figure 2-5a-e). Plankton increased to nearly 0.06 OD_{660}, while the biocathode remained fully colonized (Supplementary Figure 2-5a-c, f). In a reciprocal experiment, when new cell-free cathodes were installed in the plankton-containing bioreactors (used to obtain the biocathodes), current densities resembled the original levels (Supplementary Figure 2-5a-e). This suggests that the plankton retains the ability to attach to the electrodes after 48-hours. These data, along with $^{13}CO_2$ assimilation, suggests that planktonic cells in the bioreactors are interacting dynamically with the poised electrodes.

The uptake of $^{13}CO_2$ in the *ruBisCO* double mutant (Figure 2-4b) likely represents CO_2 consuming reactions such as non-autotrophic carboxylases shown in Figure 2-4c. Multiple carboxylases in the TIE-1 genome are expressed during EEU, however, many of these reactions are downregulated relative to chemoheterotrophic growth (Figure 2-4c). *cynS,* which encodes

cyanase is upregulated during EEU ($P < 0.05$, one-way ANOVA; Figure 2-4c). Cyanase catalyzes the bicarbonate-dependent metabolism of cyanate, that accumulates as a byproduct of urea dissociation and/or carbamoyl phosphate decomposition[46]. Overall, our data suggest that RuBisCO is the primary reaction that is catalyzing CO_2 fixation during EEU.

2.3.4 The CBB cycle is a primary electron sink for EEU

RuBisCO catalyzes a reaction between RuBP and CO_2 that results in the formation of 2 molecules of 3-phosphoglycerate (3-PGA), with no requirement for reducing equivalents[30]. The reactions that follow, however, require ATP and NAD(P)H. Phosphoglycerate kinase (PGK) catalyzes the phosphorylation of 3-PGA by ATP, which is converted in the reductive phase of the cycle by glyceraldehyde 3-phosphate dehydrogenase (GAPDH) into glyceraldehyde 3-phosphate (G3P). Thus, the CBB cycle, and not RuBisCO directly, is likely the electron sink for EEU. Because *ruBisCO* is the primary autotrophic carboxylase (Figure 2-4b) and because form I *ruBisCO* was upregulated during EEU (Figure 2-4a), we tested the effect of the lack of *ruBisCO* on this process.

We grew WT and the *ruBisCO* double mutant in bulk BESs. We chose this bioelectrochemical format because of the need for more biomass for downstream studies. After ~60 h of incubation in bulk BESs, the peak current density in the WT remained stable at ~ -1.5 µA cm^{-2} (Figure 2-5a). The *ruBisCO* double mutant had a 90% reduction in current uptake vs. WT ($P < 0.0001$, one-way ANOVA; Figure 2-5a). To assess *ruBisCO* gene expression, we performed reverse transcription quantitative PCR (RT-qPCR) on the planktonic cells. In the WT, form I *ruBisCO* was upregulated ~8-fold with an associated downregulation of form II *ruBisCO*

($P < 0.0001$, one-way ANOVA; Figure 2-5b). These expression data in the WT coincide with previous studies on EEU by TIE-1[3].

The *ruBisCO* mutants did not have a cell viability defect across incubations compared to the WT ($P = 0.3691$, one-way ANOVA; Figure 2-5c, Supplementary Figure 2-6). We also assessed $NADH/NAD^+$ and $NAD(P)H/NAD(P)^+$ ratios in the *ruBisCO* double mutant (lacking both form I and form II *ruBisCO*) and observed that these cells were more reduced under EEU compared to aerobic chemoheterotrophic conditions (Supplementary Figure 2-7). However, because these cells show very low current uptake (Figure 2-5a), these data are difficult to interpret. Additionally, we did not observe a difference in ATP levels in WT and the *ruBisCO* double mutant planktonic cells during EEU ($P = 0.2612$, one-way ANOVA; Supplementary Figure 2-8).

Upon complementation of the *ruBisCO* double mutant with form I and/or form II *ruBisCO* (Supplementary Table 2-4), current uptake reached ~-0.75 µA cm^{-2}, similar to EEU by the WT (Figure 2-5d). This was above current uptake levels by the *ruBisCO* double mutant ($P < 0.01$, one-way ANOVA; Figure 2-5d). We observed that form I and form II *ruBisCO* were expressed at levels similar to the WT (Figure 2-5e). Similar to the *ruBisCO* deletion mutants, the *ruBisCO* complementation mutants did not have a cell viability defect compared to the WT ($P = 0.0572$, one-way ANOVA; Figure 2-5f, Supplementary Figure 2-6).

2.3.5 RuBisCO deletion does not affect EEU due to a growth defect

To determine whether the EEU defect in the *ruBisCO* double mutant was growth-dependent, we inoculated WT cells into bioreactors containing a sub-lethal concentration of gentamicin to inhibit protein synthesis (Supplementary Figure 2-9). We observed that

gentamicin-treated WT cells accepted 80% more electrons during EEU compared to the *ruBisCO* double mutant ($P < 0.0001$, one-way ANOVA; Figure 2-5g). To assess a potential growth defect in the *ruBisCO* double mutant, we harvested the electrodes at the end of the incubations and used 5 mm sections as inoculum for chemoheterotrophic growth. We did not observe a growth defect in the *ruBisCO* double mutant upon re-growth compared to the WT ($P = 0.8232$, one-way ANOVA; Figure 2-5h). Planktonic colony forming units (CFUs) for the *ruBisCO* double mutant harvested at the end of incubations in the bulk bioreactors were not different from the WT ($P = 0.0804$, one-way ANOVA; Figure 2-5h). These data suggest that the lower EEU activity of the *ruBisCO* double mutant is not due to a growth defect.

We performed gene expression analysis using a set of genes that have been reported to be involved in EEU from electrodes[3]. We first assessed the expression level of the photosynthetic reaction center large subunit (*pufL*). Gene expression analysis showed a ~5-fold upregulation of *pufL* in the *ruBisCO* double mutant, very similar to the WT expression ($P = 0.0559$, one-way ANOVA; Figure 2-5i). Because previous mutant studies have shown that the *pioABC* system, a gene operon essential for phototrophic iron oxidation[47], also has a role in electron uptake[3], we performed expression analysis of *pioA* in the *ruBisCO* double mutant and the WT. We observed that the expression level of *pioA* in the *ruBisCO* double mutant was not different from the WT ($P = 0.0759$, one-way ANOVA; Figure 2-5i).

We also assessed the expression of the systems responsible for energy transduction. The TIE-1 genome contains two F-type ATPases: Atp1 and an "alternate" Atp2. *atp1* showed lower upregulation (~4-fold) than *atp2* (~7-fold) in both the WT and the *ruBisCO* double mutant (Figure 2-5i). The WT transcriptomic data corroborate the RT-qPCR data where *atp1* is downregulated during phototrophic growth conditions, including EEU, whereas *atp2* is

specifically upregulated during EEU (Supplementary Table 2-8,2-9). These results suggest that the *atp2* operon plays an important role in ATP synthesis during EEU. Overall, our data suggest that the WT and the *ruBisCO* double mutant do not show any differences in the level of gene expression for critical genes required for EEU, pETC, and energy generation. These data, in conjunction with the lack of $^{13}CO_2$ assimilation (Figure 2-4b), suggests the *ruBisCO* double mutant cells may be using cellular reserves to stay viable under the conditions tested.

2.3.6 The CBB cycle is important for phototrophic H_2 oxidation

The inability of the *ruBisCO* double mutant to take up electrons from solid electrodes suggests that the CBB cycle is the primary electron sink during EEU. This finding underscores that CO_2 fixation is tightly linked to EEU in these bacteria. In order to probe whether this coupling extends to other growth conditions, we examined the ability of the *ruBisCO* double mutant to oxidize H_2 under phototrophic conditions. We observed ~80% lower H_2 consumption in the *ruBisCO* double mutant compared to the WT ($P < 0.05$, one-way ANOVA; Figure 2-6a, Supplementary Table 2-10) with a concomitant reduction in CO_2 consumption ($P < 0.05$, one-way ANOVA; Figure 2-6b, Supplementary Table 2-10). We also observed an increase in biomass in the WT compared to the *ruBisCO* double mutant during phototrophic H_2 oxidation ($P < 0.0001$, one-way ANOVA; Supplementary Figure 2-10, 11). These data suggest that CO_2 fixation is an important electron sink under photoautotrophic conditions, where electron donors, such as H_2, are oxidized to provide cellular reducing power.

The *ruBisCO* double mutant might oxidize less H_2 because gene expression of the uptake hydrogenase[48] is lower. We therefore assessed the expression of the large subunit of the uptake hydrogenase (*hupL*) in the *ruBisCO* double mutant and found that its expression was not altered

compared to WT levels (P = 0.3222, one-way ANOVA; Figure 2-6c). This suggests that the level of phototrophic H_2 oxidation between the WT and the *ruBisCO* double mutant should be similar. However, our data show a clear reduction in H_2 oxidation of ~80% in the mutant strain. We also assessed the expression of *pufL* in the *ruBisCO* double mutant and found no difference in expression vs. the WT (P = 0.0753, one-way ANOVA; Figure 2-6c). In contrast, *atp1* gene expression was higher in the WT (P < 0.01, one-way ANOVA) while *atp2* gene expression was higher in the *ruBisCO* double mutant (P < 0.01, one-way ANOVA; Figure 2-6c). Our data suggest that the lack of *ruBisCO* affects the ability of TIE-1 to accept electrons from other electron donors such as H_2.

2.4 Discussion

Microbes have been known to exchange electrons with SPCSs for nearly a century[7]. Although we know the underlying electron transfer pathways and electron sinks employed by microbes that use SPCSs as electron acceptors, these are largely unknown for microbes that use SPCSs as electron donors[4,8]. To fill this knowledge gap, here we used an interdisciplinary approach to study the model EEU-capable microbe *R. palustris* TIE-1. Our data shows that EEU from poised electrodes is connected to pETC and CO_2 fixation (Figure 2-7). We observe that electrons enter the pETC, and eventually these electrons reduce NAD^+ for CO_2 fixation via the CBB cycle (Figures 7). Furthermore, NADH dehydrogenase plays an important role in EEU (Figure 2-2) most likely for generation of reducing equivalents for cellular metabolism.

Our inhibitor studies (Figure 2-2) and biochemical assays (Figure 2-3) suggest that during EEU, electron flow leads to NAD^+ and $NAD(P)^+$ reduction. Because the reduction potential of the electrode in our experiments is lower than that required to reduce NAD^+/ $NAD(P)^+$ directly,

reverse electron transfer has to occur. The path of reverse electron transfer has been extensively studied in chemolithoautotrophs[34,37,39,49]. In these bacteria, electrons from soluble ferrous iron enter at cytochrome c_2. These electrons can reduce oxygen to generate a PMF for ATP synthesis. The PMF can also be used to drive reverse electron flow from cytochrome bc_1 to NADH dehydrogenase to reduce NAD^+[34,37,39,49]. NADH dehydrogenase-mediated reverse electron flow has also been observed in *R. capsulatus*[34]. This pathway for electron transfer to NAD^+ has also been proposed for other anoxygenic phototrophs[50,51]. Our data implies reverse electron flow is also occurring during EEU in TIE-1.

Interestingly, we observe that EEU is reversible in TIE-1 (Figure 2-2a, b). Although artificially induced in our system (i.e. only in the presence of antimycin A or CCCP), the reversibility of extracellular electron transfer pathways is broadly observed in bacteria donating electrons to SPCSs[14,27]. For example, *Shewanella oneidensis* MR-1 uses an electron conduit called the Mtr system to transfer electrons to SPCSs[14]. Mtr can also function in reverse to facilitate EEU[14]. The PioAB system (a homolog of the MtrAB system) in TIE-1[47] plays a role in EEU from poised electrodes[3]. Anoxygenic photoheterotrophs are known to use CO_2 as an electron sink to maintain redox balance when growing on highly reduced substrates such as butyrate[52]. In nature, photoheterotrophs may use this reversibility of the EEU pathways and use SPCSs as electron sinks.

SIMS analysis demonstrates CO_2 fixation is occurring during EEU primarily via RuBisCO (Figure 2-4). We observed ^{13}C assimilation was identical in surface-attached and planktonic cells within the bulk bioreactors. Furthermore, reactors with planktonic cells have higher current densities versus plankton-free reactors (Supplementary Figure 2-5) suggesting that they contribute to EEU via an unknown mechanism (Supplementary Figure 2-12). Previously

published work from our laboratory, however, suggests no redox active molecule is detectable in the spent-medium[3]. Our laboratory has also shown that a cathode-driven Fe(II)/Fe(III) redox cycle at +100 mV vs. SHE[10], is also unlikely.

The *ruBisCO* mutant is impaired in using electron donors such as poised electrodes (Figure 2-5) and H_2 for photosynthesis (Figure 2-6). This implies that the cells ability to fix CO_2 via *ruBisCO* is relayed to the electron transfer machinery that accepts electrons from these electron donors. During EEU we observe both increased *ruBisCO* expression (Figure 2-4a) and an increased NAD(P)H/NAD(P)$^+$ ratio (Figure 2-3b). In *R. palustris* CGA009/10, which is closely related to TIE-1, form I *ruBisCO* is transcriptionally activated in response to elevated NAD(P)H and ATP levels via a regulatory system called CbbRRS[53,54]. These studies suggest that form I RuBisCO may be a sensor of cellular energy and redox balance[53,54]. In TIE-1, the regulatory CbbRRS system may also sense NAD(P)H levels and regulate form I *ruBisCO* expression. Together, this suggests that NAD(P)H is a metabolite that communicates redox status to the CBB cycle by controlling *ruBisCO* expression. This relationship between carbon metabolism and electron transfer may be conserved in other organisms, and thus be broadly relevant in many ecosystems.

Our data highlights that photosynthetic EEU is linked to the CBB cycle for CO_2 fixation. The link between EEU and the CBB cycle is the reducing equivalents produced via the pETC (Figure 2-7). Because the CBB cycle[1] and EEU[4,5] are important processes in nature, primary productivity may be attributed to this process. Future studies will focus on quantitative measurements of the prevalence of autotrophic EEU such that EEU-linked CO_2 fixation can be accounted for in global biogeochemical cycles. EEU from natural SPCSs such as rust might represent a strategy that autotrophic microbes use to access electrons for microbial survival when

other electron donors are limiting or otherwise unavailable due to spatiotemporal constraints. Photoautotrophs, which are restricted to the photic zone, are known to exchange electrons with SPCSs, including magnetite[55]. Indeed, studies have shown that SPCSs can potentiate interspecies electron transfer[55-57]. For example, *Geobacter sulfurreducens* can exchange electrons with TIE-1 via mixed valent iron oxides[55]. Furthermore, long distance extracellular electron transfer has been observed by various researchers[7,8]. Although some microbes have evolved specialized membranes to facilitate long distance extracellular electron transfer[58-60], microbes may also utilize electrically conductive minerals to access electrons in deeper sedimentary zones to overcome spatial separation from electron donors. Because SPCSs are ubiquitous[8,61], EEU might be used both for microbial growth and survival.

2.5 Methods

2.5.1 Bacterial strains and culture conditions

All strains used in this study are indicated in Supplementary Table 2-4. The *Rhodopseudmonas palustris* TIE-1 *ruBisCO* deletion mutants (Δ*cbbLS, Rpal*_1747-1748; Δ*cbbM, Rpal*_5122; and Δ*cbbLS* Δ*cbbM*) were constructed using a suicide plasmid system (Supplementary Table 2-4)[13]. A complete list of cloning and sequencing primers and restriction enzymes can be found in Supplementary Table 2-11. *Escherichia coli* strains were routinely cultivated in lysogeny broth (LB; pH 7.0) in 10 mL culture tubes or on LB agar at 37°C. TIE-1 was pre-grown chemoheterotrophically at 30°C in YP medium (0.3% yeast extract and 0.3% Bacto peptone) supplemented with 10 mM MOPS pH 7.0 (YPMOPS) in the dark. All growth experiments were carried out at 30°C unless otherwise noted. All phototrophic growth experiments were carried out with a single 60W incandescent light bulb at a distance of 25 cm.

For anaerobic photoautotrophic growth TIE-1 strains were grown on 80% hydrogen-20% carbon dioxide (H_2-CO_2) at ~50 kPa in freshwater medium[62] (FW) with 20 mM sodium bicarbonate in sterile, sealed glass serum bottles. For anaerobic photoheterotrophic growth TIE-1 was grown in 10 mL FW medium supplemented with 1 mM acetate or butyrate from stock solutions (100 mM, pH = 7). In all cases where a change in culture medium was required cells were washed 3 times in basal FW medium post-centrifugation at 5000 x *g*. Bioelectrochemical reactor studies were performed with FW medium lacking exogenous electron donors, and purged with 80%-20% nitrogen (N_2)-CO_2. The complemention experiments were carried out with 1 mM IPTG and 800 µg mL^{-1} gentamicin for plasmid selection. Doubling time was calculated using the equation $g = \ln(2)/k$, where k was determined from the slope of OD_{660} versus time on a $\log_{10}$ scale.

2.5.2 Complementation of *ruBisCO* knockouts

The TIE-1 form I *ruBisCO* (*cbbLS*) and form II *ruBisCO* (*cbbM*) genes were cloned such that the start site overlapped with an NdeI restriction site for cloning into pSRKGm (Supplementary Table 2-4). A complete list of primers and restriction enzymes used in cloning can be found in Supplementary Table 2-11. Post-cloning, the *ruBisCO* complementation plasmids were conjugated into the *ruBisCO* double mutant (Δ*cbbLS* Δ*cbbM*) using the mating strain *E. coli* S17-1/λpir and selected on 800 µg mL^{-1} YPMOPS agar plates. A single colony was chosen and grown on 1 mM IPTG. Colonies were PCR screened using the primers in Supplementary Table 2-11. The pSRKGm empty vector was introduced into the WT and the *ruBisCO* double mutant to serve as controls (Supplementary Table 2-4).

2.5.3 RNA isolation and RT-qPCR

For bioelectrochemical studies, planktonic cells were sampled in an anaerobic chamber and immedietly mixed 1:1 with RNA*later*® (Qiagen, USA). RNA was extracted using the

RNeasy® Mini Kit according to the manufacturer's recommendations (Qiagen, USA). DNA removal was performed using Turbo DNA-*free*™ Kit (Ambion, USA). RNA samples were tested for purity using PCR. Gene expression analysis of *ruBisCO* was performed using RT-qPCR with the comparative Ct method. Primer efficiencies were determined according to the manufacturers reccommendations. Purified RNA was used to synthesize cDNA with the iScript™ cDNA synthesis kit. *clpX* and *recA* were used as internal standards based on previous studies[3]. Primers for RT-qPCR outlined in Supplementary Table 2-12 were designed in Primer3 v4.1.0 (http://primer3.ut.ee) using the programs default parameters. The Bio-Rad iTaq™ Universal SYBR® Green Supermix and the Bio-Rad CFX Connect™ Real-Time System Optics ModuleA machine (Bio-Rad Laboratories, Inc., Hercules, CA) were used for all quantitative assays according to the manufacturer's recommendations.

2.5.4 Differential expression (RNA-seq) analysis

Transcriptomic data sets were downloaded from NCBI (BioProject: PRJNA417278) and differential expression and statistical analysis was performed. Trimmomatic version 0.36 was used to trim Illumina sequencing reads (threshold = 20) and length filter (min = 60bp)[63]. Processed reads were mapped to the published *R. palustris* TIE-1 genome using TopHat2 version 2.1.1 and the gff3 annotation file as a guide for sequence alignment[64]. Bowtie 2 version 2.3.3.1 was used to index the reference genome FASTA file[65]. The number of reads mapping to each feature were counted by HTSeq version 0.9.1[66]. Differentially expressed genes were determined in DESEQ2 version 1.16.1 using the HTSeq read counts. To determine if genes were significantly differentially expressed an adjusted p-value cutoff of 0.05 was used. Heat maps were drawn in R using ggplot2[67].

2.5.6 Quantification of NADH/NAD$^+$ and NAD(P)H/NAD(P)$^+$ ratios

NADH/NAD$^+$ and NAD(P)H/NAD(P)$^+$ ratios were quantified using the "high-sensitivity" reagent mixture and sampling procedure[41]. Briefly, two separate 2 mL cell aliquots were sampled in an anaerobic chamber and centrifuged for 1 minute at 21,000 x *g* to remove the supernatant. Cell pellets were then resuspended in 200 µL 0.2 M hydrochloric acid (for NAD$^+$ and NAD(P)$^+$) or sodium hydroxide (for NADH and NAD(P)H) for 10 minutes at 50°C, then chilled on ice for 5 min. The reaction was then neutralized dropwise with equal volume 0.1 M acid or base and centrifuged for 5 min at 21,000 x *g*. The supernatant was stored at -80°C for no more than one week. The enzyme cycling assays were performed on a BioTek Synergy™ HTX 96-well plate reader measuring absorbance at 570 nm[41]. A standard curve of known concentrations of NAD$^+$ and NAD(P)$^+$ was used to determine the concentration of samples.

2.5.7 ATP quantitation

ATP was extracted using the boiling water method[68]. Briefly, 2 mL of cells were centrigured at 21,000 x *g* for 1 minute and the cell pellet was resuspended in 50 µL boiling sterile-filtered Milli-Q® water and allowed to sit at room temperature for 10 minutes. Samples were then centrifuged at 21,000 x *g* for 1 minute and the supernatant was transferred to fresh microcentrifuge tubes and stored at -80°C for no more than one week. The ATP Determination Kit (Molecular Probes, Eugene, OR) was used to measure ATP concentrations using a standard curve of known concentrations according to the manufacturers reccomendations. Absorbance was measured at 560 nm. ATP concentrations were normalized to biomass (OD_{660}).

2.5.8 Bulk bioelectrochemical system (BES) setup and conditions

Bioelectrochemical systems (BESs) were configured as previously described[10]. Briefly, FW media (70 mL) was dispensed into sterile, sealed, three-electrode BESs which were bubbled

for 60 minutes with 80%:20% N_2-CO_2 to make remove oxygen, and pressurized to ~50 kPa. The three electrodes were configured as follows: graphite working electrodes were approximately 3.2 cm^2; reference eletrodes (Ag/AgCl) were submerged in 3 M KCl; and counter electrodes were composed of 5 cm^2 platinum foil. Working electrodes were poised at +100 mV versus Standard Hydrogen Electrode (SHE) using a multichannel potentionstat (Gamry Instruments, Warmister, PA) and operated continuously with a single 60W incandescent light bulb at 26°C. Data were collected every 1 minute using the Gamry Echem Analyst™ (Gamry Instruments, Warmister, PA) software package. The biomass (OD_{660}) of inoculated BESs was monitored with a BugLab Handheld OD Scanner (Applikon Biotechnology, Inc., Foster City, CA).

2.5.9 Quantification of live/dead bacteria on electrodes

Graphite electrodes were washed 3 times with anoxic 1X phosphate-buffered saline (PBS) to remove unattached cells in an anaerobic chamber. Sections of the electrode were cut with a sterile razor blade and immediately placed in sterile microfuge tubes containing anoxic 1X PBS. Prior to imaging, the electrode was immersed in LIVE/DEAD® stain (10 µM SYTO 9 and 60 µM propidium iodide, L7012, Life Technologies) and incubated for 15 min in the dark. Samples were then placed in 1X PBS in a glass bottom Petri dish (MatTek Corporation, Ashland, MA). For imaging biofilms in the intact µ-BEC, LIVE/DEAD® stain was flowed into the µ-BEC and allowed to incubate for 15 min in the dark. The excess stain was washed with sterile anoxic 1X PBS. Electrodes were imaged on a Nikon A1 inverted confocal microscope using 555 and 488 nm lasers and a 100X objective (Washington University in St. Louis Biology Department Imaging Facility). Attached cells were quantified in Fiji v1.0 (https://fiji.sc) using the analysis pipeline described below. Briefly, images (n = 3) were inverted then converted to a 1-bit image by auto-thresholding. The "Watershed" tool was then applied to separate object edges. The

"Analyze Particles" tool was used to generate cell counts for each image based on an area range (min = 16 pixels, max = 210 pixels) that was empirically determined from manually masking 100 cells. The red and green channels were split, and the "Analyze Particles" tool was used to count bacteria on each image (1024 × 1024 pixels).

2.5.10 Micro-bioelectrochemical cell (µ-BEC) setup and conditions

The µ-BECs were assembled from polymer fluidic layers, indium tin oxide (ITO) coverslips, and a glass layer with integrated reference and counter electrodes. Inlet, outlet, and connecting channels were laser cut into a 40 mm × 12.25 mm × 254-µm thick acetal polyoxymethylene (POM) adhesive tape. Four 4 mm diameter reaction chambers were cut into a second 127-µm thick acetal POM tape, aligned, and bonded to the channel layer using a pressure-sensitive acrylic adhesive. Prior to assembly, 1-mm diameter inlet/outlet holes were drilled into Borofloat® 33 1.75-mm thick glass capping layer (Schott AG, Mianz, Germany). 500-µm deep grooves were diced into the glass above the chamber midlines to locate 250-µm silver and platinum wires used for reference (RE) and counter (CE) electrodes, respectively (Xi'an Yima Opto-electrical Technology Co., Ltd, Shaanxi, China). Each 1.6 µL (0.125 cm^2) well was enclosed by a 6 mm × 10 mm × 170-µm thick ITO-coated coverslip (30-60 Ω) (SPI supplies, West Chester, PA) to serve as the working electrode. Inlet and outlet tubes (Saint-Gobain TYGON® b-44-3; 1/16" ID x 1/8" OD) (United States Plastic Corp., Lima, OH) were attached on the glass capping layer and the 1/16" tube ends were capped with male/female luer lock fittings (World Precision Instruments, Sarasota, FL). Microbial samples were injected into the µ-BEC using a FLOW EZ™ Fluigent Microflow Controller (Le Kremlin-Bicêtre, France) with 5 kPa 80%-20% N_2-CO_2. Microbial cells were incubated in µ-BECs with working electrodes poised at +100 mV vs. SHE for ~120 h under illuminated conditions with a single

60W incandescent light bulb at a distance of 25 cm to establish biofilms. Once we obtained stable current densities under illuminated conditions (~-100 nA cm^{-2}), planktonic cells were washed out of the system with microfluidic control and biofilms were immedietly treated with chemical inhibitors under dark conditions. Light "on-off" experiments were subsequently carried out at an interval of 10 seconds for a total of 200 seconds. Microfluidic flow was not applied during electrochemical data collection.

2.5.11 Analytical techniques

In order to quantify the amounts of H_2 and CO_2 consumption during photoautotrophic growth of with H_2, gas concentrations in headspace at the initial and final time points were measured. 20 µL of gas sample from the headspace was withdrawn using a Hamilton™ gas-tight syringe and analyzed using a Tracera GC-BID 2010 Plus, (Shimadzu Corp., Japan) equipped with Rt®-Silica BOND PLOT Column (30 m × 0.32 mm; Restek, USA). Based on the measured partial pressures of H_2 and CO_2, their concentrations in headspace (moles of gas) were calculated using the ideal gas law ($PV = nRT$).

2.5.12 Secondary ion mass spectrometry (SIMS)

For planktonic assessments, 2 mL of cells were harvested from the bulk BESs and centrifuged at 4000 x *g* for 10 minutes. For biofilm assessments, cells were manually dislodged from the electrode by scraping with a sterile razor and resuspended in 950 µL of 1X PBS. Cells were then fixed with 50 µL of 20% paraformaldehyde fixative to a 1% final concentration and incubated at 4°C for 24 h. After incubation, cells were pelleted by centrifugation, and washed with 1X PBS buffer twice to remove any residual fixative. Lastly, the cells were resuspended in 500 µL 100% ethanol and stored at -20°C. Carbon isotopic compositions of individual cells were

measured on a Cameca IMS 7f-GEO (Ametek Inc., USA) secondary ion mass spectrometer. Areas of interest (~100 μm^2) were selected via scanning ion imaging, using the criterion of maximizing cell density, without compromising unambiguous individual cell identification. Scanning ion images of $^{12}C^{14}N^-$ were used for this step, which was preceded by several minutes of pre-sputtering, in order to overcome the surface ion-yield transient region and achieve steady state secondary ion yield. Note that for biological specimens, nitrogen is monitored as CN^- which provides a strong, unambiguous signal with which to locate the microbes[69]. Nominal primary ion settings were a 1.5-μm diameter, 20-keV net impact energy, 10 pA Cs^+ beam rastered over a square area 100 microns per side. $^{12}C^-$ and $^{13}C^-$ scanning ion images were acquired, sequentially, using magnet switching and a single electron multiplier (EM) detector. In order to avoid EM saturation or aging, the instantaneous secondary ion count rate was restricted to $<3x10^5$ counts per second. A magnetic field settling time of 1 second was included prior to each new image acquisition. The acquisition time per image was nominally 5 seconds for $^{12}C^-$ and 55 seconds for $^{13}C^-$. Image acquisition cycling continued until most cellular material was sputtered through (typically between 2-4 hours). Between 2-6 fields of view were measured for each sample, depending on cell spacing. For these specimens, the most egregious isobaric interference was $^{12}C^1H^-$, which required a mass resolving power (MRP) of 2909 (M/dm) to achieve mass peak separation from $^{13}C^-$. Therefore, the entrance and exit slits were set to achieve a flat-topped peak with MRP = 3000.

2.5.13 SIMS data analysis

Each region of interest (ROI; i.e. one individual cell) was selected using Cameca WinImage software (Ametek Inc., USA), and all count rates were exported for all ROIs for all cycles. Electron multiplier dead time and quasi-simultaneous arrival corrections (QSA) were

applied[70]. Note that these corrections made a relative change to the corrected ratio from the raw data ratio of only ~ 0.5% and ~ 0.2%, respectively. For each field of view, isotope ratios for all ROIs were plotted against cycle number. Based on numerous 'blank' analyses of unlabeled microbes, isotope ratios are not statistically 'normally' distributed around the mean value as the cell is sputtered through, being skewed at the onset of sputtering (despite pre-loading with Cs) and also when the cell is almost consumed. However, excluding these cycles, histograms of percent deviation from natural abundance of populations of 'blank' cells are, indeed, statistically normal, with a typical *relative* standard deviation < 1% (1 second, for >100 cells). (Note that a 1% *relative* standard deviation indicates, for example, that a 20% measured label isotope ratio increase would have a standard deviation of 0.2%). Once the cycles for each field of view were chosen, the ratios were averaged across those cycles for each region of interest. The data were then translated to deviations from unlabeled. For each test, a reference ratio, that is, the mean $R^{13}C$ (i.e., $^{13}C/^{12}C$) of the unlabeled data set, is calculated. Then all ratios in that test were recalculated as ‰ (permil, or part per thousand) deviations from the unlabeled mean using the equation $\delta^{13}C_{test} = (R^{13}C_{test}/R^{13}C_{ref} - 1)*1000$ with Microsoft® Excel.

2.5.14 Electron transport chain inhibitors

Stock solutions (100X) of rotenone, antimycin A, and carbonyl cyanide *m*-chlorophenyl hydrazine (CCCP) (MilliporeSigma, USA) were solubilized in 100% DMSO and stored as aliquots at -20°C for no more than one day before use. For µ-BEC experiments, the stock solutions were suspended in 1X PBS before use.

2.5.15 Statistical analysis

All statistical analyses (Student's *t*-test, one-way ANOVA with Bonferroni adjustment) were performed with Microsoft® Excel "Data Analysis" tools.

2.5.16 Data availability

All data in this study are available from the corresponding authors upon request. The source data underlying Figs 1d, 2a-b, 3a-d, 4a-c, 5a-i, 6a-c; Supplementary Figs 2a-d, 3, 4, 5d-e, 6a-i, 7a-b, 8-11; and Supplementary Tables 1-3 and 5-7 and 10 are provided as a Source Data file. Sequencing reads used for differential expression analysis are available under BioProject PRJNA417278.

2.6 Figures

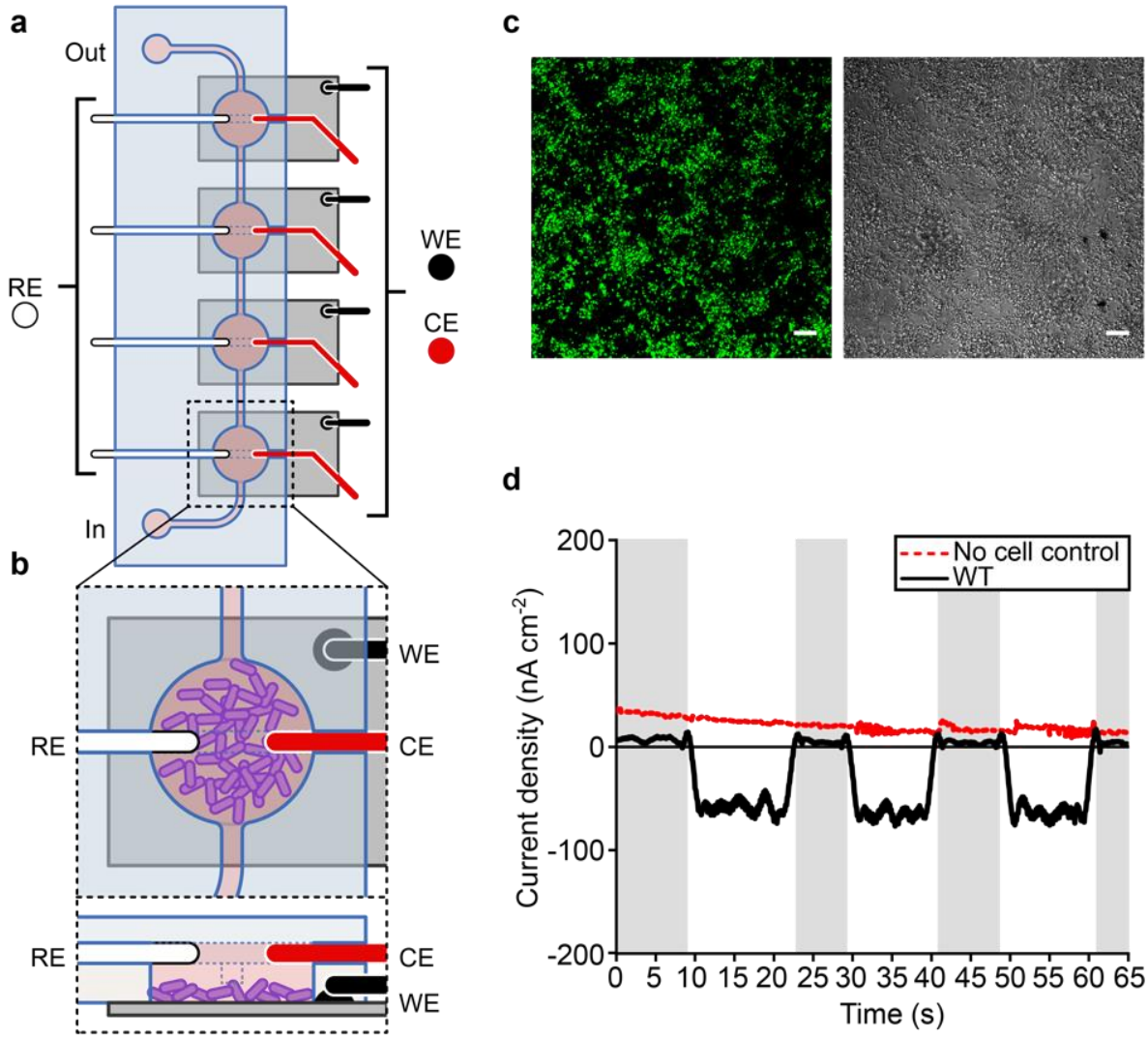

Figure 2.1. Extracellular electron uptake in the micro-bioelectrochemical cell. (a) Schematic drawing of a single, four-chamber micro-bioelectrochemical (μ-BEC) with (b) microbial cells attached to the indium tin oxide (ITO) working electrode (WE). The reference (RE) and counter (CE) electrodes are silver and platinum wires, respectively (not drawn to scale). (c) Confocal micrograph *of R. palustris* TIE-1 biofilms attached to the WE under poised conditions using

LIVE/DEAD® staining. Green cells are viable. Scale bars are 10 μm (d) Current densities for TIE-1 wild-type (WT) (black) in the μ-BEC under illuminated and dark conditions (shaded regions) compared to a 'No cell control' reactor (red). Data shown are representative of three experiments. Source data are provided as a Source Data File.

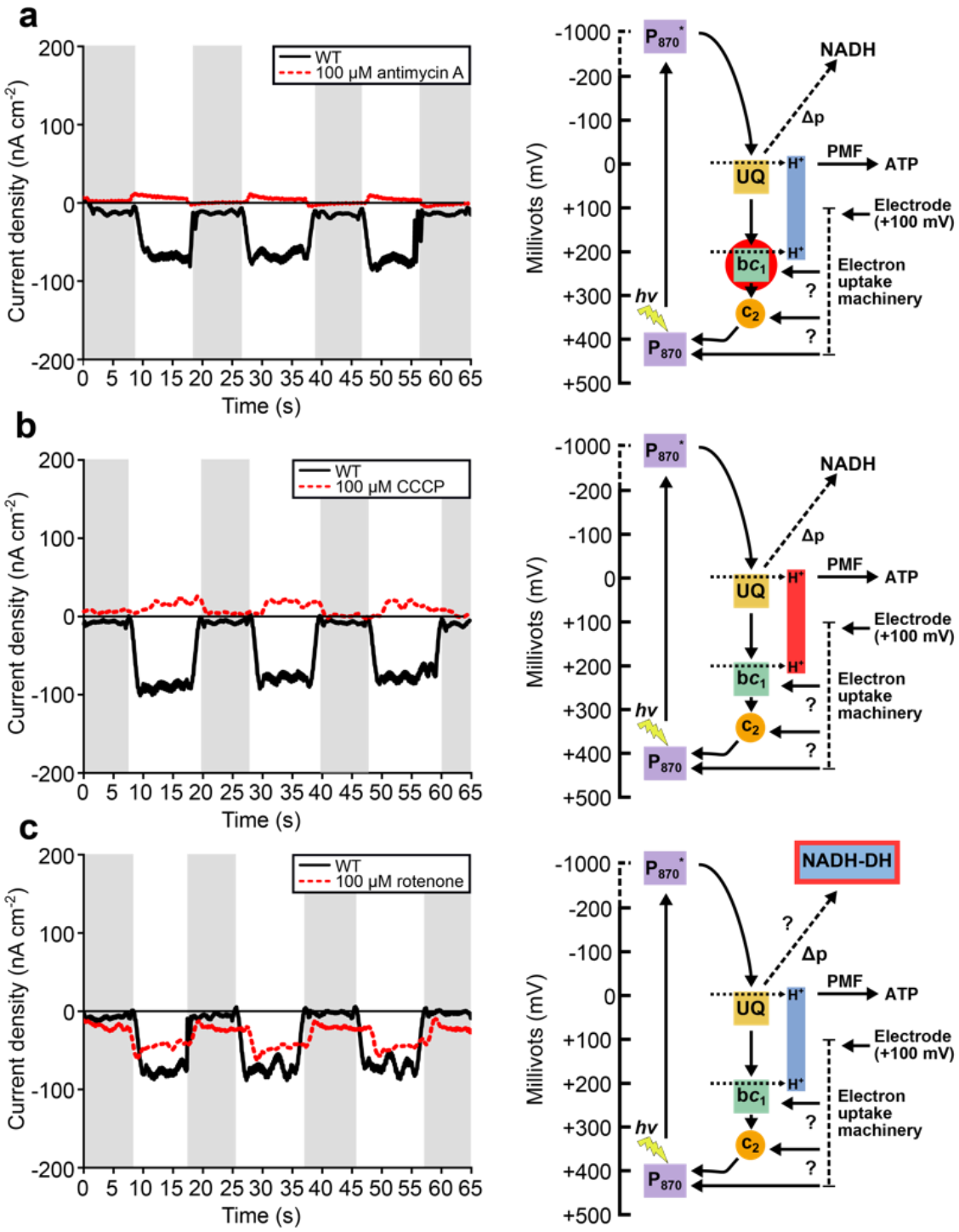

Figure 2.2. Photosynthetic electron transfer is required for extracellular electron uptake. Current densities of TIE-1 wild-type (WT) in response to inhibition of the photosynthetic ETC under illuminated and dark (shaded regions) conditions with (a) antimycin A, (b) carbonyl

cyanide *m*-chlorophenyl hydrazine (CCCP), and (c) rotenone. Data shown are representative of three experiments. Each current density diagram (left) is followed by the proposed path of electron flow (right). The site of chemical inhibition is indicated by a red halo on the electron path diagrams. P_{870} (photosystem), P_{870}* (excited photosystem), UQ (ubiquinone), bc_1 (cytochrome bc_1), c_2 (cytochrome c_2), NADH-DH (NADH dehydrogenase), Δp (proton gradient), H^+ (protons), *hv* (light), ? (currently unknown), PMF (proton motive force) and ATP (adenosine triphosphate). Source data are provided as a Source Data File.

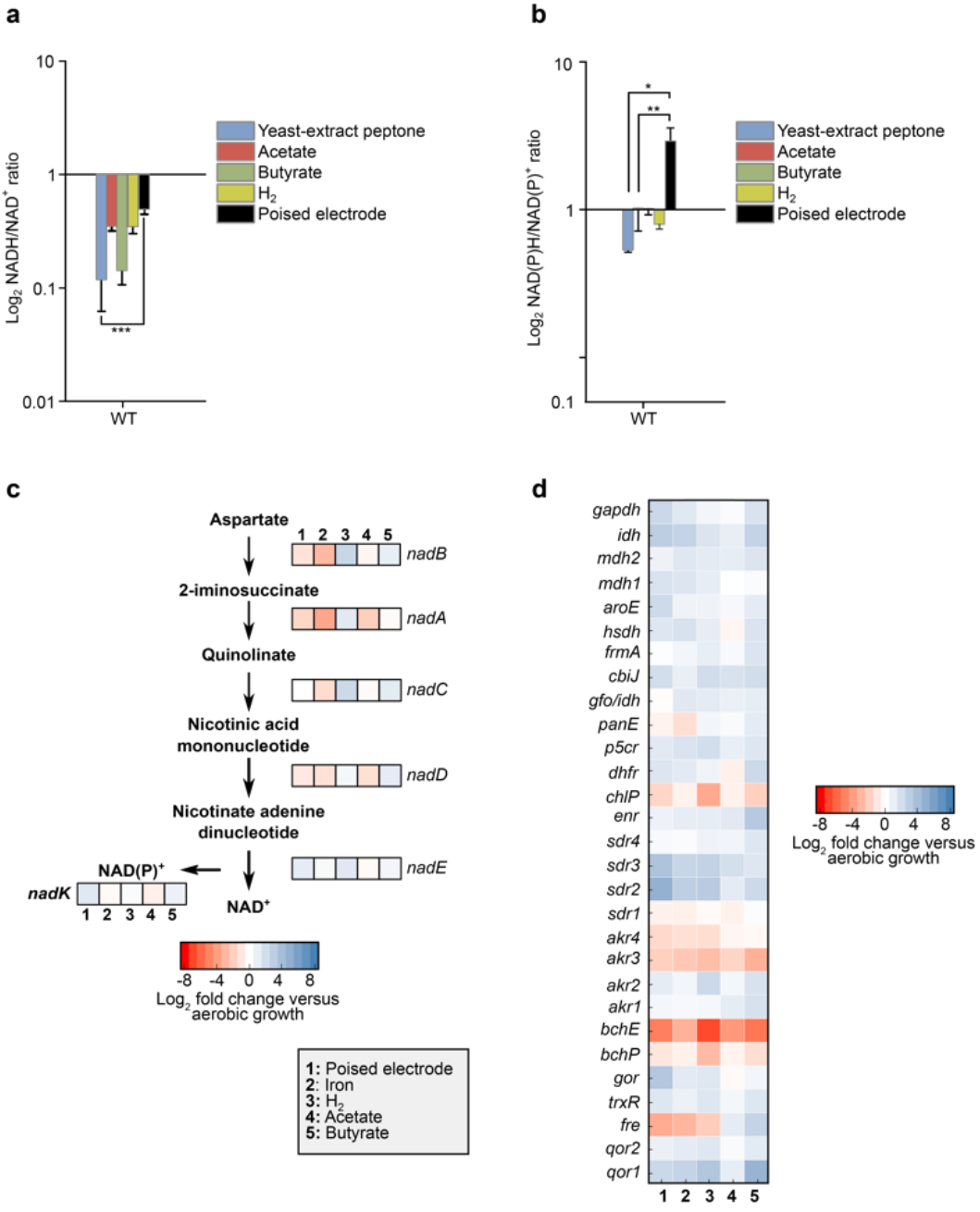

Figure 2.3. Extracellular electron uptake leads to a reducing intracellular redox environment. (a) TIE-1 WT NADH/NAD^+ and (b) NAD(P)H/$NAD(P)^+$ ratios under various growth conditions. Conditions tested: yeast-extract peptone (blue); photoheterotrophy with acetate (red) and butyrate (green); and photoautotrophy with H_2 (yellow) or a poised electrode

(black). Data are means ± s.e.m. of three biological replicates assayed in triplicate. The *P* values were determined by one-way ANOVA followed by a pairwise test with Bonferroni adjustment (*$P < 0.05$, **$P < 0.01$, ***$P < 0.0001$; ns, not significant). (c) Transcriptomic analysis of the *de novo* NAD biosynthesis pathway under various photoautotrophic and photoheterotrophic growth conditions. (d) Genome-wide transcriptomic analysis of NAD(P)$^+$/H-requiring reactions. Source data (and reactions not mentioned in text) are provided as a Source Data File.

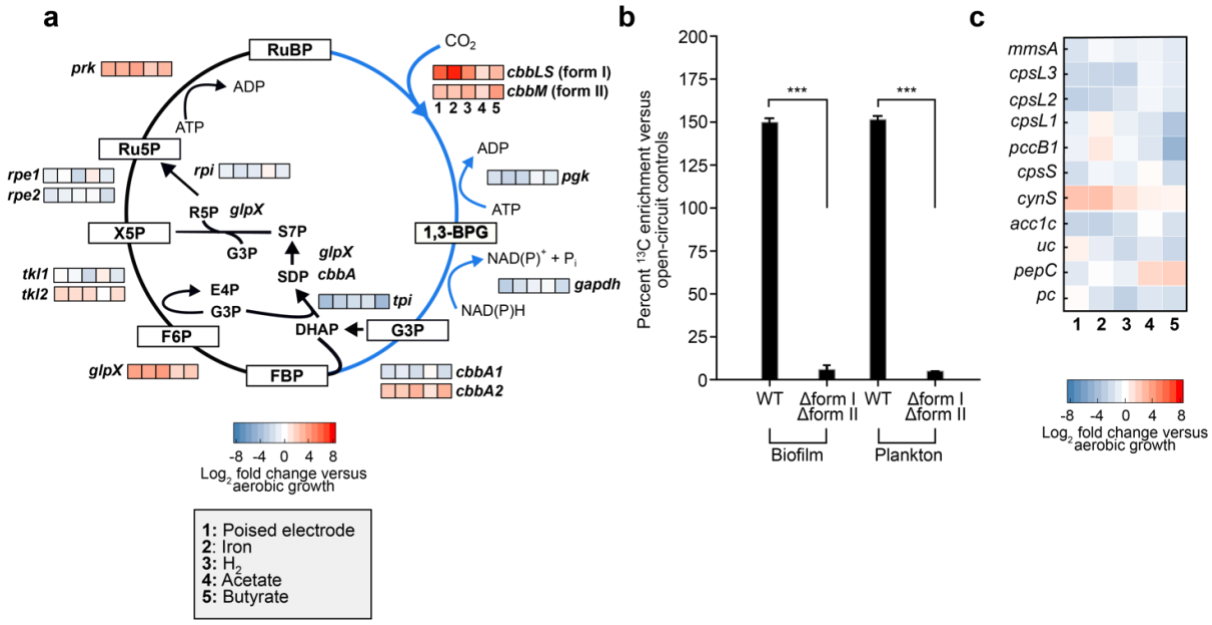

Figure 2.4. Extracellular electron uptake leads to carbon dioxide fixation. (a) Differential expression analysis of genes encoding Calvin-Benson-Bassham (CBB) cycle enzymes in *R. palustris* TIE-1 wild-type (WT) under various photoautotrophic (poised electrodes, iron oxidation, and H_2 oxidation) and photoheterotrophic growth conditions (acetate and butyrate). (b) $^{13}CO_2$ incorporation under cathodic conditions in *R. palustris* TIE-1 WT and the *ruBisCO* double mutant (Δform I Δform II) biofilms and planktonic cells determined by secondary ion mass spectrometry (SIMS). Data are means ± s.e.m. of at least 25 cells. The *P* values were determined by one-way ANOVA followed by a pairwise test with Bonferroni adjustment (*$P < 0.05$, **$P < 0.01$, ***$P < 0.0001$; ns, not significant). (c) Differential expression analysis of CO_2 and HCO_3^- consuming reactions in *R. palustris* TIE-1 WT. RuBP (Ribulose 1,5-bisphosphate), 1,3 BPG (I,3-bisphosphoglycerate), G3P (Glyceraldehyde 3-phosphate), FBP (Fructose 1,6-bisphosphate), F6P (Fructose 6-phosphate), X5P (Xylulose 5-phosphate), Ru5P (Ribulose 5-phosphate) and R5P (Ribose 5-phosphate). Source data (and reactions not mentioned in text) are provided as a Source Data File.

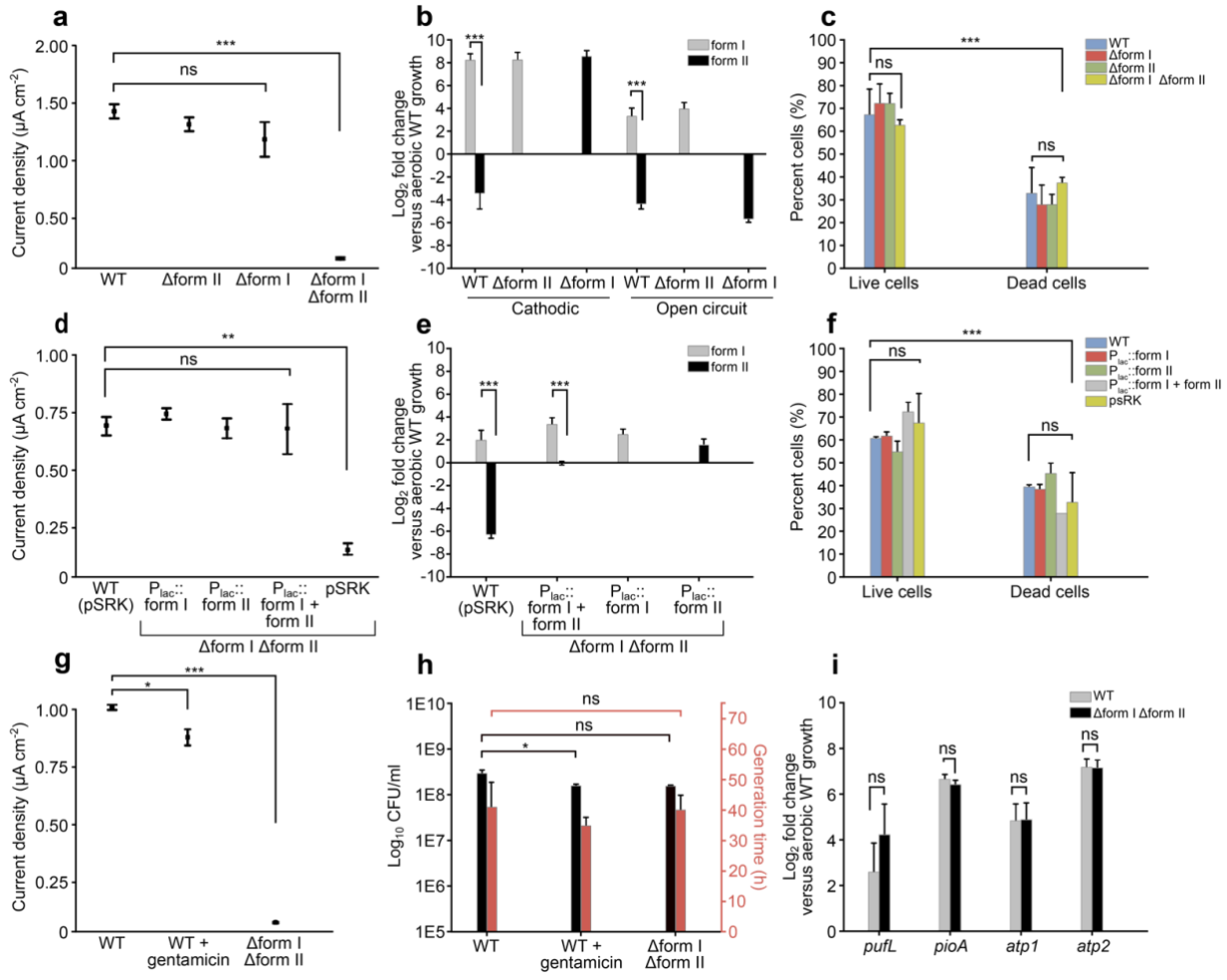

Figure 2.5. RuBisCO is required for extracellular electron uptake. (a) Endpoint current densities for *ruBisCO* deletion mutants compared to *R. palustris* TIE-1 wild-type (WT). Data are means ± s.e.m. of three biological replicates. (b) *ruBisCO* mRNA $\log_2$ fold change under poised current (cathodic) and no current (open-circuit) conditions for TIE-1 WT and *ruBisCO* deletion mutants. (c) LIVE/DEAD® staining of electrode-attached cells under cathodic conditions. Data are means ± s.e.m. of three biological replicates assayed in triplicate. % represents the percent cells in relation to the total number of cells counted. (d) Endpoint current densities for *ruBisCO* complementation mutants. Data are means ± s.e.m. of three biological replicates. (e) *ruBisCO*

mRNA $\log_2$ fold change under cathodic conditions for *R. palustris* TIE-1 WT and *ruBisCO* complementation mutants. (f) LIVE/DEAD® staining of electrode-attached cells under cathodic conditions. Data are means ± s.e.m. of three biological replicates assayed in triplicate. (g) Endpoint current densities under standard conditions (WT) and when treated with gentamicin (WT + gentamicin). Data are means ± s.e.m. of three biological replicates. (h) Log_{10} colony forming units (CFU) and generation time (h) of planktonic cells incubated under standard conditions (WT) and when treated with gentamicin (WT + gentamicin). Data are means ± s.e.m. of at least two biological replicates assayed in triplicate. (i) mRNA $\log_2$ fold change of photosynthetic reaction center (*pufL*), *pio* operon (*pioA*), and ATP synthase homologs (*atp1*, *atp2*) in *R. palustris* TIE-1 WT and the *ruBisCO* double mutant. RT-qPCR data are means ± s.e.m. of two biological replicates assayed in triplicate. The *P* values were determined by one-way ANOVA followed by a pairwise test with Bonferroni adjustment (*$P < 0.05$, **$P < 0.01$, ***$P < 0.0001$; ns, not significant). Source data are provided as a Source Data File.

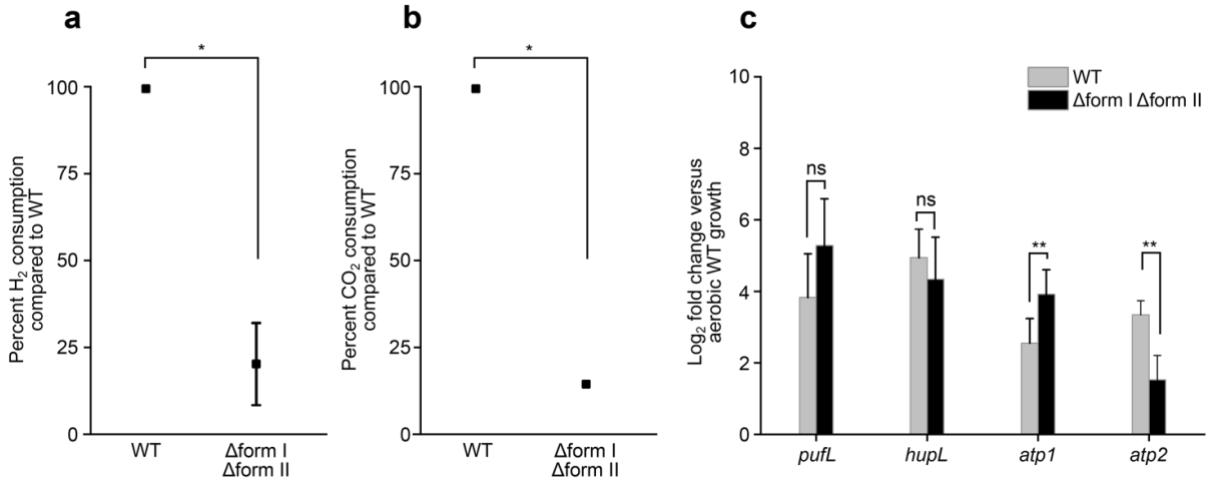

Figure 2.6. RuBisCO is important for phototrophic hydrogen (H_2) oxidation. (a) Hydrogen (H_2) oxidation and (b) carbon dioxide (CO_2) consumption by the *ruBisCO* double mutant (Δform I Δform II) as a percent of consumption by *R. palustris* TIE-1 wild-type (WT). Data are means ± s.e.m. of two biological replicates assayed in triplicate. (c) mRNA $\log_2$ fold change of photosynthetic reaction center (*pufL*), NiFe hydrogenase (*hupL*), and ATP synthase homologs (*atp1*, *atp2*) in WT and the *ruBisCO* double mutant. RT-qPCR data are means ± s.e.m. of two biological replicates assayed in triplicate. The *P* values were determined by one-way ANOVA followed by a pairwise test with Bonferroni adjustment (*$P < 0.05$, **$P < 0.01$, ***$P < 0.0001$; ns, not significant). Source data are provided as a Source Data File.

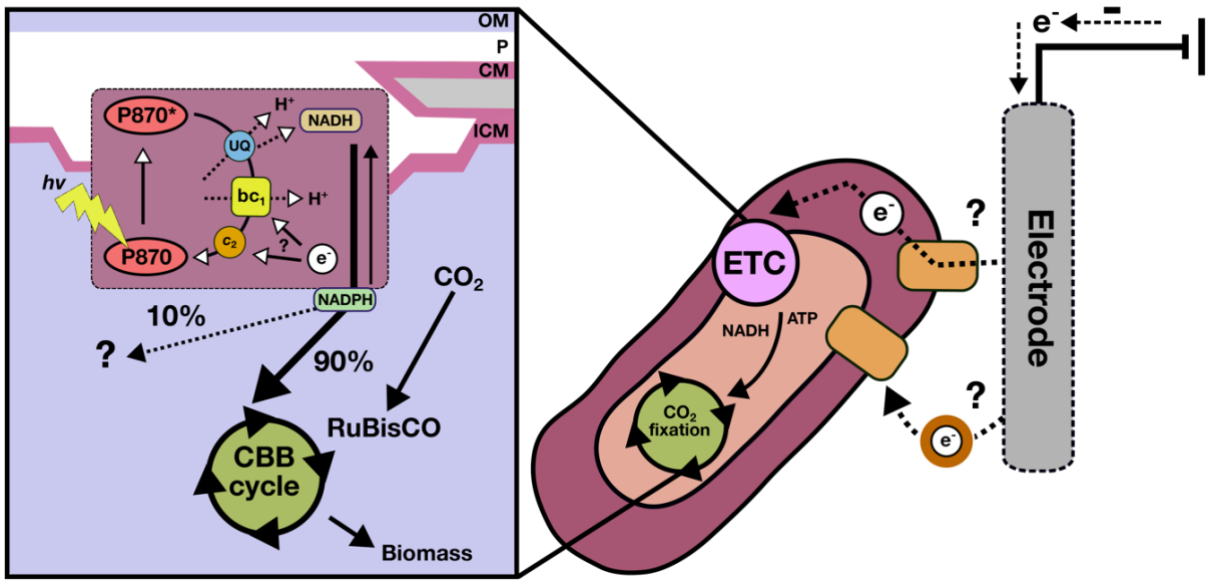

Figure 2.7. Conceptual model of phototrophic extracellular electron uptake. Extracellular electron uptake is connected to the photosynthetic electron transport chain (pETC) and carbon dioxide (CO_2) fixation in *R. palustris* TIE-1. The CBB cycle (Calvin-Benson-Bassham) uses RuBisCO and is the primary sink for electrons that enter the photosystem from poised electrodes. The electrons are used by the CBB cycle as NAD(P)H (reduced nicotinamide adenine dinucleotide phosphate) that is exchanged with NADH (reduced nicotinamide adenine dinucleotide) produced via reverse electron flow. For details please read the text. ATP (adenosine triphosphate), e^- (electrons), P_{870} (photosystem), P_{870}* (excited photosystem), UQ (ubiquinone), *bc*$_1$ (cytochrome *bc*$_1$), c_2 (cytochrome *c*$_2$), H^+ (protons), *hv* (light), ? (currently unknown), OM (outer membrane), P (periplasm), CM (cytoplasmic membrane) and ICM (inner cytoplasmic membrane).

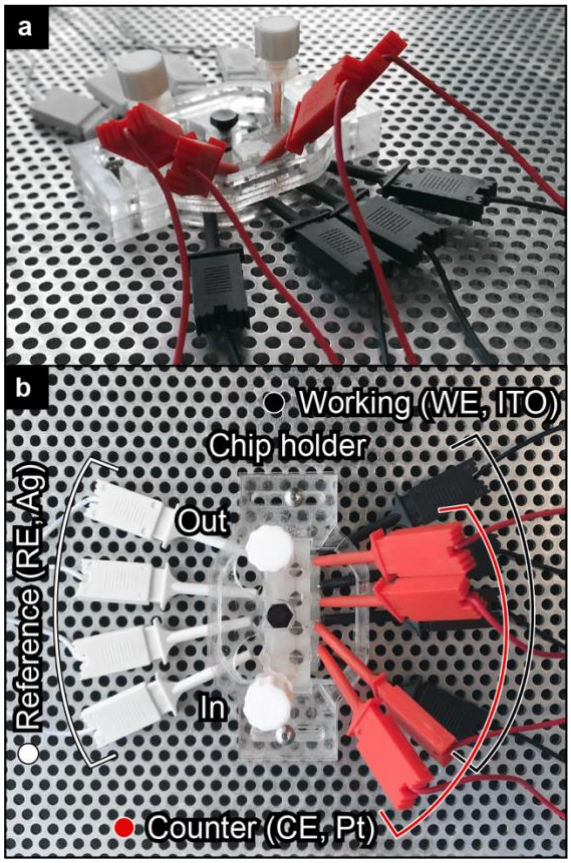

Supplementary Figure 2.1. Micro-bioelectrochemical cell (µ-BEC). (a) Instrument assembly with inlet/outlet capped for incubation. (b) Top-down view of four-chamber µ-BEC configuration shown with reference electrode (RE), counter counter (CE), and working electrode (WE) leads connected to integrated silver (Ag) and platinum (Pt) wires, and indium tin oxide (ITO) coverslips (WE).

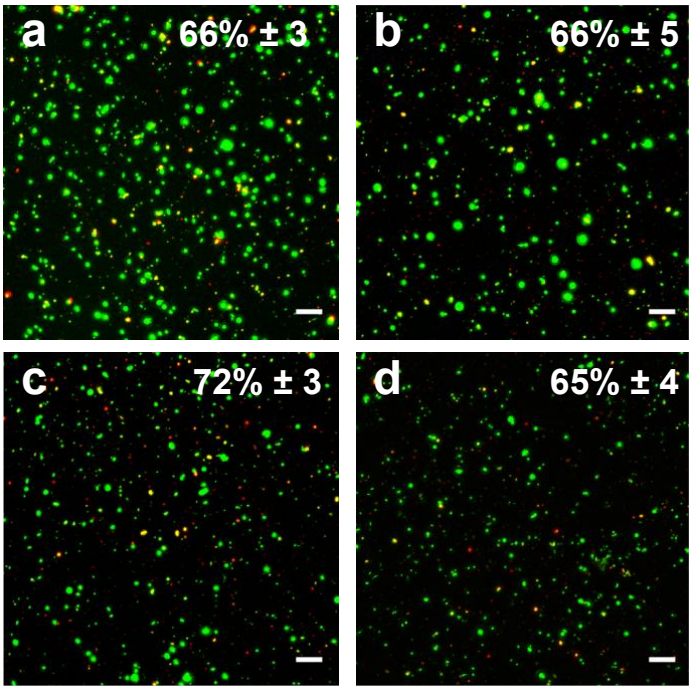

Supplementary Figure 2.2. Fluorescent micrographs of *Rhodopseudomonas palustris* TIE-1 wild-type (WT) biofilms in μ-BEC. Representative confocal micrographs of TIE-1 biofilms attached to the cathode and stained with LIVE/DEAD® dyes. (a) Untreated control, (b) antimycin A, (c) carbonyl cyanide *m*-chlorophenyl hydrazone (CCCP), and (d) rotenone treated cells. Data are the mean percentages of live cells ± s.e.m. of three biological replicates assayed in triplicate. All cells in the field of view were counted. Image manipulation and cell counts were performed in Fiji v1.0 (see Methods). Scale bars are 10 μm. Source data are provided as a Source Data File.

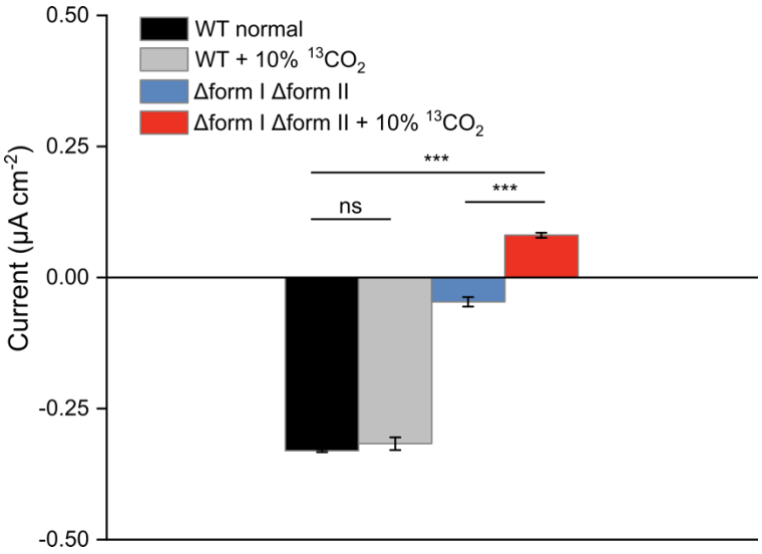

Supplementary Figure 2.3. Average current densities for *R. palustris* TIE-1 cells harvsted for secondary ion mass spectrometry studies. Current uptake for *R. palustris* TIE-1 WT and the *ruBisCO* double mutant (Δform I Δform II) after 60 h incubations in bulk bioelectrochemical cells (BECs) with and without 10% $^{13}CO_2$. Data are means ± s.e.m. of current passed over 60 h with a 10 second interval between measurements (number of measurements per condition, n = 25527). The P values were determined by one-way ANOVA followed by a pairwise test with Bonferroni adjustment (*$P < 0.05$, **$P < 0.01$, ***$P < 0.0001$; ns, not significant). Source data are provided as a Source Data File.

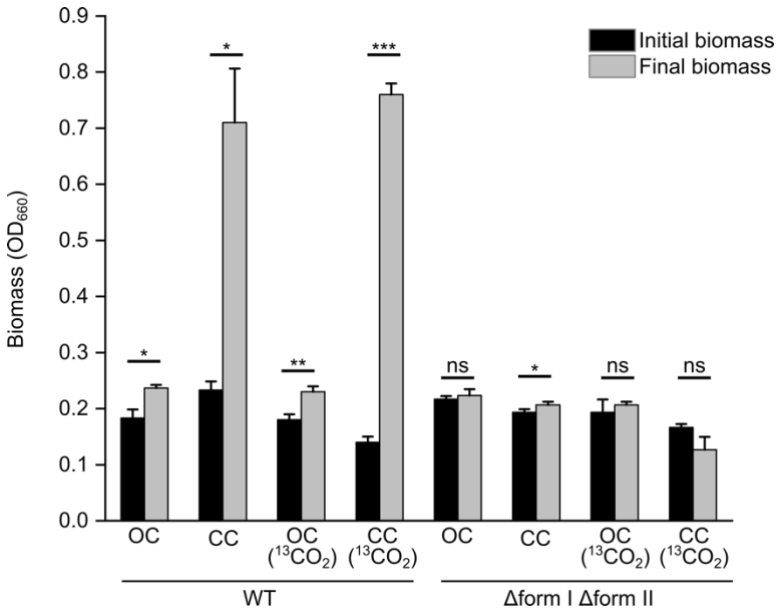

Supplementary Figure 2.4. Planktonic cell growth of *R. palustris* TIE-1 wildtype (WT) and the *ruBisCO* double mutant (Δform I Δform II) harvested for secondary ion mass spectrometry. Initial and final optical density (OD_{660}) in bulk BECs after 60 h incubations under open-circuit (OC, reactor not passing current) and standard closed-circuit (CC, reactors passing current) conditions with and without 10% $^{13}CO_2$. Data are means ± s.e.m. of three technical replicates. The *P* values were determined by one-way ANOVA followed by a pairwise test with Bonferroni adjustment (*$P < 0.05$, **$P < 0.01$, ***$P < 0.0001$; ns, not significant). Source data are provided as a Source Data File.

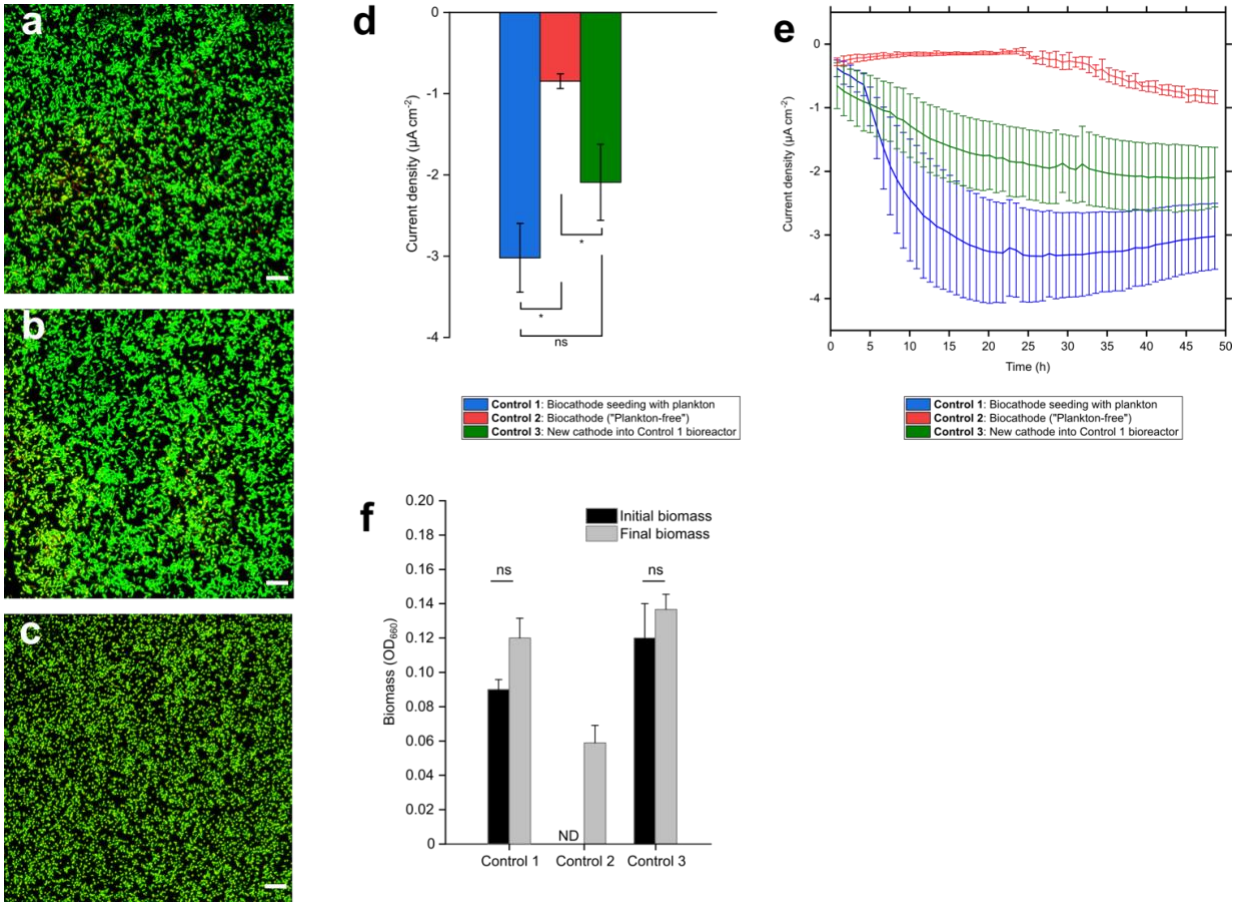

Supplementary Figure 2.5. *R. palustris* TIE-1 wild-type (WT) biocathode seeding in plankton-free bioreactors. Representative confocal micrographs of TIE-1 biofilms attached to cathode and stained with LIVE/DEAD® dyes. (a) "Control 1" biocathode. (b) "Control 2" biocathode. (c) "Control 3" biocathode. Scale bars are 10 μM. "Control 1" bioreactors were seeded with planktonic cells to generate the biocathodes that were then installed into the "Control 2" bioreactors. "Control 2" bioreactors are plankton-free and contain only biocathodes (with fresh media). "Control 3" bioreactors are the initial "Control 1" bioreactors replaced with new, cell-free cathodes (media was not replaced). (d) Mean current densities after 48-hour incubations. (e) Mean current density over time. (f) Initial and final optical density (OD_{660}) of bioreactors. Data are means ± s.e.m. of three biological replicates. The *P* values were determined

by one-way ANOVA followed by a pairwise test with Bonferroni adjustment (*$P < 0.05$, **$P < 0.01$, ***$P < 0.0001$; ns, not significant). ND (not detectable). Source data are provided as a Source Data File.

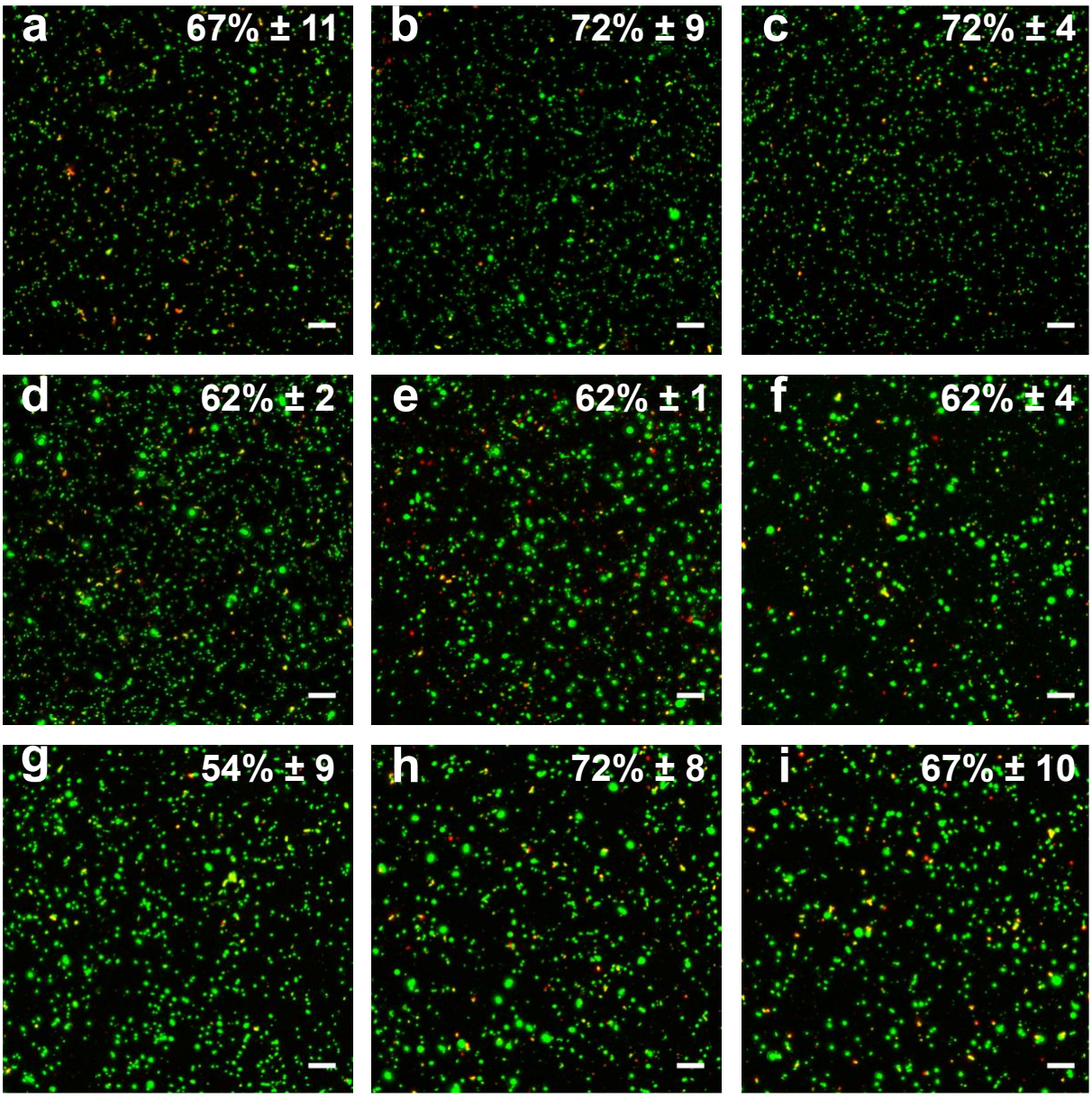

Supplementary Figure 2.6. Confocal micrographs of *R. palustris* TIE-1 wild-type (WT) and *ruBisCO* deletion and complementation mutant biofilms. Representative images of biofilms attached to cathode in bulk BECs and stained with LIVE/DEAD® dyes: (a) WT, (b) Δform I, (c) Δform II, (d) Δform I Δform II, (e) WT (pSRK), (f) Δform I Δform II (P_{lac}::form I), (g) Δform I Δform II (P_{lac}::form II), (h) Δform I Δform II (P_{lac}::form I + form II), (i) Δform I Δform II

(pSRK). Data are the mean percentages of live cells ± s.e.m. of three biological replicates assayed in triplicate. All cells in the field of view were counted. Image manipulation and cell counts were performed in Fiji v1.0 (see Methods). Scale bars are 10 μm. Source data are provided as a Source Data File.

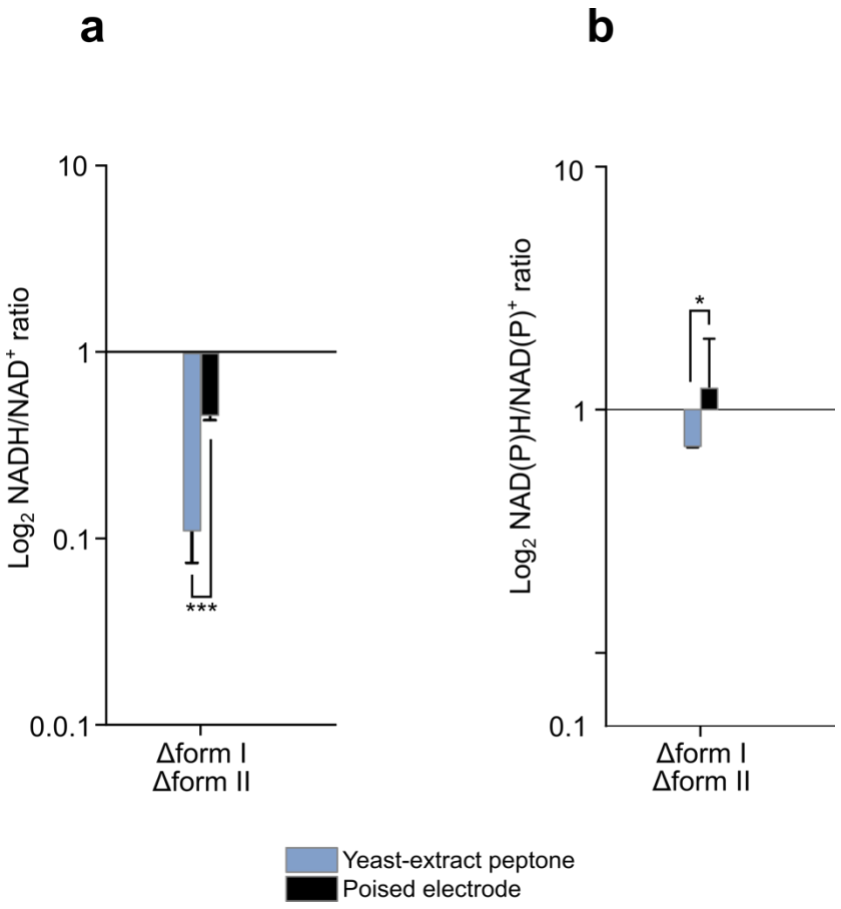

Supplementary Figure 2.7. NADH/NAD$^+$ and NAD(P)H/NAD(P)$^+$ ratios from *R. palustris* TIE-1 *ruBisCO* double mutant (Δform I Δform II). (a) Log_2 NADH/NAD$^+$ and (b) NAD(P)H/NAD(P)$^+$ ratios for *ruBisCO* double mutant cells. Data are means ± s.e.m. of three biological replicates assayed in triplicate. The *P* values were determined by one-way ANOVA followed by a pairwise test with Bonferroni adjustment (*$P < 0.05$, **$P < 0.01$, *** $P < 0.0001$; ns, not significant). Source data are provided as a Source Data File.

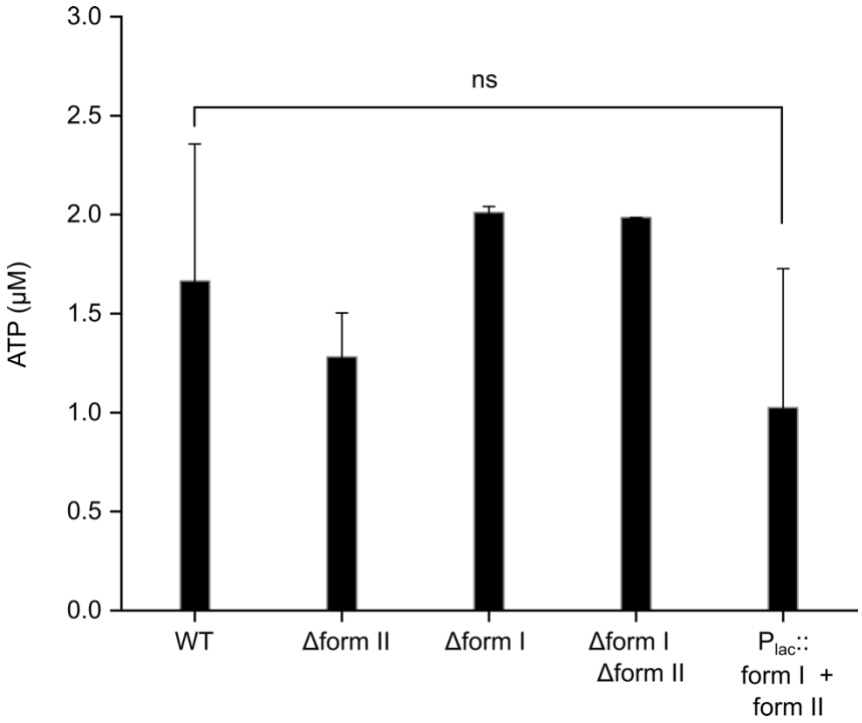

Supplementary Figure 2.8. ATP quantitation from planktonic *R. palustris* TIE-1 wild-type (WT) and *ruBisCO* deletion and complementation. ATP levels from TIE-1 cells after 60 h incubations in bulk BECs. Data are means ± s.e.m. of at least two biological replicates assayed in triplicate. The *P* values were determined by one-way ANOVA followed by a pairwise test with Bonferroni adjustment (*$P < 0.05$, **$P < 0.01$, ***$P < 0.0001$; ns, not significant). Source data are provided as a Source Data File.

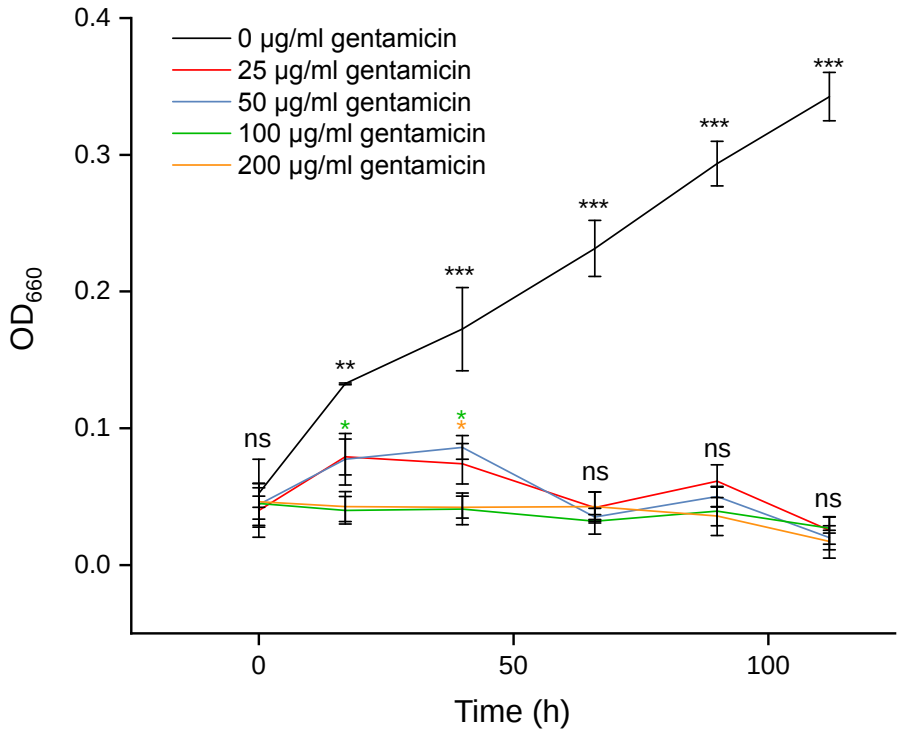

Supplementary Figure 2.9. Minimum inhibitory concentration (MIC) determination for photoautotrophically-grown *R. palustris* TIE-1 wild-type (WT). Optical density (OD_{660}) during photoautotrophic growth on 80% hydrogen:20% carbon dioxide (H_2:CO_2) with increasing concentrations of gentamicin. Data are means ± s.d. of at least two biological replicates assayed in triplicate. The *P* values were determined by one-way ANOVA followed by a pairwise test with Bonferroni adjustment (*$P < 0.05$, **$P < 0.01$, ***$P < 0.0001$; ns, not significant). Source data are provided as a Source Data File.

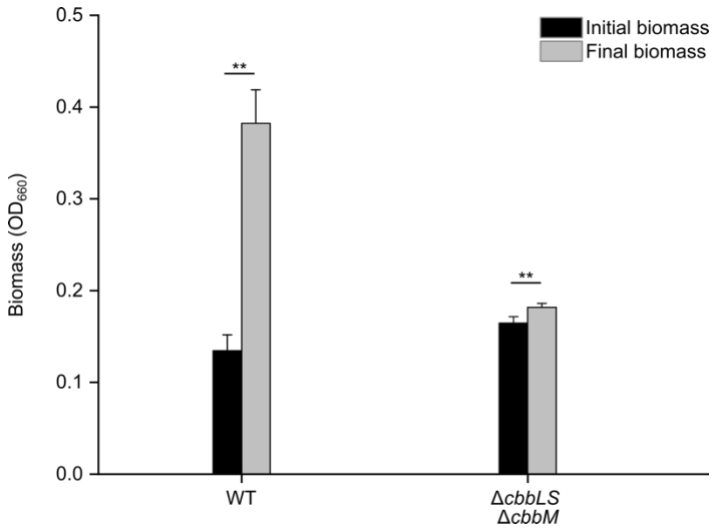

Supplementary Figure 2.10. Planktonic cell growth of *R. palustris* TIE-1 wild-type (WT) and *ruBisCO* double mutant (Δform I Δform II) during photoautotrophic growth on H_2:CO_2. Initial and final optical density (OD_{660}) from cells used for quantification of H_2 and CO_2 consumption. Data are means ± s.e.m. of three biological replicates assayed in triplicate. The *P* values were determined by one-way ANOVA followed by a pairwise test with Bonferroni adjustment (*$P < 0.05$, **$P < 0.01$, ***$P < 0.0001$; ns, not significant). Source data are provided as a Source Data File.

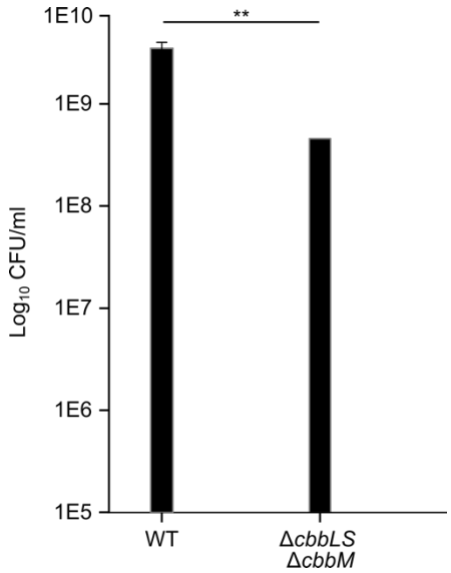

Supplementary Figure 2.11. Log_{10} colony forming units (CFU) per mL during photoautotrophic growth with H_2. Log_{10} colony forming units of TIE-1 wild-type (WT) and *ruBisCO* double mutant planktonic cells. Cells were plated aerobically onto rich media at the end of incubations that typically lasted 60 hours. Data are means ± s.e.m. of three biological replicates. The *P* values were determined by one-way ANOVA followed by a pairwise test with Bonferroni adjustment (*$P < 0.05$, **$P < 0.01$, ***$P < 0.0001$; ns, not significant). Source data are provided as a Source Data File.

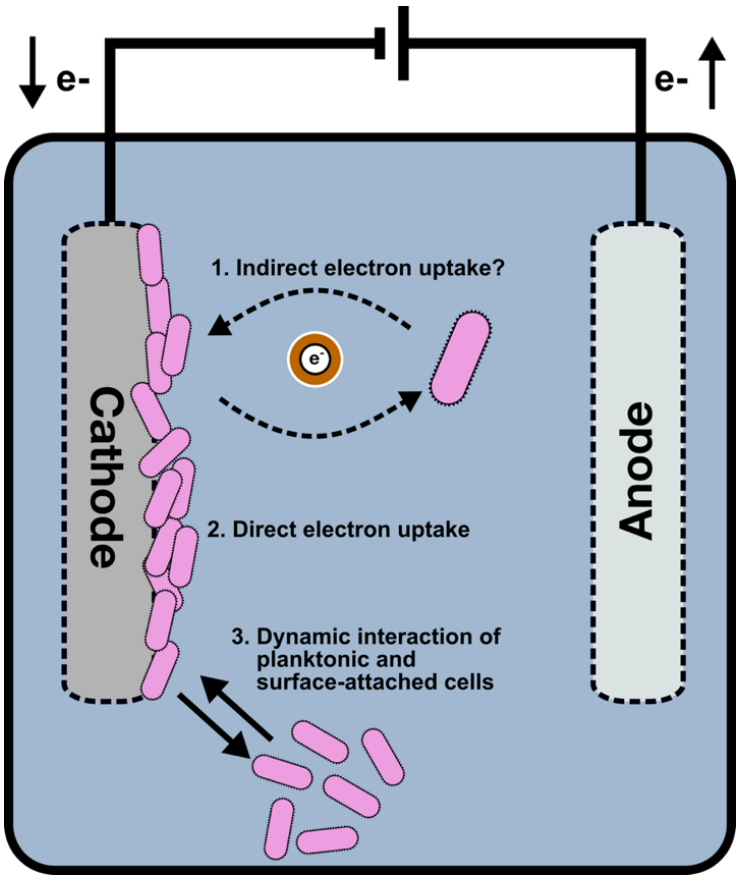

Supplementary Figure 2.12. Potential mechanisms involved in extracellular electron uptake (EEU) from a poised electrode by planktonic cells. (1) Indirect electron uptake via a soluble redox active compound; (2) Direct electron uptake; (3) Dynamic interaction of planktonic and surface-attached cells.

Supplementary Table 2.1. Average maximum current density under light and dark conditions with antimycin A treatment in µ-BECs for *R. palustris* TIE-1 wild-type (WT). Data are means ± s.e.m. of three biological replicates. The *P* values were determined by pairwise *t*-test. *P*-values across rows are for comparisons between light and dark treatments. *P*-values in columns are for comparisons between untreated and treated reactors. Source data are provided as a Source Data File.

	Maximum current density (nA cm^{-2})			**Coulombs (C)**		
	Light	Dark	*P* (Light vs. Dark)	Light	Dark	*P* (Light vs. Dark)
Untreated control	-85.5 ± 21.7	-9.70 ± 3.59	*P*<0.0001	-121 ± 6.12	-23.5 ± 1.14	*P*<0.0001
100 µM antimycin A	12.5 ± 1.34	-3.46 ± 1.80	*P*<0.0001	4.74 ± 3.34	-2.02 ± 1.14	*P*<0.0001
P (untreated vs. 100 µM antimycin A)	*P*<0.0001	*P*=0.0006		*P*<0.0001	*P*<0.0001	

Supplementary Table 2.2. Average maximum current density under light and dark conditions with carbonyl cyanide *m*-chlorophenyl hydrazine (CCCP) treatment in µ-BECs for *R. palustris* TIE-1 wild-type (WT). Data are means ± s.e.m. of three biological replicates. The *P* values were determined by pairwise *t*-test. *P*-values across rows are for comparisons between light and dark treatments. *P*-values in columns are for comparisons between untreated and treated reactors. Source data are provided as a Source Data File.

	Maximum current density (nA cm^{-2})			**Coulombs (C)**		
	Light	Dark	*P* (Light vs. Dark)	Light	Dark	*P* (Light vs. Dark)
Untreated control	-114 ± 21.7	-17.5 ± 3.41	*P*<0.0001	-119 ± 3.22	-9.65 ± 1.03	*P*<0.0001
25 µM CCCP	21.2 ± 9.13	-18.4 ± 14.01	*P*<0.0001	6.73 ± 4.31	-7.84 ± 2.44	*P*<0.0001
100 µM CCCP	19.3 ± 5.46	-12.9 ± 6.40	*P*<0.0001	18.3 ± 3.74	0.740 ± 5.21	*P*<0.0001
P (untreated vs. 25 µM CCCP)	*P*<0.0001	*P*=0.8666		*P*<0.0001	*P*=0.0025	
P (untreated vs. 100 µM CCCP)	*P*<0.0001	*P*=0.0906		*P*<0.0001	*P*<0.0001	

Supplementary Table 2.3. Average maximum current density under light and dark conditions with rotenone treatment in µ-BECs for *R. palustris* TIE-1 wild-type (WT). Data are means ± s.e.m. of three biological replicates. The *P* values were determined by pairwise *t*-test. *P*-values across rows are for comparisons between light and dark treatments. *P*-values in columns are for comparisons between untreated and treated reactors. Source data are provided as a Source Data File.

	Maximum current density (nA cm^{-2})			**Coulombs (C)**		
	Light	Dark	*P* (Light vs. Dark)	Light	Dark	*P* (Light vs. Dark)
Untreated control	-94.7 ± 3.61	-12.0 ± 4.02	*P*<0.0001	-120 ± 3.73	-16.7 ± 3.73	*P*<0.0001
25 µM rotenone	-71.8 ± 2.02	-25.2 ± 1.60	*P*<0.0001	-73.5 ± 2.32	-38.9 ± 3.07	*P*<0.0001
50 µM rotenone	-60.3 ± 1.81	-19.5 ± 4.94	*P*<0.0001	-64.6 ± 5.67	-34.3 ± 3.42	*P*<0.0001
100 µM rotenone	-41.6 ± 4.55	-25.2 ± 0.820	*P*<0.0001	-60.7 ± 1.88	-26.7 ± 2.41	*P*<0.0001
P (untreated vs. 25 µM rotenone)	*P*<0.0001	*P*<0.0001		*P*<0.0001	*P*<0.0001	
P (untreated vs. 50 µM rotenone)	*P*<0.0001	*P*=0.0050		*P*<0.0001	*P*<0.0001	
P (untreated vs. 100 µM rotenone)	*P*<0.0001	*P*<0.0001		*P*<0.0001	*P*<0.0001	

Supplementary Table 2.4. Strains and plasmids used in this study.

Strain or plasmid	Genotype and use	Source
***E. coli* strains**		
WM6026	[*lacI*^{q} *rrnB3* Δ*lacZ*4787 *hsdR514*Δ*araBAD567* Δ*rhaBAD5 68 rph-1 att*l::pAE12(Δ*ori*R6K-*cat*::Frt5) Δ*endA*::Frt *uidA*(ΔMluI)::*pir att*HK::pJK1006Δ(*ori*R6K-*cat*::Frt5;*trfA*::Frt)]. Donor strain for conjugation.	W. Metcalf, University of Illinois, Urbana-Champaign
DH10B	F^{-} *endA1 recA1 galE15 galK16 nupG rpsL ΔlacX74* Φ80*lacZΔM15 araD139 Δ(ara,leu)7697 mcrA Δ(mrr-hsdRMS-mcrBC)* λ$^{□}$. Used as standard cloning strain.	Casadaban, M. J. & Cohen, S. N. Analysis of gene control signals by DNA fusion and cloning in *Escherichia coli*. *J. Mol. Biol.* **138**, 179-207 (1980).
***R. palustris* strains**		
TIE-1	Wild-type (WT). Isolated from Woods Hole, MA.	Jiao, Y., Kappler, A., Croal, L. R. & Newman, D. K. Isolation and characterization of a genetically tractable photoautotrophic Fe(II)-oxidizing bacterium, *Rhodopseudomonas palustris* strain TIE-1. *Appl. Environ. Microbiol.* **71**, 4487-4496 (2005).
AB135	Δ*cbbLS* Δ*cbbM* (Rpal_1747- Rpal_1748, Rpal_5122)	This study
AB136	Δ*cbbLS* (Rpal_1747)	This study
AB143	Δ*cbbM* (Rpal_5122)	This study
AB114	WT TIE-1 with pSRKGm	This study
AB142	AB135 with pSRKGm	This study
AB138	AB135 complemented with pAB721	This study
AB139	AB135 complemented with pAB709	This study
AB140	AB135 complemented with pAB720	This study
Plasmids		
pAB709	pSRKGm with Rpal_1747-1748 (*cbbLS*) cloned into *Nde*I and *Spe*I sites using primers cbbL-For/cbbLS-Rev.	This study
pAB720	pSRKGm with Rpal_5122 (*cbbM*) cloned into *Spe*I and *Sma*I sites using primers pSRKGm-CbbM-For4-AclI-NdeI/pSRKGm-CbbM-Rev3-AclI-SmaI.	This study
pAB721	pSRKGm with Rpal_1747-1748 (*cbbLS*) and Rpal_5122 (*cbbM*). pAB720 insert was digested and cloned into the *Spe*I and *Sma*I sites of pAB709.	This study
pSRKGm	Complementation plasmid modified from pBBR1MCS-5; Gm^{R}.	Khan, S. R., Gaines, J., Roop, R. M. & Farrand, S. K. Broad-host-range expression vectors with tightly regulated promoters and their use to examine the influence of TraR and

		TraM expression on Ti plasmid quorum sensing. *Appl. Environ. Microbiol.* **74**, 5053-5062 (2008).
pJQ200KS	*sacB*, Gm^R. Suicide vector.	Quandt, J. & Hynes, M. F. Versatile suicide vectors which allow direct selection for gene replacement in gram-negative bacteria. *Gene* **127**, 15-21 (1993).
pAB621	1 kilobase (kb) upstream and 1 kb downstream of the WT *Rhodospeudmonas* palustris TIE-1 *cbbLS* gene cloned into the *Not*I and *Bam*HI sites of pJQ200KS using primers Rpal_1747_upfor/Rpal_1747_uprev (upstream of *cbbL*) and Rpal_1748_dnfor/ Rpal_1747_dnrev (downstream of *cbbS*).	This study
pAB622	1 kilobase (kb) upstream and 1 kb downstream of the WT *Rhodospeudmonas* palustris TIE-1 *cbbM* gene cloned into the *Not*I and *Bam*HI sites of pJQ200KS using primers Rpal_5122upforNotI/Rpal_5122uprev (upstream of *cbbM*) and Rpal_5122dnfor/ Rpal_5122dnrev (downstream of *cbbM*).	This study

Supplementary Table 2.5. Doubling time (hours) for aerobic chemoheterotrophic, photoheterotrophic (with butyrate and acetate), and photoautotrophic growth by *R. palustris* TIE-1 wild-type (WT) and *ruBisCO* deletion mutants. Data are means ± s.d. of three biological replicates. Source data are provided as a Source Data File.

Growth condition	WT	Δform I	Δform II	Δform I Δform II
Yeast-extract peptone	3.1 ± 0.11	3.6 ± 0.17	4.6 ± 0.95	3.2 ± 0.26
Acetate	5.7 ± 1.1	13 ± 1.4	8.8 ± 1.5	23 ± 0.7
Butyrate	4.6 ± 0.17	4.9 ± 0.29	4.9 ± 0.84	30 ± 2.5
Phototrophic H_2 oxidation	4.3 ± 0.02	4.3 ± 0.01	8.7 ± 0.05	No growth

Supplementary Table 2.6. Average delta $^{13}C/^{12}C$ ratio values for *R. palustris* TIE-1 wild-type (WT). Data are means ± s.e.m. of at least 25 cells. "Non-poised" refers to open-circuit conditions. "Plankton" are free-living cells sampled from the bioreactors, whereas "electrode" refers to biofilms attached to the cathode (i.e. surface-attached cells). Source data are provided as a Source Data File.

	Condition	**Current**	**$^{13}CO_2$**	**Delta $^{13}C/^{12}C$**
1	Control 1 (electrode non-poised)	No	No	0.20 ± 0.19
2	Control 2 (electrode poised)	Yes	No	-0.29 ± 0.21
3	Control 3 (electrode non-poised)	No	Yes	14.4 ± 2.67
4	Test condition 1 (electrode poised)	Yes	Yes	150 ± 2.81
5	Control 4 (plankton non-poised)	No	No	1.55 ± 1.21
6	Control 5 (plankton poised)	Yes	No	3.01 ± 1.95
7	Control 6 (plankton non-poised)	No	Yes	46.4 ± 3.22
8	Test condition 2 (plankton poised)	Yes	Yes	151 ± 2.72

Supplementary Table 2.7. Average delta $^{13}C/^{12}C$ ratio values for *R. palustris* TIE-1 *ruBisCO* double mutant (Δform I Δform II). Data are means ± s.e.m. of at least 25 cells. "Non-poised" refers to open-circuit conditions. "Plankton" are free-living cells sampled from the bioreactors, whereas "electrode" refers to biofilms attached to the cathode (i.e. surface-attached cells). Source data are provided as a Source Data File.

	Condition	**Current**	**$^{13}CO_2$**	**Delta $^{13}C/^{12}C$**
1	Control 1 (electrode non-poised)	No	No	ND
2	Control 2 (electrode poised)	Yes	No	0.00 ± 0.630
3	Control 3 (electrode non-poised)	No	Yes	ND
4	Test condition 1 (electrode poised)	Yes	Yes	5.91 ± 2.80
5	Control 4 (plankton non-poised)	No	No	-1.57 ± 0.220
6	Control 5 (plankton poised)	Yes	No	-1.40 ± 0.240
7	Control 6 (plankton non-poised)	No	Yes	18.6 ± 0.420
8	Test condition 2 (plankton poised)	Yes	Yes	4.93 ± 0.430

Supplementary Table 2.8. *Atp1* series gene expression reported as log_2 fold-change.

Locus	**Annotation**	**Acetate**	*P*-value	**Butyrate**	*P*-value	**H_2**	*P*-value	***Iron**	*P*-value	**Poised electrode**	*P*-value
Rpal_0170	ATP synthase F1, epsilon	-1.37	0.387	0.900	0.957	2.87	0.094	3.86	0.009	3.59	0.003
Rpal_0171	ATP synthase F1, beta	-0.317	0.901	0.156	0.560	2.04	0.340	3.29	0.068	3.71	0.008
Rpal_0172	ATP synthase F1, gamma	-0.536	0.812	-2.06	0.481	2.49	0.249	3.86	0.027	3.19	0.011
Rpal_0173	ATP synthase F1, alpha	-0.820	0.633	2.49	0.220	2.68	0.126	-3.42	0.024	-3.89	0.001
Rpal_0174	ATP synthase F1, delta	0.020	0.993	4.01	0.009	0.873	0.846	2.75	0.095	-2.99	0.011
Rpal_0914	ATP synthase F0, A	-0.207	0.940	2.42	0.332	1.98	0.408	3.53	0.044	-4.10	0.005
Rpal_0911	H^+-transporting two-sector	-0.935	0.647	1.36	0.787	3.40	0.069	-4.40	0.010	5.06	0.001
Rpal_0913	H^+-transporting two-sector	-0.415	0.857	1.14	0.872	2.62	0.200	4.19	0.011	3.85	0.009
	Average fold change	**0.572**		**1.78**		**2.37**		**-3.66**		**3.80**	

All log_2 fold-change values are from a comparison of the conditions listed to aerobic chemoheterotrophic growth on yeast-extract peptone (see methods for further details).

Acetate = Photoheterotrophic growth using acetate

Butyrate = Photoheterotrophic growth using butyrate

Hydrogen = Photoautotrophic hydrogen oxidation

Iron = Photoautotrophic iron oxidation

Poised electrode = Extracellular electron uptake

* = Growth condition for which values are from n = 2 biological replicates, otherwise n = 3

P-values were determined in DESEQ2 (see Methods)

Reactions were determined from KEGG (https://www.kegg.jp) pathway analysis of the analyzed genes

Supplementary Table 2.9. *Atp2* series gene expression reported as log_2 fold-change.

Locus	Annotation	Acetate	*P*-value	Butyrate	*P*-value	H_2	*P*-value	*Iron	*P*-value	Poised electrode	*P*-value
Rpal_1049	H^+-transporting two-sector	-0.320	0.637	-1.02	0.787	-1.26	0.224	-0.648	0.379	1.60	0.734
Rpal_1050	ATP synthase F1, alpha	-0.872	0.209	-1.33	0.507	-1.80	0.048	-0.823	0.363	0.916	0.646
Rpal_1051	H^+-transporting two-sector	-1.06	0.284	-0.963	0.916	-1.77	0.196	-0.488	0.835	1.87	0.238
Rpal_1052	ATP synthase F0, C subunit	-0.488	0.771	-0.425	0.792	-1.34	0.564	-0.592	0.832	1.39	0.236
Rpal_1053	ATP synthase F0, A subunit	0.470	0.755	-1.21	0.793	-1.29	0.570	0.162	0.882	0.791	0.157
Rpal_1055	F0F1-ATPase subunit	0.579	0.828	-0.231	0.801	-0.317	0.924	0.908	0.715	4.71	0.001
Rpal_1056	alternate F1F0 ATPase, F1	1.13	0.241	0.854	0.050	-0.357	0.868	1.33	0.189	2.18	0.003
Rpal_1057	ATP synthase F1, beta	1.10	0.641	-0.968	0.954	-0.507	0.989	1.53	0.517	4.52	0.006
	Average fold change	**0.069**		**-0.662**		**-1.08**		**0.172**		**2.25**	

All log_2 fold-change values are from a comparison of the conditions listed to aerobic chemoheterotrophic growth on yeast-extract peptone (see methods for further details).

Acetate = Photoheterotrophic growth using acetate

Butyrate = Photoheterotrophic growth using butyrate

Hydrogen = Photoautotrophic hydrogen oxidation

Iron = Photoautotrophic iron oxidation

Poised electrode = Extracellular electron uptake

* = Growth condition for which values are from n = 2 biological replicates, otherwise n = 3

P-values were determined in DESEQ2 (see Methods)

Reactions were determined from KEGG (https://www.kegg.jp) pathway analysis of the analyzed genes

Supplementary Table 2.10. Gas chromatography barrier ionization discharge (GC-BID) quantification of H_2 and CO_2 consumption. GC-BID analysis of TIE-1 wild-type (WT) and *ruBisCO* double mutant cells during photoautotrophic growth on H_2. Data are means ± s.e.m. of three biological replicates. Source data are provided as a Source Data File.

Strain	**H_2 (µM)**	**CO_2 (µM)**
WT	3957 ± 211.3	5395.5 ± 594.0
Δform I Δform II	717.0 ± 418.0	774.2 ± 8.90

Supplementary Table 2.11. Primers used in this study for plasmid construction.

Primer	Sequence
Plasmid construction	
Rpal_1747_upfor	CATATGGCGGCCGCCGCAGGTCCATTGCAGTCGT
Rpal_1747_uprev	CATATGGGATCCGTCGTCCTCCTTGAAAGCCCTGGC
Rpal_1748_dnfor	CATATGGGATCCTACGGAGGCTGATCGTGGAC
Rpal_1748_dnrev	CATATGCTGCAGGACCAAGACGAGCATCAGCGT
Rpal_5122dnfor	CATATGACTAGTTAAGCTGGCCTAGTCGACACG
Rpal_5122dnrev	CATATGGGATCCAGTGCACCGAGACCCGACAG
Rpal_5122uprev	CATATGACTAGTGGTGATCTCCTGCAATGCGAG
Rpal_5122upforNotI	CATATGGCGGCCGCGACATCATGCTGGCGAAGATGAT
cbbL-For	CATATGAACGAAGCAGTCACCAT
cbbLS-Rev	ACTAGTTCAGCCTCCGTAGC
pSRKGm-CbbM-For4-AclI-NdeI	AACGTTCATATGGACCAGTCGAACCGCTACG
pSRKGm-CbbM-Rev3-AclI-SmaI	CCCGGGTTACGCCGCCTGCG
Plasmid Sanger sequencing	
pSRKGM-For1-seq	TATGCTTCCGGCTCGTATGT
pSRKGM-CbbL-Rev1-Seq	GAACTTGTCCATGCGCTCGC
cbbLS-Rev1-seq	TGCAGCAGCTGATGCATCTG
Rpal_5122-PCR-screen_F	CAAAGAGAGCGAGCTGATCG
Rpal_5122 P6 Knockout Rev	TGATTACCGAGGACGCTGCTG

Supplementary Table 2.12. Primers used in this study for RT-qPCR.

Gene name (locus tag)	Primer name	Sequence
ruBisCO form I (Rpal_1747)	Rpal_1747qPCR_for	ACCAAGGACGACGAGAACAT
ruBisCO form I (Rpal_1747)	Rpal_1747qPCR_rev	CATGCAGTATTGGAAGCGCT
ruBisCO form II (Rpal_5122)	Rpal_5122qPCR_for	GGCGTATCTCAAGCTGTTCG
ruBisCO form II (Rpal_5122)	Rpal_5122qPCR_rev	CGATGAAGCCACCGTTGATC
clpX (Rpal_3308)	TIE-1clpXqRT-PCRFor	GGAGATCTGCAAGGTTCTCG
clpX (Rpal_3308)	TIE-1clpXqRT-PCRRev	CCGCTTGTAGTGATTGTGGA
recA (Rpal_4376)	TIE-1recAqRT-PCRFor	ATCGGCCAGATCAAGGAAC
recA (Rpal_4376)	TIE-1recAqRT-PCRRev	GAATTCGACCTGCTTGAACG
photosynthetic reaction center L subunit (Rpal_1716)	Rpal_1716_pufL_for	GAGAAGAAATACCGCGTTCG
photosynthetic reaction center L subunit (Rpal_1716)	Rpal_1716_pufL_rev	CCGAAGATCCCAACGTAGAA
F-type H+-transporting ATPase subunit beta (Rpal_1057)	Rpal_1057_atp1_for	ATTCTGAACGCCATCGAAAC
F-type H+-transporting ATPase subunit beta (Rpal_1057)	Rpal_1057_atp1_rev	GACGGTCGATTCACCAAGAT
F-type H+-transporting ATPase subunit beta (Rpal_0171)	Rpal_0171_atp2_for	GACGATCGCGGAGTATTTTC
F-type H+-transporting ATPase subunit beta (Rpal_0171)	Rpal_0171_atp2_rev	CAGGCTGGATAACTCGCTTC
pioA (Rpal_0817)	pioAqRTPCRfor	AAATTTCGACGACACCATCGA
pioA (Rpal_0817)	pioAqRTPCRrev	CTTGGCGGCGAGGATCT
hydrogenase large subunit (Rpal_1153)	Rpal_1153qPCRfor	GTGCAACTGCTGTCGATCAT
hydrogenase large subunit (Rpal_1153)	Rpal_1153qPCRrev	CCAGCACGTTGTCGAGAC

2.7 References

1. Kirchman, D. L. *Processes in Microbial Ecology* 55-78 (Oxford University Press, 2018).

2. Imhoff J.F. *Anoxygenic Photosynthetic Bacteria* (eds Blankenship, R.E., Madigan, M.T. & Bauer, C.E.) 1-15 (Kluwer Academic Publishers, 1995).

3. Bose, A., Gardel, E.J., Vidoudez, C., Parra, E.A. & Girguis, P.R. Electron uptake by iron-oxidizing phototrophic bacteria. *Nat. Commun.* **5**, 3391 (2014).

4. Tremblay, P.L., Angenent, L.T. & Zhang, T. Extracellular electron uptake: among autotrophs and mediated by surfaces. *Trends Biotechnol.* **35**, 1-12 (2016).

5. Rosenbaum, M., Aulenta, F., Villano, M. & Angenent, L.T. Cathodes as electron donors for microbial metabolism: which extracellular electron transfer mechanisms are involved? *Bioresour. Technol.* **102**, 324-333 (2011).

6. Rabaey, K., Rodriguez, J., Blackall, L.L., Keller, J., Gross, P., Batstone, D., Verstraete, W. & Nealson, K.H. Microbial ecology meets electrochemistry: electricity-driven and driving communities. *ISME J.* **1**, 9-18 (2007).

7. Lovley, D. R. Extracellular electron transfer: wires, capacitors, iron lungs, and more. *Geobiology* **6**, 225-231 (2008).

8. Shi, L., Dong, H., Reguera, G., Beyenal, H., Lu, A., Liu, J., Yu, H.Q. & Fredrickson, J.K. Extracellular electron transfer mechanisms between microorganisms and minerals. *Nat. Rev. Microbiol.* **14**, 651-662 (2016).

9. Nevin, K.P., Hensley, S.A., Franks, A.E., Summers, Z.M., Ou, J., Woodard, T.L., Snoeyenbos-West, O.L. & Lovley, D.R. Electrosynthesis of organic compounds from carbon dioxide catalyzed by a diversity of acetogenic microorganisms. *Appl. Environ. Microbiol.* **77**, 2882-2886 (2011).

10. Rengasamy, K., Ranaivoarisoa, T., Singh, R. & Bose, A. An insoluble iron complex coated cathode enhances direct electron uptake by *Rhodopseudomonas palustris* TIE-1. *Bioelectrochemistry* **122**, 164-173 (2018).

11. Doud, D. F. & Angenent, L. T. Toward electrosynthesis with uncoupled extracellular electron uptake and metabolic growth: enhancing current uptake with *Rhodopseudomonas palustris*. *Environ. Sci. Technol. Lett.* **1**, 351-355 (2014).

12. Ha, P.T., Lindemann, S.R., Shi, L., Dohnalkova, A.C., Fredrickson, J.K., Madigan, M.T. & Beyenal, H. Syntrophic anaerobic photosynthesis via direct interspecies electron transfer. *Nat. Commun.* **8**, 13924 (2017).

13. Jiao, Y., Kappler, A., Croal, L.R. & Newman, D.K. Isolation and characterization of a genetically tractable photoautotrophic Fe(II)-Oxidizing bacterium, *Rhodopseudomonas palustris* strain TIE-1. *Appl. Environ. Microbiol.* **71**, 4487-4496 (2005).

14. Ross, D.E., Flynn, J.M., Baron, D.B., Gralnick, J.A. & Bond, D.R. Towards electrosynthesis in *Shewanella*: energetics of reversing the Mtr pathway for reductive metabolism. *PLoS ONE* **6**, e16649 (2011).

15. Ishii, T., Kawaichi, S., Nakagawa, H., Hashimoto, K. & Nakamura, R. From chemolithoautotrophs to electrolithoautotrophs: CO_2 fixation by Fe(II)-oxidizing bacteria coupled with direct uptake of electrons from solid electron sources. *Front. Microbiol.* **6**, 994 (2015).

16. Summers, Z. M., Gralnick, J. A. & Bond, D. R. Cultivation of an obligate Fe(II)-oxidizing lithoautotrophic bacterium using electrodes. *mBio* **4**, e00420-00412 (2013).

17. Lohner, S. T., Deutzmann, J. S., Logan, B. E., Leigh, J. & Spormann, A. M. Hydrogenase-independent uptake and metabolism of electrons by the archaeon *Methanococcus maripaludis*. *ISME J* **8**, 1673-1681 (2014).

18. Strycharz, S.M., Glaven, R.H., Coppi, M.V., Gannon, S.M., Perpetua, L.A., Liu, A., Nevin, K.P. & Lovley, D.R. Gene expression and deletion analysis of mechanisms for electron transfer from electrodes to *Geobacter sulfurreducens*. *Bioelectrochemistry* **80**, 142-150 (2011).

19. Nevin, K.P., Hensley, S.A., Franks, A.E., Summers, Z.M., Ou, J., Woodard, T.L., Snoeyenbos-West, O.L. & Lovley, D.R. Electrosynthesis of organic compounds from carbon dioxide catalyzed by a diversity of acetogenic microorganisms. *Appl. Environ. Microbiol.* **77**, 2882-2886 (2011).

20. Beese-Vasbender, P. F., Nayak, S., Erbe, A., Stratmann, M. & Mayrhofer, K. J. Electrochemical characterization of direct electron uptake in electrical microbially influenced corrosion of iron by the lithoautotrophic SRB *Desulfopila corrodens* strain IS4. *Electrochim. Acta* **167**, 321-329 (2015).

21. Rowe, A.R., Chellamuthu, P., Lam, B., Okamoto, A. & Nealson, K.H. Marine sediments microbes capable of electrode oxidation as a surrogate for lithotrophic insoluble substrate metabolism. *Front. Microbiol.* **5**, 784 (2014).

22. Wang, Z., Leary, D.H., Malanoski, A.P., Li, R.W., Hervey, W.J., Eddie, B.J., Tender, G.S., Yanosky, S.G., Vora, G.J., Tender, L.M., Lin, B., & Strycharz-Glaven, S.M. A previously uncharacterized, nonphotosynthetic member of the *Chromatiaceae* is the primary CO_2-fixing constituent in a self-regenerating biocathode. *Appl. Environ. Microbiol.* **81**, 699-712 (2015).
23. Lam, B. R., Rowe, A. R. & Nealson, K. H. Variation in electrode redox potential selects for different microorganisms under cathodic current flow from electrodes in marine sediments. *Environ. Microbiol.* **20**, 2270-2287 (2018).

24. Rowe, A.R., Rajeev, P., Jain, A., Pirbadian, S., Okamoto, A., Gralnick, J.A., El-Naggar, M.Y. & Nealson, K.H. Tracking electron uptake from a cathode into *Shewanella* cells: implications for energy acquisition from solid-substrate electron donors. *mBio* **9**, e02203-02217 (2018).

25. Ren, H., Lee, H.S. & Chae, J. Miniaturizing microbial fuel cells for potential portable power sources: promises and challenges. *Microfluid. Nanofluidics* **13**, 353-381 (2012).

26. Deutzmann, J. S., Sahin, M. & Spormann, A. M. Extracellular enzymes facilitate electron uptake in biocorrosion and bioelectrosynthesis. *MBio* **6**, e00496-00415 (2015).

27. Gregory, K.B., Bond, D.R. & Lovley, D.R. Graphite electrodes as electron donors for anaerobic respiration. *Environ. Microbiol.* **6**, 596-604 (2004).

28. Strycharz, S.M., Woodard, T.L., Johnson, J.P., Nevin, K.P., Sanford, R.A., Löffler, F.E. & Lovley, D.R. Graphite electrode as a sole electron donor for reductive dechlorination of tetrachlorethene by *Geobacter lovleyi*. *Appl. Environ. Microbiol.* **74**, 5943-5947 (2008).

29. Strycharz, S.M., Gannon, S.M., Boles, A.R., Franks, A.E., Nevin, K.P. & Lovley, D.R. Reductive dechlorination of 2-chlorophenol by *Anaeromyxobacter dehalogenans* with an electrode serving as the electron donor. *Environ. Microbiol. Rep.* **2**, 289-294 (2010).

30. White, D. *The Physiology and Biochemistry of Prokaryotes* 112-117 (Oxford Press, 2007).

31. Trumpower, B.L. Cytochrome bc_1 complexes of microorganisms. *Microbiol. Mol. Biol. Rev.* **54**, 101-129 (1990).

32. Knaff, D.B. The cytochrome bc_1 complexes of photosynthetic purple bacteria. *Photosynth. Res.* **35**, 117-133 (1993).

33. Heytler, P. Uncoupling of oxidative phosphorylation by carbonyl cyanide phenylhydrazones. I. Some characteristics of *m*-CI-CCP action on mitochondria and chloroplasts. *Biochemistry* **2**, 357-361 (1963).

34. Herter, S.M., Kortlüke, C. M. & Drews, G. Complex I of *Rhodobacter capsulatus* and its role in reverted electron transport. *Arch. Microbiol.* **169**, 98-105 (1998).

35. Spero, M.A., Brickner, J.R., Mollet, J.T., Pisithkul, T., Amador-Noguez, D. & Donohue, T.J. Different functions of phylogenetically distinct bacterial complex I isozymes. *J. Bacteriol.* **198**, 1268-1280 (2016).

36. Tichi, M.A., Meijer, W.G. & Tabita, F.R. Complex I and its involvement in redox homeostasis and carbon and nitrogen metabolism in *Rhodobacter capsulatus*. *J. Bacteriol.* **183**, 7285-7294 (2001).

37. Dupuis, A., Darrouzet, E., Duborjal, H., Pierrard, B., Chevallet, M., Van Belzen, R., Albracht, S.P. & Lunardi, J. Distal genes of the *nuo* operon of *Rhodobacter capsulatus* equivalent to the mitochondrial ND subunits are all essential for the biogenesis of the respiratory NADH-ubiquinone oxidoreductase. *Mol. Microbiol.* **28**, 531-541 (1998).

38. Palmer, G., Horgan, D.J., Tisdale, H., Singer, T.P. & Beinert, H. Studies on the Respiratory chain-linked reduced nicotinamide adenine dinucleotide dehydrogenase XIV. Location of the sites of inhibition of rotenone, barbiturates, and piericidin by means of electron paramagnetic resonance spectroscopy. *J. Biol. Chem.* **243**, 844-847 (1968).

39. Dupuis, A. Genetic disruption of the respiratory NADH-ubiquinone reductase of *Rhodobacter capsulatus* leads to an unexpected photosynthesis-negative phenotype. *FEMS Microbiol. Lett.* **148**, 107-113 (1997).

40. Jackson, J. The proton-translocating nicotinamide adenine dinucleotide transhydrogenase. *J. Bioenerg. Biomembr.* **23**, 715-741 (1991).

41. Kern, S.E., Price-Whelan, A. & Newman, D.K. Extraction and measurement of NAD(P)(+) and NAD(P)H. *Methods Mol. Biol.* **1149**, 311-323 (2014).

42. Begley, T.P., Kinsland, C., Mehl, R.A., Osterman, A. & Dorrestein, P. The biosynthesis of nicotinamide adenine dinucleotides in bacteria. *Vitam. Horm.* **61**, 103-119 (2001).

43. Tabita, F.R., Satagopan, S., Hanson, T.E., Kreel, N.E. & Scott, S.S. Distinct form I, II, III, and IV Rubisco proteins from the three kingdoms of life provide clues about Rubisco evolution and structure/function relationships. *J. Exp. Bot.* **59**, 1515-1524 (2008).

44. Sirevåg, R., Buchanan, B., Berry, J. & Troughton, J. Mechanisms of CO_2 fixation in bacterial photosynthesis studied by the carbon isotope fractionation technique. *Arch. Microbiol.* **112**, 35-38 (1977).

45. Shiba, H., Kawasumi, T., Igarashi, Y., Kodama, T. & Minoda, Y. The CO_2 assimilation via the reductive tricarboxylic acid cycle in an obligately autotrophic, aerobic hydrogen-oxidizing bacterium, *Hydrogenobacter thermophilus*. *Arch. Microbiol.* **141**, 198-203 (1985).

46. Ebbs, S. Biological degradation of cyanide compounds. *Curr. Opin. Biotechnol.* **15**, 231-236 (2004).

47. Jiao, Y. & Newman, D.K. The *pio* operon is essential for phototrophic Fe(II) oxidation in *Rhodopseudomonas palustris* TIE-1. *J. Bacteriol.* **189**, 1765-1773 (2007).

48. Rey, F. E., Oda, Y. & Harwood, C. S. Regulation of uptake hydrogenase and effects of hydrogen utilization on gene expression in *Rhodopseudomonas palustris*. *J. Bacteriol.* **188**, 6143-6152 (2006).

49. Marrs, B., Stahl, C.L., Lien, S. & Gest, H. Biochemical physiology of a respiration-deficient mutant of the photosynthetic bacterium *Rhodopseudomonas capsulata*. *Proc. Natl. Acad. Sci. USA* **69**, 916-920 (1972).

50. Bird, L.J., Bonnefoy, V. & Newman, D.K. Bioenergetic challenges of microbial iron metabolisms. *Trends Microbiol.* **19**, 330-340 (2011).

51. Bird, L.J. Interactions of Fe(II) with the iron oxidizing bacterium *Rhodopseudomonas palustris* TIE-1. *Diss. Massachusetts Institute of Technology*, 1-172 (2013).

52. McKinlay, J.B. & Harwood, C.S. Carbon dioxide fixation as a central redox cofactor recycling mechanism in bacteria. *Proc. Natl. Acad. Sci. USA.* **107**, 11669-11675 (2010).

53. Romagnoli, S. & Tabita, F.R. A novel three-protein two-component system provides a regulatory twist on an established circuit to modulate expression of the *cbbI* region of *Rhodopseudomonas palustris* CGA010. *J. Bacteriol.* **188**, 2780-2791 (2006).

54. Joshi, G.S., Bobst, C.E. & Tabita, F.R. Unravelling the regulatory twist–regulation of CO_2 fixation in *Rhodopseudomonas palustris* CGA010 mediated by atypical response regulator(s). *Mol. Microbiol.* **80**, 756-771 (2011).

55. Byrne, J.M., Klueglein, N., Pearce, C., Rosso, K.M., Appel, E. & Kappler, A. Redox cycling of Fe(II) and Fe(III) in magnetite by Fe-metabolizing bacteria. *Science* **347**, 1473-1476 (2015).

56. Kato, S., Hashimoto, K. & Watanabe, K. Microbial interspecies electron transfer via electric currents through conductive minerals. *Proc. Natl. Acad. Sci. USA* **109**, 10042-10046 (2012).

57. Shrestha, P.M. & Rotaru, A.E. Plugging in or going wireless: strategies for interspecies electron transfer. *Front. Microbiol.* **5**, 237 (2014).

58. Reguera, G., McCarthy, K.D., Mehta, T., Nicoll, J.S., Tuominen, M.T. & Lovley, D.R. Extracellular electron transfer via microbial nanowires. *Nature* **435**, 1098 (2005).

59. El-Naggar, M.Y., Wanger, G., Leung, K.M., Yuzvinsky, T.D., Southam, G., Yang, J., Lau, W.M., Nealson, K.H. & Gorby, Y.A. Electrical transport along bacterial nanowires from *Shewanella oneidensis* MR-1. *Proc. Natl. Acad. Sci. USA* **107**, 18127-18131 (2010).

60. Pfeffer, C., Larsen, S., Song, J., Dong, M., Besenbacher, F., Meyer, R.L., Kjeldsen, K.U., Schreiber, L., Gorby, Y.A., El-Naggar, M.Y. & Leung, K.M. Filamentous bacteria transport electrons over centimetre distances. *Nature* **491**, 218 (2012).

61. Hernandez, M. & Newman, D. Extracellular electron transfer. *Cell. Mol. Life Sci.* **58**, 1562-1571 (2001).

62. Ehrenreich, A. & Widdel, F. Anaerobic oxidation of ferrous iron by purple bacteria, a new type of phototrophic metabolism. *Appl. Environ. Microbiol.* **60**, 4517-4526 (1994).

63. Bolger, A. M., Lohse, M. & Usadel, B. Trimmomatic: a flexible trimmer for Illumina sequence data. *Bioinformatics* **30**, 2114-2120 (2014).

64. Kim, D., Pertea, G., Trapnell, C., Pimentel, H., Kelley, R. & Salzberg, S.L. TopHat2: accurate alignment of transcriptomes in the presence of insertions, deletions and gene fusions. *Genome Biol.* **14**, R36 (2013).

65. Langmead, B. & Salzberg, S. L. Fast gapped-read alignment with Bowtie 2. *Nat. Methods* **9**, 357 (2012).

66. Anders, S., Pyl, P. T. & Huber, W. HTSeq—a Python framework to work with high-throughput sequencing data. *Bioinformatics* **31**, 166-169 (2015).

67. Wickman, H. *ggplot2: Elegant Graphics for Data Analysis* (Springer, 2016).

68. Yang, N.C., Ho, W.M., Chen, Y.H. & Hu, M.L. A convenient one-step extraction of cellular ATP using boiling water for the luciferin-luciferase assay of ATP. *Anal. Biochem.* **306**, 323-327 (2002).

69. Hoppe, P., Cohen, S. & Meibom, A. NanoSIMS: technical aspects and applications in cosmochemistry and biological geochemistry. *Geostand. Geoanalytical Res.* **37**, 111-154 (2013).

70. Jones, C., Fike, D.A. & Peres, P. Investigation of the quasi-simultaneous arrival (QSA) effect on a CAMECA IMS 7f-GEO. *Rapid Commun. Mass Spectrom.* **31**, 623-630 (2017).

Chapter 3: Extracellular electron uptake by a phototrophic sulfur-oxidizing bacterium

Preface

The following authors contributed to the work in this chapter. Michael Singh Guzman, Arpita Bose, Karthikeyan Rengasamy, Dinesh Gupta, and Rajesh Singh designed the research. Michael Singh Guzman, Karthikeyan Rengasamy, Rajesh Singh, and Dinesh Gupta collected the data. Michael Singh Guzman, Karthikeyan Rengasamy, Rajesh Singh, Dinesh Gupta, Emily Davenport and Arpita Bose analyzed and interpreted the data. Michael Singh Guzman, Dinesh Gupta, and Arpita Bose wrote the manuscript.

We thank the following members of the Washington University community: Bradley Evans and Shin-Cheng Tzeng at The Donald Danforth Place Science Center Proteomics and Mass Spectrometry Facility; and the Genome Access and Technology Center for help with RNA-Sequencing. M.S.G. was supported by the Initiative for Maximizing Student Development (IMSD) training grant from the U.S. National Institutes of Health (grant number R25-GM103757). This work was supported by the following grants to A.B.: The David and Lucile Packard Foundation Fellowship (grant no. 201563111), the U.S. Department of Energy (grant no. DESC0014613; also to D.A.F.), and the U.S. Department of Defense, Army Research Office (grant no. W911NF-18-1-0037). This work was also funded by a Collaboration Initiation Grant, an Office of the Vice Chancellor of Research Grant, and an International Center for Energy, Environment and Sustainability Grant from Washington University in St. Louis.

3.1 Abstract

Phototrophic extracellular electron uptake (phototrophic EEU) is a metabolism that allows photoautotrophic bacteria to transport electrons from solid-phase conductive substances (SPCSs) into the cell. Although recent work has advanced our understanding of the molecular and bioenergetic underpinnings of this process, very little is known about the ecological role that phototrophic EEU plays in marine environments. Here we investigated whether electrodes poised over a range of potentials that mimic elemental sulfur oxidation could serve as electron donors for the phototrophic sulfur-oxidizing bacterium *Rhodovulum sulfidophilum* AB26. Using multi-omics approaches, we show that cellular metabolism is activated by this process. We also identify EEU-specific electron-transfer proteins upregulated at the protein level. This work establishes the basis for molecular, biochemical, and genetic studies of the EEU pathway. Overall, these results provide evidence that marine phototrophic bacteria engage in EEU and that SPCSs may be important for energy acquisition and CO_2 fixation in marine ecosystems.

3.2 Introduction

Photoautotrophic organisms perform a complex series of biochemical reactions that couple light-energy transduction to CO_2 fixation to generate virtually all the biomass that supports life on Earth[1]. In anoxic environments, purple nonsulfur bacteria (PNSB) utilize an array of inorganic compounds as their electron donors for photosynthesis. These include soluble or gaseous phase compounds (H_2, H_2S, Fe^{+2}), as well as solid-phase and/or insoluble minerals such as rust (mixed-valent iron minerals)[2-4], sulfide minerals[5,6], or elemental sulfur[7]. Most recently, they have been shown to utilize solid-phase conductive substances (SPCSs) such as

poised electrodes[8,9] as proxies for minerals. To access insoluble minerals and SPCSs, phototrophs typically utilize an extracellular electron transfer process called phototrophic extracellular electron uptake (phototrophic EEU)[10]. Studies have shown that extracellular electron transfer to minerals is common in anoxic nutrient-poor environments[11]. The EEU-potential of microbes thriving in marine sediments or the photic zone of marine ecosystems, is incompletely understood. Knowledge of microbial EEU is critical to our understanding of global biogeochemical cycles, the microbial ecology of marine environments, and the evolution of microbial EEU.

Marine sediments are enriched in insoluble iron and sulfur minerals as well as elemental sulfur[11-13]. Anoxygenic phototrophs, such as *Rhodovulum* species, are broadly distributed marine phototrophs that use inorganic sulfur compounds as electron donors for carbon dioxide (CO_2) fixation[7]. To understand phototrophic EEU in marine ecosystems we used electrochemical, biochemical, bioinformatic, and microscopic approaches to characterize the electron uptake process of a genetically-tractable marine phototrophic bacterium, *Rhodovulum sulfidophilum* AB26 (hereafter referred to as AB26). Our data shows that AB26 is EEU-active at -200 mV vs. Standard Hydrogen Electrode (SHE), suggesting marine phototrophs may use an extracellular electron transfer mechanism to access SPCSs as electron donors for photosynthesis. We compared genome-wide transcriptomes of AB26 cultivated under different phototrophic conditions, including EEU, and found that genes related to energy-transduction, electron-transfer, and CO_2 fixation were upregulated, supporting this hypothesis. Mass spectrometry analysis provides further evidence that electron-transfer proteins, including *c*-type cytochromes and ferredoxins, are upregulated during phototrophic EEU. Lastly, using comparative genomics

we examine the metabolic and phylogenetic diversity of *Rhodovulum* species. These findings improve our understanding of biogeochemical cycling and suggest phototrophic EEU might represent an important microbial survival strategy in marine ecosystems.

3.3 Results

3.3.1 Phototrophic EEU from a poised electrode

Since the discovery of metal-reducing bacteria, microbe-mineral interactions have been shown to play an important role in biogeochemical cycling in marine sediments and subsurface marine environments[11]. The role of microbial EET in facilitating EEU in marine ecosystems, where solid-phase reduced sulfur compounds are prevalent[13], has recently gained interest[14-16]. Whether phototrophic microbes living in these environments can access SPCSs as electron donors, however, has not been evaluated. To investigate if SPCSs can serve as electron donors for anoxygenic phototrophs in marine environments, we cultivated AB26 cells photoautotrophically in artificial seawater media on poised electrodes in bioelectrochemical systems (BESs). BESs mimic microbial interactions with SPCSs, wherein an electrode can operate as an electron donor for microbial metabolism[8,17]. The electrodes were poised from +200 mV to -200 mV (vs. SHE) to mimic the potential range of solid phase and/or insoluble minerals AB26 may utilize in its natural environment.

We observed the highest current densities on electrodes poised at -200 mV (-126.6 nA cm^{-2} ± 4.81) [an electrode potential slightly higher than the redox couple of S/H_2S ($E^{\circ\prime}$ = -274 mV)][18] (Figure 3.1a). This magnitude of current uptake is similar to that observed for *R. palustris* TIE-1 cells cultivated on electrodes poised at +100 mV[10]. We performed cyclic voltammetry of

the electrodes at the end of incubations (Figure 3.1b). For electrodes poised at -200 mV, we observed increased cathodic current densities in cyclic voltammograms at the end of 45 h incubations compared to abiotic control reactors (Figure 3.1b). Cathodic current densities were higher than abiotic control reactors from +500 mV to -600 mV and were typically higher at more electronegative potentials. We also observed a reversible redox peak with a midpoint potential of +450 mV (Figure 3.1b).

To determine if AB26 releases extracellular redox-active molecules during EEU we filtered the spent media after the incubations and performed cyclic voltammetry with sterile electrodes. We observed an increase in cathodic current densities in cyclic voltammograms between -200mV to -600 mV compared to abiotic control reactors (Figure 3.1c). The increased current densities in the cyclic voltammograms could reflect a microbially-produced redox active molecule. Over the 45 h incubations there was modest cell growth reflected by an increase in the planktonic cell density within bioreactors where electrodes were poised at 0 mV ($P < 0.05$, one-way ANOVA) and -200 mV ($P < 0.001$, one-way ANOVA) (Figure 3.1d). We did not observe a significant increase in planktonic cell density in bioreactors where electrodes were poised at +200 mV ($P = 0.708$, one-way ANOVA) (Figure 3.1d). Whether this increase in planktonic cell density is a result of direct electron uptake from the electrode, or via an indirect mechanism requires further investigation.

Scanning electron microscopy (SEM) revealed that electrodes poised at 0 mV and -200 mV were colonized by microbial cells (Figure 3.2b-c). No electrode-attached cells were observed on electrodes poised at +200 mV (Figure 3.2a). We observed that cellular aggregates formed on electrodes poised at -200 mV (Figure 3.2c). These aggregates appeared to reach several cell-

layers in thickness and were entirely encapsulated by an extracellular matrix-like substance (Figure 3.2c). Microscopy of the biocathodes revealed that this substance contains exopolysaccharide and extracellular protein (Supplementary Figure 3.1). We performed viability staining on these electrodes using LIVE/DEAD® dyes (Figure 3.2d-f). Viable attached cells were observed only on electrodes poised at 0 mV and -200 mV (Figure 3.2d-f). However, increased numbers of dead cells were observed on electrodes poised at 0 mV (Figure 3.2e). No attached and/or viable cells were observed on electrodes poised at +200 mV (Figure 3.2d). Overall, our data indicates that AB26 can utilize solid electrodes for cellular survival and growth and suggest that cellular attachment is important for electron uptake.

3.3.2 Highly responsive and EEU-specific gene expression

Very few studies have investigated the molecular and bioenergetic pathways that allow photoautotrophs to use SPCSs as electron donors[19]. Subsequently, we have a limited understanding of the electron-transfer pathways, physiological electron sinks, and regulatory mechanisms that govern this process. To better understand phototrophic EEU in AB26 we performed whole-genome transcriptomic analysis (RNA-Seq) (Figure 3.3a). We performed RNA-Seq on AB26 cells incubated in bioreactors (where electrodes were poised at -200 mV vs. SHE) and under four other growth conditions: (1) anaerobic photoautotrophic growth with H_2, (2) anaerobic photoautotrophic growth with thiosulfate, (3) anaerobic photoheterotrophic growth with acetate, and lastly, (4) aerobic chemoheterotrophic growth (Supplementary Figure 3.1, Supplementary Table 3.1,3.2).

We performed differential expression analysis of these growth conditions to identify genes specifically upregulated during EEU (Figure 3.3b). When cells performed EEU from the electrode, 383 out of the 4077 genes in the AB26 genome were EEU-specific (i.e. specifically upregulated during EEU when compared to the other growth conditions) (Figure 3.3b). An additional 257 genes were upregulated and shared between EEU and phototrophic thiosulfate oxidation (Figure 3.3b). Genes involved in energy metabolism, including F-type ATPase, were EEU-specific (~2-fold; $P < 0.0001$) (Figure 3.3c). Porphyrin, chlorophyll and heme biosynthesis genes were also EEU-specific (Figure 3.3c). We observed the EEU-specific upregulation of an operon encoding an NAD^+-dependent formate dehydrogenase (~2-fold; $P < 0.05$) (Figure 3.3c). Formate dehydrogenase catalyzes formate oxidation to CO_2 and H^+ but can also function in reverse to catalyze CO_2 fixation to produce formate[20-22]. CO_2 fixation via formate dehydrogenase has been observed in *Rhodobacter capsulatus*[23] and other microbes[24,25]. Studies have also shown that formate dehydrogenase is an electrochemically active enzyme that can participate in direct electron uptake from electrodes[22,26,27]. Together, these data suggest that cellular metabolism is activated by the poised electrode.

Two distinct two-component systems (TCS) were EEU-specific (Figure 3.3c). These TCS are arranged in typical gene clusters which encode a sensor histidine kinase adjacent to a DNA-binding response regulator[28]. BV509_11515 and BV509_11520 encode a poorly characterized TCS called NtrY-NtrX (~3-fold; $P < 0.0001$) (Supplementary Figure 3.3). NtrY-NtrX has been observed to control a variety of cellular processes including cell motility, extracellular polymeric substance (EPS) production, and nitrogen metabolism[29-32]. These genes are immediately downstream of NtrB-NtrC. In *Rhodobacter capsulatus*, NtrB-NtrC is a TCS that controls the

expression of a number of genes involved in nitrogen fixation and assimilation[30]. The other TCS (encoded by BV509_19210 and BV509_19215) shares sequence similarity with YesM-YesN from *Bacillus subtilis* (~2-fold; $P < 0.0001$) (Supplementary Figure 3.3)[33]. This TCS is nonessential in *B. subtilis* and has an unknown function[33].

3.3.3 Gene expression related to carbon fixation and carbon reserves

Previous studies have shown that CO_2 fixation is an important electron sink in anoxygenic phototrophs during EEU. For example, in the phototrophic Fe(II)-oxidizing bacterium *Rhodopseudomonas palustris* TIE-1, CO_2 fixation via the Calvin-Benson-Bassham (CBB) cycle is the primary sink for phototrophic EEU[10]. In the genome of AB26, the CBB cycle is the sole pathway for CO_2 fixation. Form I and form II ribulose-1,5-bisphosphate carboxylase/oxygenase (*ruBisCO*) are organized in gene clusters typical of PNSB (Supplementary Table 3.3). Form I *ruBisCO*, but not form II *ruBisCO*, was upregulated during EEU (~2-fold; $P < 0.05$) (Figure 3.4a). Each *ruBisCO* gene is adjacent to a divergently transcribed LysR-family transcriptional regulator, CbbR[34] (BV509_05530 and BV509_15210). The *cbbR* homolog adjacent to form I *ruBisCO* in AB26 is expressed highest during EEU, even when compared to other phototrophic growth conditions (~3.5-fold; $P < 0.0001$) (Figure 3.4a). CbbR is known to activate the transcription of form I *ruBisCO* in *R. palustris* and *R. sphaeroides* in response to the redox, energy, and carbon status of the cell[35-37].

Many microbes synthesize intracellular and/or extracellular carbon storage molecules for survival under organic carbon-limiting conditions. These include the intracellular carbon polymers polyhydroxybutyrate (PHB) and glycogen, as well as EPS[38-41]. To determine if AB26

synthesizes and/or utilizes carbon reserves during EEU we identified pathways encoding PHB, glycogen, and EPS biosynthesis in the AB26 genome and determined their expression. The PHB biosynthesis pathway, including a PhaC homolog responsible for PHB polymerization, was expressed but typically downregulated during EEU (Figure 3.4b). However, a polyhydroxyalkanoate synthesis repressor *phaR* homolog (BV509_06285) (~0.6-fold; $P < 0.0001$) and a PHA depolymerase *phaZ* homolog (BV509_06270) (~0.4-fold; $P < 0.0001$) were upregulated during EEU and other phototrophic conditions (Figure 3.4b). Furthermore, a phasin-domain containing protein was highly upregulated during EEU (~4-fold; $P < 0.0001$) (Figure 3.4b). Phasins localize to the surface of PHB granules and are synthesized under conditions permissive for PHB production[42]. The glycogen synthesis pathway of AB26 is encoded by an ADP-glucose pyrophosphorylase homolog (GlgC: BV509_13230) which is responsible for catalyzing the first step in the pathway[40]. In this gene cluster is also the glycogen synthetase (GlgA: BV509_13225), the branching enzyme (GlgB: BV509_13235), and the enzymes involved in glycogen degradation, including the glycogen debranching enzyme GlgX (BV509_13220) and the glycogen phosphorylase GlgP2 (BV509_13240). The glycogen biosynthesis pathway is expressed at low levels under all phototrophic growth conditions (Figure 3.4b).

Bacteria produce EPS to aid in biofilm formation[43]. Genes involved in capsular polysaccharide and exopolysaccharide biosynthesis were upregulated during EEU (Figure 3.3c). A capsular polysaccharide export protein (BV509_20210) is specifically upregulated during EEU (~3-fold; $P < 0.0001$) (Figure 3.3c). This gene is in a cluster that encodes a variety of genes involved in nucleotide sugar metabolism (BV509_20220-BV509_20235). Capsular

polysaccharide (CPS) biosynthesis[43,44] pathways are present in other gram-negative bacteria, including *Rhodobacter sphaeroides*[45]. By integrating data for carbohydrate metabolism (based on KEGG, GO, and IPS assignments) with RNASeq analysis, we identified a putative EPS pathway in AB26 (Supplementary Figure 3.4). This analysis included the identification of pathways encoding the enzymes for sugar nucleotide biosynthesis, glycosyltransferases, and genes involved in EPS export—including several ABC transporters and a *wza* homolog (Supplementary Figure 3.4). Wza is an outer membrane lipoprotein that is involved in the production of the extracellular polysaccharide colanic acid[43]. These results corroborate our microscopic analysis of AB26 biocathodes and suggest that EPS may be an extracellular carbon sink during EEU.

3.3.4 Identification of potential extracellular electron transfer pathways

EET-capable microorganisms have specialized membranes evolved for electron exchange between solid-phase electron-donors and -acceptors. These include diverse molecular mechanisms, such as porin-cytochrome-mediated pathways[46], nanowires[47,48], and multicellular filaments[49]. One common feature between EET pathways is that they require *c*-type cytochromes[19]. To better understand the extracellular electron transfer pathway in AB26 we identified *c*-type cytochromes in the genome and examined the expression of these genes. We identified ~40 heme-binding proteins in AB26 with the characteristic CXXCH motif (Supplementary Table 3.4)[50]. This included many well-characterized *c*-type cytochromes, such as those in the sulfur oxidation (*sox*) system[51], along with diheme cytochrome *c* peroxidase family homologs (BV509_14915, BV509_20295) that are involved in cellular detoxification in

related bacteria[45]. This analysis also identified potential respiratory pathways including a *cbb3*-type cytochrome *c* oxidase (BV509_18680-BV509_18695) and a cytochrome *bd* respiratory complex (BV509_19445-BV509_19455). These oxidases are typically found in PNSB related to AB26 and are important terminal oxidases in oxygen-limited environments[52,53]. We did not detect homologs of known *c*-type cytochromes involved in EET and/or iron-oxidation[19].

We identified several hypothetical cytochrome *c*-like proteins in the genome of AB26 that were expressed during EEU. This included multiple monoheme, diheme, and a single tetraheme *c*-type cytochrome. Multiheme *c*-type cytochrome proteins are typically involved in EET[19] so we investigated these proteins further. BV509_01335 was the most significantly differentially expressed cytochrome *c*-like gene (~3-fold; $P < 0.0001$) (Figure 3.5a). This gene is a periplasmic diheme *c*-type cytochrome that is upstream of a transmembrane cytochrome *b*-domain containing protein (BV509_01340). BV509_01335 is expressed under all phototrophic conditions and is upregulated ~3-fold during EEU ($P < 0.0001$) (Figure 3.5a). BV509_09650 is a diheme *c*-type cytochrome downstream of the *sox* operon and is adjacent to a flavocytochrome *c* sulfide dehydrogenase (BV509_09655; ~3-fold; $P < 0.0001$) and a transmembrane flavin reductase-like gene (BV509_09665; ~5-fold; $P < 0.0001$) (Figure 3.5a). Additionally, several diheme *c*-type cytochromes near gene clusters encoding for metal transport were upregulated. This includes BV509_10070 which is a diheme cytochrome *c* near gene clusters encoding for molybdenum, nickel, and cobalt transport (~2-fold; $P < 0.0001$) (Figure 3.5a). Lastly, a hypothetical protein with a single *c*-type cytochrome domain (BV509_18570) was specifically upregulated during EEU (~1-fold; $P < 0.05$) and phototrophic thiosulfate oxidation (~1-fold; $P < 0.05$) (Figure 3.5a).

Other electron-transfer proteins identified included iron-sulfur cluster containing proteins, such as ferredoxins. Iron-sulfur proteins have been reported to be involved in iron oxidation in Fe(II)-oxidizing[54,55] and EEU-capable[56] bacteria. In some Fe(II)-oxidizing bacteria iron-sulfur proteins function to bifurcate electron flow in the periplasm for the generation of a proton gradient for ATP production[57]. Gene clusters containing iron-sulfur proteins have also been identified in purple sulfur bacteria within biocathode communities and have been proposed to be involved in EEU in these organisms[56]. We identified 13 iron-sulfur genes in the genome of AB26 (Supplementary Table 3.5). These genes did not share significant sequence homology to iron-sulfur proteins identified in Fe(II)-oxidizing bacteria in previous studies[56]. Of note is a 4Fe-4S ferredoxin-like gene (BV509_04265) that was specifically upregulated during EEU (~2-fold; $P < 0.0001$) and phototrophic thiosulfate oxidation (~2-fold; $P < 0.0001$) (Figure 3.5b).

To determine the proteins upregulated during phototrophic EEU, we compared and analyzed total protein (soluble and insoluble) fractions of AB26 cells cultivated under different phototrophic conditions. We observed a distinct protein band (between 56 and 72 kDa) specific to phototrophic EEU in both the soluble and insoluble fractions (Figure 3.5c). Interestingly, mass spectrometry analysis of these bands identified the presence of a 61 kDa periplasmic diheme cytochrome *c* (BV509_10070) that was a top hit in both the soluble and insoluble fractions (Supplementary Table 3.6,3.7). We also identified a 60 kDa periplasmic 4Fe-4S ferredoxin-like protein (BV509_08685) that was a top hit specifically in the soluble fraction (Supplementary Table 3.6). These proteins were also upregulated during phototrophic EEU in our transcriptomic analysis (Figure 3.5a).

C-type cytochromes are involved in EET pathways in diverse bacterial genera[19]. Interestingly, phylogenetic analysis of BV509_10070 indicates this gene is highly conserved in *Rhodovulum* species (Supplementary Figure 3.6). Homologs of BV509_10070 are also present in *Rhizobiales*, including two *R. palustris* strains and a *Mesorhizobium*. BV509_10070 is absent from *R. palustris* TIE-1 and other known phototrophic Fe(II)-oxidizing/EEU-capable bacteria. The presence of BV509_10070 in both the soluble and insoluble fractions might suggest that this protein could interact with the membrane of AB26. Overall, this data establishes the basis for interrogating the electron-transfer proteins important for phototrophic EEU in AB26.

3.3.5 Comparative genomics and physiology of *Rhodovulum* species

We recently sequenced the draft genome of AB26 and two closely related isolates (AB14 and AB30) from the Trunk River estuary in Woods Hole, MA[58]. The initial assembly of AB26 revealed a single chromosome and two extrachromosomal sequences. Here, we provide a further analysis of the AB26 genome, its phylogenetic placement, and its metabolic features in light of its ability to perform phototrophic EEU. Based upon phylogenetic analysis of its 16S rRNA gene AB26 clades with *Rhodovulum*, which is a genus typically found in marine environments (Figure 3.6). AB26 has ~99% 16S rRNA nucleotide sequence identity to *R. sulfidophilum* type-strains W4 (DSM 1374) and W12 (DSM 2351). AB26 also has ~99% nucleotide sequence identity to new isolates AB14 and AB30[58], and SNK001. AB26 clusters outside of clades containing phototrophic Fe(II)-oxidizing bacteria: *Rhodopseudomonas palustris* TIE-1[59], *Rhodovulum robiginosum*[60], *Rhodovulum iodosum*[60], and *Rhodobacter* sp. SW2[61] (Figure 3.6).

As we've previously reported, the chromosome of AB26 is ~4.2 Mb, and the genome

contains two plasmid-like contig sequences which are ~100 Kb and ~80 Kb, respectively[58] (Figure 3.7a-c). The single chromosome of AB26 shares a high degree of synteny to those of other *Rhodovulum sulfidophilum* strains (Figure 3.7a). BLAST analysis indicates that ~90% of protein-coding genes have a top-hit to *R. sulfidophilum* strains in the NCBI database (Supplementary Figure 3.7). The ~80 Kb contig sequence is homologous to "Plasmid 3" from the finished genome of *R. sulfidophilum* DSM 2351[62] (Figure 3.7b). The ~100 Kb plasmid contig sequence (which we refer to here as Plasmid 4), however, does not appear to be conserved within the genome of *R. sulfidophilum* DSM 2351 but instead to a plasmid sequence in the genome of *Rhodovulum* sp. MB263 (Figure 3.7c).

Rhodovulum species are exceptionally metabolically versatile microbes that play an important role in the biogeochemical cycling of C, N, S, and Fe[7]. To support photoautotrophic growth, *Rhodovulum* are known to oxidize a variety of inorganic compounds as electron donors for anoxygenic photosynthesis. This includes molecular hydrogen (H_2), reduced sulfur compounds, and iron. The ability to oxidize reduced sulfur compounds, including thiosulfate, is also broadly conserved among *Rhodovulum* (Figure 3.6 and 3.7d)[7]. This process is typically carried out by the Sox system[63]. It has been suggested that the Sox system is also responsible for the oxidation of elemental sulfur (S^0), however, this process is poorly understood[7]. Because many of the *Rhodovulum* strains that carry the Sox system cannot carry out S^0 oxidation, its role in this process is unclear. Some PNSB also encode sulfide:quinone oxidoreductase and sulfide dehydrogenase, enzymes involved in sulfide oxidation (Figure 3.7d). Although some *Rhodovulum* species encode these two enzymes, they are absent from AB26 and most *R. sulfidophilum* strains (Figure 3.7d). *R. sulfidophilum* DSM 1374 is the only sequenced strain that

possesses these genes (Figure 3.7d). Interestingly, AB26 is the only *R. sulfidophilum* stain with the metabolic potential for sulfur assimilation via a sulfite reductase homolog (Figure 3.7d)[64-66].

The AB26 genome contains a number of notable features, including the metabolic potential to oxidize one-carbon compounds. We identified a gene cluster encoding a methanol oxidation system found on Plasmid 4 that shared no sequence homology to the genomes of PNSB available in public databases (Figure 3.7d). NCBI BLAST analysis of this region revealed >80% nucleotide sequence identity to the methanol oxidation gene cluster of *Methylobacterium* sp. C1. This gene cluster encodes the methanol dehydrogenase (MDH) large and small subunit (*mxaF*: BV509_20585; *mxaI*: BV509_20600), the MDH-specific cytochrome c_L (*mxaG*: BV509_20595), and homologs to its accessory factors (*mxaJ*: BV509_20590; *mxaR*: BV509_20605; *mxaS*: BV509_20610; *mxaA*: BV509_20615; *mxaC*: BV509_20620; *mxaC*: BV509_20620; *mxaK*: BV509_20625; *mxaL: BV509_20630*; *mxaD*: BV509_20635). These results expand our understanding of the metabolic versatility of *R. sulfidophilum* in marine ecosystems.

3.4 Discussion

Solid-phase conductive substances (SPCSs), such as iron minerals, are ubiquitous in natural environments. Microbes that exchange electrons with these materials via extracellular electron transfer (EET) play an important role in biogeochemical cycles[19]. Recent studies have shown that anoxygenic phototrophs can use SPCSs as electron donors for CO_2 fixation[2,8-10,67]. The possibility and extent to which this process contributes to primary productivity in marine ecosystems, however, is unclear. To better understand this process, we isolated and characterized

a PNSB from a marine microbial mat. We demonstrated that *R. sulfidophilum* AB26 is capable of taking up electrons from electrodes poised at -200 mV vs. SHE, close to the redox couple of S/H_2S ($E^{\circ\prime}$ = -274 mV)][18] (Figure 3.1a). Furthermore, cyclic voltammograms of the spent media revealed a cathodic peak ~ -200 mV vs. SHE (Figure 3.1c). Anode-respiring microbes are known to secrete redox-active molecules, such as flavins, to mediate EET[68-70]. The redox peak we observed in our study falls into the range of known EET redox mediators ($E^{\circ\prime}$ = -219 mV (FMN and FAD) and $E^{\circ\prime}$ = -208 mV (riboflavin))[71]. Future studies will characterize the electrochemical properties of this redox peak and determine its molecular identity.

AB26 is distinct from other EEU-capable PNSB in that it can use electrodes at relatively low potentials (i.e. -200 mV vs. SHE) and does not contain homologs of known genes involved in EET (e.g. the Mtr system of Shewanella oneidensis MR-1[46]). Using transcriptome sequencing we identified the expression of *c*-type cytochromes in the AB26 genome. We identified several periplasmic *c*-type cytochromes that were upregulated during EEU (Fig. 3.6). One periplasmic *c*-type cytochrome and a *cbb3*-type cytochrome *c* oxidase were specifically upregulated during EEU and phototrophic thiosulfate oxidation (Figure 3.5a). This suggests AB26 may use conserved electron transfer mechanisms to mediate these two cellular metabolisms. Interestingly, we also identified multiple sulfur oxidation genes in our mass spectrometry analysis (Supplementary Table 3.8). This data corroborates our transcriptomic data and suggests the poised electrode is simulating sulfur metabolism.

One of the top hits in our mass spectrometry analysis of total protein was a periplasmic diheme *c*-type cytochrome BV509_10070 (Supplementary Table 3.7,3.8). BV509_10070 contains a Sec-signal peptide and thus is likely a periplasmic protein. Because of its cytochrome

c-like properties (Supplementary Figure 3.5), increased transcription (Figure 5a), and distinct protein expression (Supplementary Table 3.6,3.7), BV509_10070 may be involved in electron transfer during EEU. Future biochemical work needs to be performed to determine whether BV509_10070 is heme-attached and if it is a functional oxidoreductase protein. Future genetic studies should also determine its involvement in EEU. Because AB26 does not contain known EET genes, identification of the extracellular electron pathways in this organism will provide new genetic markers for studying EET in the environment.

EEU-capable microbes identified in previous studies typically make monolayer-thick biofilms on electrodes[8,10,72]. This is consistent with a direct electron uptake mechanism by these microbes. In contrast, we observed that AB26 biofilms were several cell-layers in thickness (Figure 3.2c). We also identified that AB26 produces an EPS-like substance on electrodes (Figure 3.2c and Supplementary Figure 3.1) and that pathways leading to EPS production were upregulated during EEU (Figure 3.3c and Supplementary Figure 3.4). Interestingly, EPS has been shown to be electrochemically active and to mediate EET in diverse microbial biofilms[60,61]. EPS can also serve as a carbon source for microbial survival[73] and studies have shown that EPS represents an important source of dissolved organic matter in marine ecosystems[41]. Future studies should determine the role of EPS in AB26 and examine whether it has electron-transfer properties.

Studies have suggested that electroactive bacteria can sense electrically conductive surfaces and elicit specific responses that augment their ability to carry out EET. For example, in *Shewanella*, "electrokinesis" has been described as a microbial behavior characterized by increased cell swimming speeds and protracted paths of motion in response to minerals and

poised electrodes[74]. Cell tracking analysis with outer-membrane *c*-type cytochrome mutants of *Shewanella* has furthermore confirmed that this response is likely mediated by extracellular electron shuttles (e.g. flavins)[75]. Studies have also shown that electroactive bacteria sense electrode potentials[76] and accordingly regulate catabolic pathways to maximize their growth rate[77]. The molecular details of how EEU-capable bacteria sense and respond to electrically conductive surfaces, however, remains unclear. In our study, we identified TCS that were specifically upregulated during EEU (Figure 3.3c). TCS integrate a variety of external inputs to induce transcriptional changes and allow the cell to respond to a stimulus[28]. Although TCS have not been identified in EET pathways, because they control a number of cellular processes important for biofilm formation and are redox-responsive[28], the TCS identified in AB26 may play a role in EEU.

During EEU in AB26 we observe that the gene encoding form I *ruBisCO* is upregulated, whereas form II *ruBisCO* is expressed at low levels (Figure 3.4a). In *R. palustris* TIE-1 increased expression of form I *ruBisCO* has also been observed during EEU[8,10]. Furthermore, CO_2 fixation (via RuBisCO) is the primary sink for cathodic electrons[10]. This suggests that form I *ruBisCO* may also be the primary autotrophic carboxylase in AB26 and that electrons from the cathode may be used for CO_2 fixation. In *R. sphaeroides* and related microbes the LysR transcriptional regulator CbbR is a positive regulator of the CBB cycle operons[35,78]. The AB26 genomes encodes CbbR-homologs adjacent to each CBB cycle operon (Supplementary Table 3.3). The expression of these genes is highest during EEU, even when compared to other photoautotrophic growth conditions (Figure 3.4a). The involvement of CbbR in activating CBB cycle expression and its intracellular signals should be investigated in future studies.

CO_2 fixation via phototrophic EEU has biotechnological applications because of metabolic potential for the production of intracellular polymers, including poly(3-hydroxybutyrate) (PHB) (Figure 3.4b). *R. sulfidophilum* W-1S has the capability to accumulate PHB under photoheterotrophic conditions, and can use PHB as a substrate for H_2 production[79]. In a previous study by our lab, we observed microbial PHB production via phototrophic EEU from poised electrodes in *R. palustris* TIE-1[67]. Others have also observed PHB production via indirect EEU from electrodes[26,80]. Because AB26 has the metabolic potential for PHB production, and is capable of EEU from electrodes, microbial PHB production could represent a bioplastic production strategy[38,39].

Our data shows that phototrophic PNSB from marine environments are capable of accepting electrons from poised electrodes. By using genome and transcriptome sequencing this work provides new insights into the molecular and bioenergetic pathways that enable photoautotrophs to use SPCSs for cellular survival. This work also expands the known diversity of organisms capable of EEU and provides a new microbe for use in electrochemical and physiological studies. Furthermore, since AB26 utilizes electrodes poised as sufficiently more negative potentials than PNSB previously characterized, this microbe may have utility in applications including energy storage, carbon-capture, and microbial electrosynthesis. Future studies will characterize the electron-conduit responsible for EEU and examine how this process is connected to photosynthesis and carbon fixation. This will enable use of this microbe in electrochemical applications and further our understanding of the role of marine PNSB in biogeochemical cycles.

3.5 Methods

3.5.1 Microbial isolation and cultivation conditions

AB26 was isolated in July 2014 from a microbial mat in the Trunk River estuary in Woods Hole, MA. Enrichments were cultivated photoheterotrophically in anoxic artificial seawater medium supplemented with 20 mM acetate. Enrichments were cultivated with ~850-nm light at 30°C and passaged six times, followed by streaking oxically 6 times on Bacto agar with Difco marine broth 2216 (BD Diagnostic Systems, Sparks, MD, USA) to isolate single colonies. AB26 can oxidize a variety of compounds to support photolithoautotrophy, including molecular hydrogen (H_2) and reduced sulfur compounds (Supplementary Table 3.1). All growth experiments were carried out at 30°C unless otherwise noted. All phototrophic growth experiments were performed with a single 60W incandescent light bulb at a distance of 25 cm. For anaerobic photoautotrophic growth cells were grown on 80% hydrogen-20% carbon dioxide (H_2-CO_2) at ~50 kPa or 10 mM sodium thiosulfate in artificial seawater (SW) medium with 70 mM sodium bicarbonate and 1 mM sodium sulfate. For anaerobic photoheterotrophic growth, cells were grown in 10 mL SW medium supplemented with 10 mM acetate from stock solutions (1 M, pH = 7). Anaerobic cultivations were performed in sterile, sealed glass serum bottles. Bioelectrochemical studies were performed with SW medium lacking exogenous electron donors, and purged with 80%-20% nitrogen (N_2-CO_2).

3.5.2 BES setup and conditions

Bioelectrochemical systems (BESs) were configured as previously described[10]. SW media (70 mL) was dispensed into anoxic, sterile, sealed, three-electrode BESs which were

pressurized to ~50 kPa with 80%:20% N_2-CO_2. The three electrodes were configured as follows: indium tin oxide (ITO) working electrodes were approximately 0.28 cm^2; reference eletrodes (Ag/AgCl) were submerged in 3 M KCl; and counter electrodes were composed of 5 cm^2 platinum foil. Working electrodes were poised using a multichannel potentionstat (Gamry Instruments, Warmister, PA). Reactors were operated continuously with a single 60W incandescent light bulb at 26°C. Chronoamperometry data were collected every 1 minute using the Gamry Echem Analyst™ (Gamry Instruments, Warmister, PA) software package. Mid-log phase H_2-CO_2 grown cells were used as inoculum for all bioelectrochemical cultivations. The biomass (OD_{660}) of inoculated BESs was monitored with a BugLab Handheld OD Scanner (Applikon Biotechnology, Inc., Foster City, CA). Cyclic voltammetry (CV) was performed at the end of incubations with potential sweep from +800 mV to -900 mV versus SHE and a 5 s scan rate.

3.5.3 Staining of electrodes

Electrodes were washed twice with anoxic 1X phosphate-buffered saline (PBS) to remove unattached cells in an anaerobic chamber. The exposed ITO surface was cut in half with a glass cutter and immediately placed in sterile microfuge tubes containing anoxic 1X PBS. Prior to imaging, the electrode was immersed in either: (1) LIVE/DEAD® stain (10 µM SYTO 9 and 60 µM propidium iodide, L7012, Life Technologies); (2) Concanavalin A Alexa Fluor™ 488 Conjugate (100 µg mL^{-1}); or (3) FilmTracer™ SYPRO™ Ruby Biofilm Matrix Stain. Samples were incubated for 30 min in the dark. Samples were placed in 1X PBS in a glass bottom Petri dish (MatTek Corporation, Ashland, MA) for imaging. Samples were imaged on a Nikon A1 inverted confocal microscope using 555 and 488 nm lasers and a 100X objective (Washington

University in St. Louis Biology Department Imaging Facility). Images were processed in Fiji version 2.0.0 to add scale bars[81].

3.5.4 Scanning electron microscopy

Cells were first fixed in an anaerobic chamber for 30 minutes using 2% formaldehyde and 2.5% glutaraldehyde in a 0.05 M sodium cacodylate buffer (pH 7.2) at a 1:1 ratio followed by sequential dehydration using varying proportions of ethanol (25%, 50%, 75%, 95%, 100%). A few drops of sample suspension were placed over the surface of a glass coverslip followed by critical point drying using EMS 850 Critical Point Drier. Critical point dried samples were coated with gold (7 nm) using a Leica ACE 600 sputter coater. A JEOL JSM-7001 LVF Field Emission SEM coupled with energy dispersive spectroscopy (SEM/EDS) was employed for morphological and compositional analyses of cells.

3.5.5 Molecular phylogenetic analysis

16S rRNA gene sequences were downloaded from GenBank. Evolutionary analyses were conducted in MEGA X[82]. The evolutionary history was inferred using the Maximum Likelihood method and the Tamura 3-parameter model. The tree with the highest log likelihood (-6546.83) is shown. The percentage of trees in which the associated taxa clustered together is shown next to the branches. Bootstrap values below 50% were omitted. Initial tree(s) for the heuristic search were obtained automatically by applying Neighbor-Join and BioNJ algorithms to a matrix of pairwise distances estimated using the Maximum Composite Likelihood (MCL) approach, and then selecting the topology with superior log likelihood value. A discrete Gamma distribution was used to model evolutionary rate differences among sites (2 categories (+G, parameter =

0.7388)). The rate variation model allowed for some sites to be evolutionarily invariable ([+I], 33.07% sites). The tree is drawn to scale, with branch lengths measured in the number of substitutions per site. This analysis involved 26 nucleotide sequences. All positions containing gaps and missing data were eliminated (complete deletion option). There were a total of 1261 positions in the final dataset.

3.5.6 Functional analysis

The draft genome sequences of AB26 were downloaded from NCBI (BioSample: SAMN05876236). Genome alignments were performed with BLAST Ring Image Generator (BRIG)[83] version 0.95 using the programs default parameters and NCBI BLAST+ version 2.9.0. The genome was mapped and annotated with the Blast2GO® bioinformatics platform using the programs default parameters. Metabolic pathway analysis was performed using BlastKOALA and KEGG-Decoder version 0.8 (https://github.com/bjtully/BioData/tree/master/KEGGDecoder) using the programs default parameters[84]. The metabolic pathway definitions used for this analysis can be found at https://github.com/bjtully/BioData/blob/master/KEGGDecoder/KOALA_definitions.txt.

3.5.7 Screening for known iron oxidation genes

FeGenie version 1.0 (https://github.com/Arkadiy-Garber/FeGenie/) was used to screen the genome assembly against known genes involved in iron oxidation using the program's default parameters.

3.5.8 RNA isolation

Microbial cells were sampled in an anaerobic chamber and immediately mixed 1:1 with RNA*later*® (Qiagen, USA). RNA was extracted using the RNeasy® Mini Kit according to the manufacturer's recommendations (Qiagen, USA). DNA removal was performed using Turbo DNA-*free*™ Kit (Ambion, USA). RNA samples were tested for purity using PCR.

3.5.9 RNA sequencing (RNA-Seq) and differential expression analysis

Illumina single-end 50-bp libraries were prepared and sequenced at Washington University's Genome Technology Access Center on an Illumina HiSeq3000 (Illumina Inc., San Diego, CA, USA). Reads were mapped to the AB26 genome using TopHat2 version 2.1.1 and the gff3 annotation file as a guide for sequence alignment. Bowtie 2 version 2.3.3.1 was used to index the reference genome FASTA file. The number of reads mapping to each feature were counted by HTSeq version 0.9.1. Differentially expressed genes were determined in DESEQ2 version 1.16.1 using the HTSeq read counts. To determine if genes were significantly differentially expressed an adjusted p-value cutoff of 0.05 was used. Marine broth (chemoheterotrophy) was used in differential expression analysis to "calibrate" expression values for each test condition. Figures were drawn in R.

3.5.10 Preparation of soluble and membrane fractions for mass spectrometry

AB26 cells cultivated under phototrophic conditions were harvested and stored at -80°C. Cell pellets were thawed on ice for ~30 min, resuspended in B-PER™ Bacterial Protein Extraction Reagent (ThermoFisher Scientific, USA), and then sonicated (Branson Ultrasonic

Bath, Branson Ultasonics Corp., USA). The lysates were centrifuged at 14,000 rpm for 30 min to separate the soluble and membrane fractions. The pellet was solubilized in 3X SDS buffer and used as the membrane fraction. The proteins in the soluble and membrane fractions were resolved via SDS-PAGE. Distinct protein bands were cut out of the gels, stored at -80°C, and sent to the Proteomics and Mass Spectrometry Facility at the Donald Danforth Plant Science Center (St. Louis, MO) for sequencing.

3.5.11 Statistical analysis

Statistical analyses (Student's *t*-test, one-way ANOVA with Bonferroni adjustment) were performed with Microsoft® Excel "Data Analysis" tools.

3.5.12 Data availability

Sequencing reads were deposited in the NCBI database under BioProject PRJNA546270. Accession numbers for individual sequencing libraries can also be found in Supplementary Table 3.2.

3.6 Figures

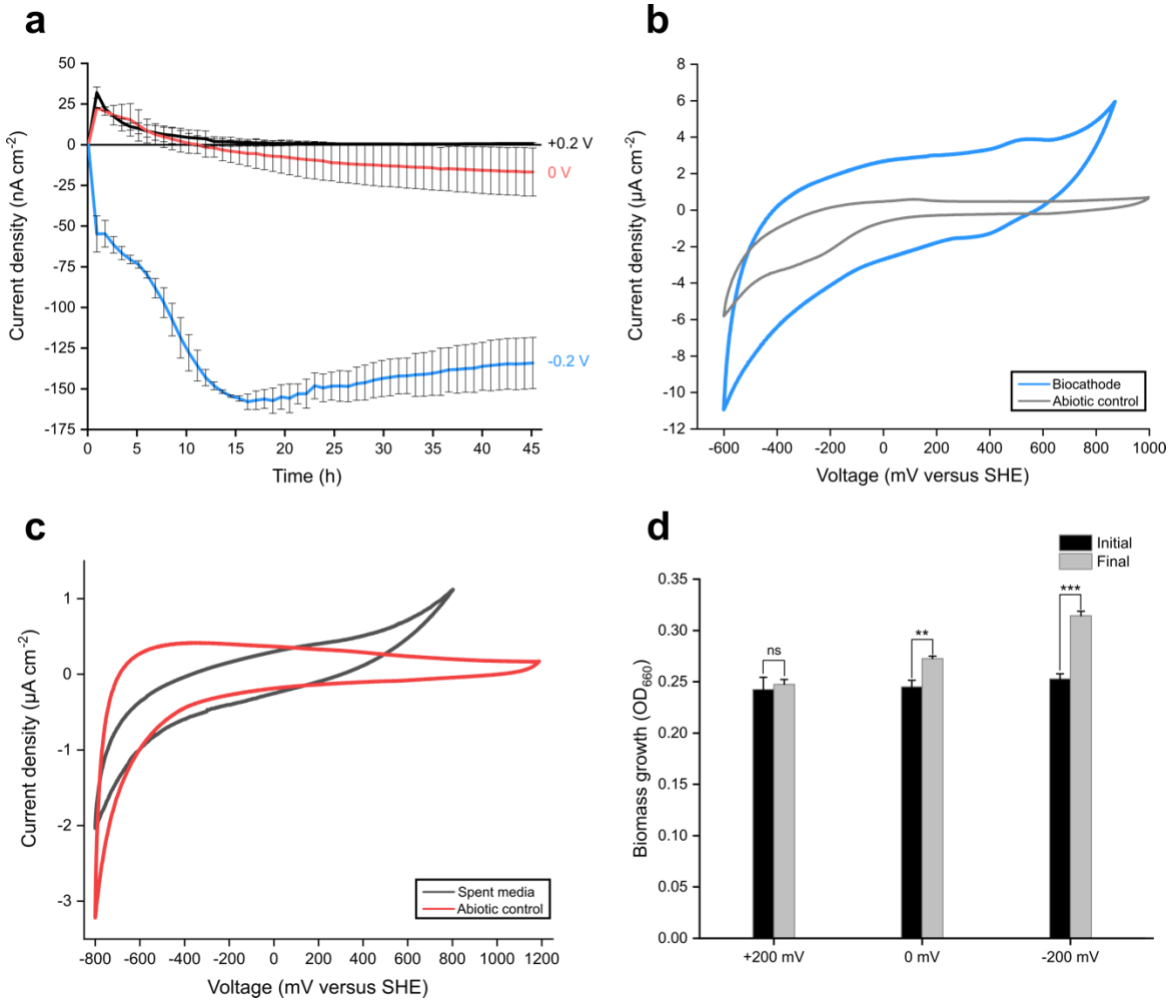

Figure 3.1. Solid electrode as the sole electron donor for anoxygenic photosynthesis. (a) Cathodic current densities vs. time at +200 mV, 0 mV, and -200 mV versus SHE. (b) Cyclic voltammograms after 45 h of electrochemical incubation at -200 mV versus SHE (blue) compared to an abiotic control reactor (grey). (c) Cyclic voltammograms of filtered, spent media after 45 h of electrochemical incubation at -200 mV versus SHE (grey) compared to fresh media (red). (d) Planktonic cell growth (OD_{660}) in bioreactors. Data are mean ± s.d. of at least two

biological replicates. The *P* values were determined by one-way ANOVA followed by a pairwise test with Bonferroni adjustment (*$P < 0.05$, **$P < 0.01$, ***$P < 0.0001$; ns, not significant).

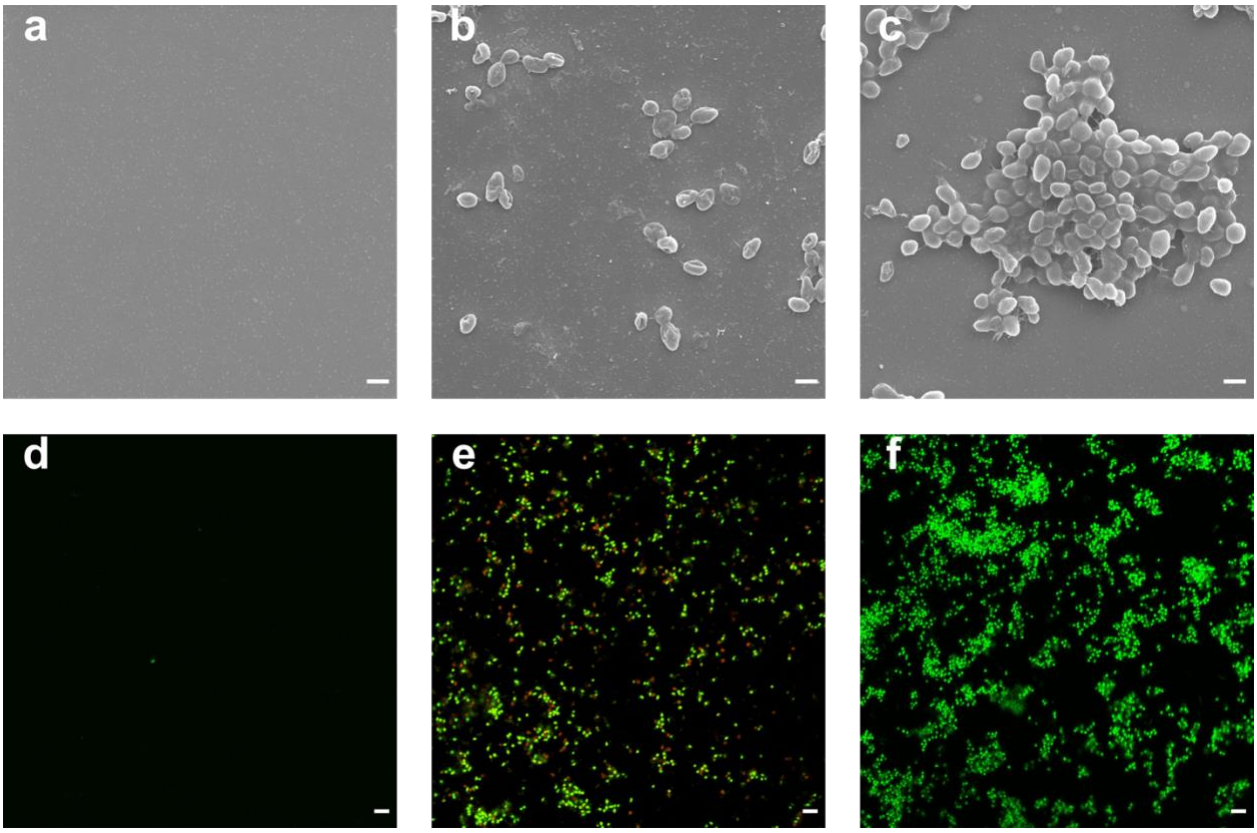

Figure 3.2. Bacterial cells attached to electrodes poised at different potentials. Microscopic images of bacterial cells attached to electrodes poised at: (a, d) +200 mV, (b, e) 0 mV, and (c, f) -200 mV versus SHE. (a-c) Scanning electron micrographs. Scale bar is 5 μM. (d-f) LIVE/DEAD staining. Green indicates live cells. Red indicates dead cells. Scale bar is 5 μM. Data are representative of at least two biological replicates.

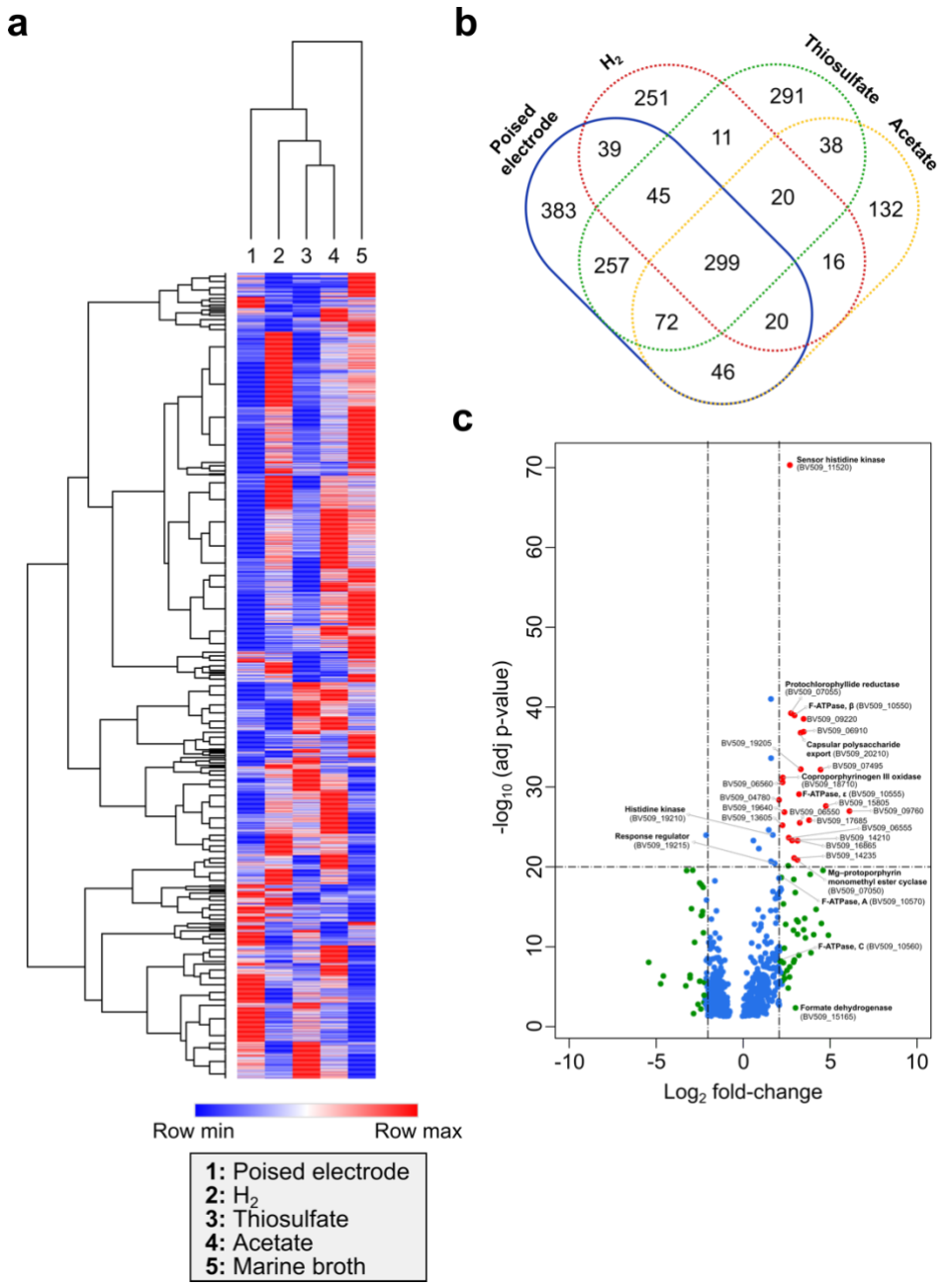

Figure 3.3. Identification of EEU-specific differentially expressed genes. (a) Hierarchical clustering of expression values (mean fragments per kilobase of transcript per million mapped reads, FPKM) of each condition (columns) for all 4077 genes (rows) in the AB26 genome. (b) Venn diagram of differentially expressed genes. (c) Genes specifically differentially expressed

during EEU. Blue denotes genes with a $P \leq 0.05$. Green denotes genes with a $P \leq 0.05$ and $\log_2$ fold-change ≥ 2. Red denotes genes with a $P \leq 10^{-20}$ and a $\log_2$ fold-change ≥ 2. Data are the average of at least three biological replicates.

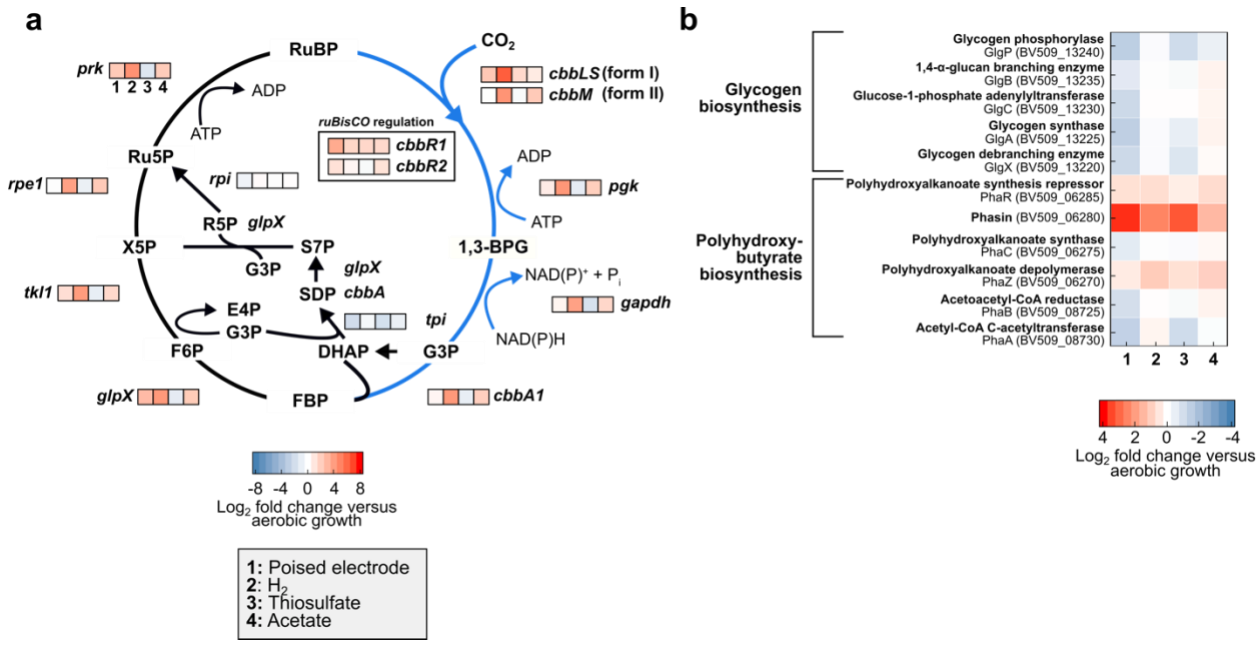

Figure 3.4. Expression analysis of carbon fixation and storage pathways. (a) Expression analysis of genes encoding the Calvin-Benson-Bassham cycle and (b) potential carbon storage pathways in the genome. RuBP (Ribulose 1,5-bisphosphate), 1,3 BPG (1,3-bisphosphoglycerate), G3P (Glyceraldehyde 3- phosphate), FBP (Fructose 1,6-bisphosphate), F6P (Fructose 6-phosphate), X5P (Xylulose 5-phosphate), Ru5P (Ribulose 5-phosphate) and R5P (Ribose 5- phosphate). Data are the average of at least three biological replicates.

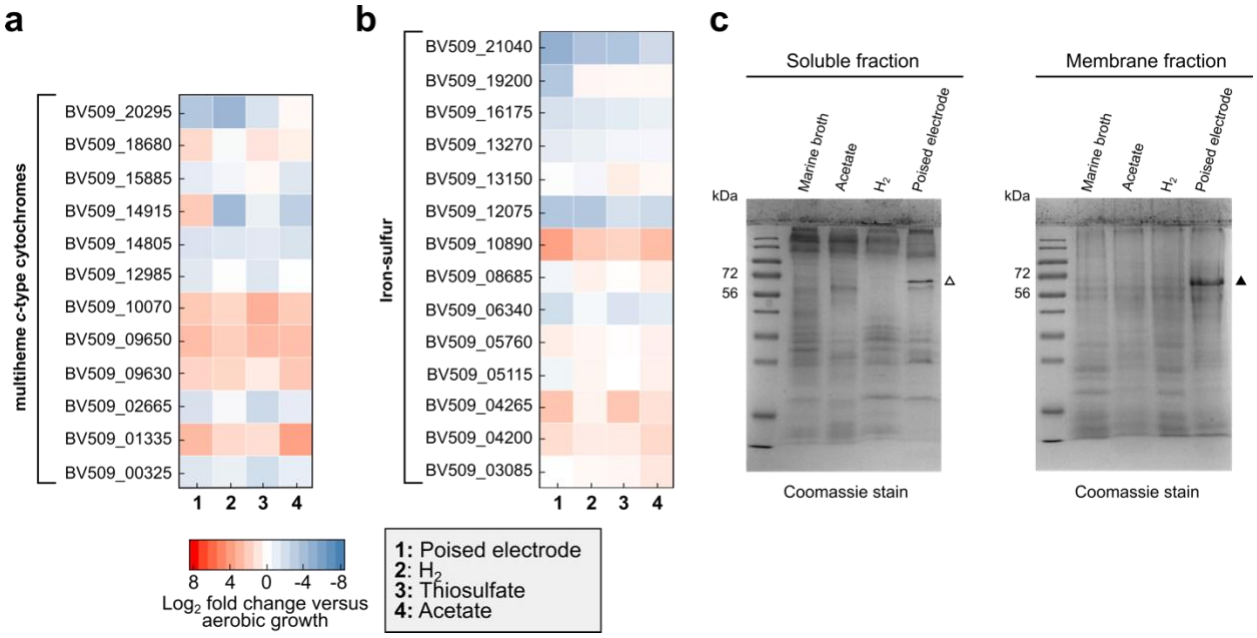

Figure 3.5. Expression of electron-transfer proteins under phototrophic conditions.

Expression analysis of (a) multiple *c*-type cytochromes and (b) iron-sulfur cluster genes in the AB26 transcriptome. Data are the average of at least three biological replicates. (c) Total protein (soluble and insoluble fraction) from AB26 cells cultivated under different phototrophic conditions. Mass spectrometry analysis was performed on the bands denoted by the open triangle (soluble fraction) and closed triangle (membrane fraction).

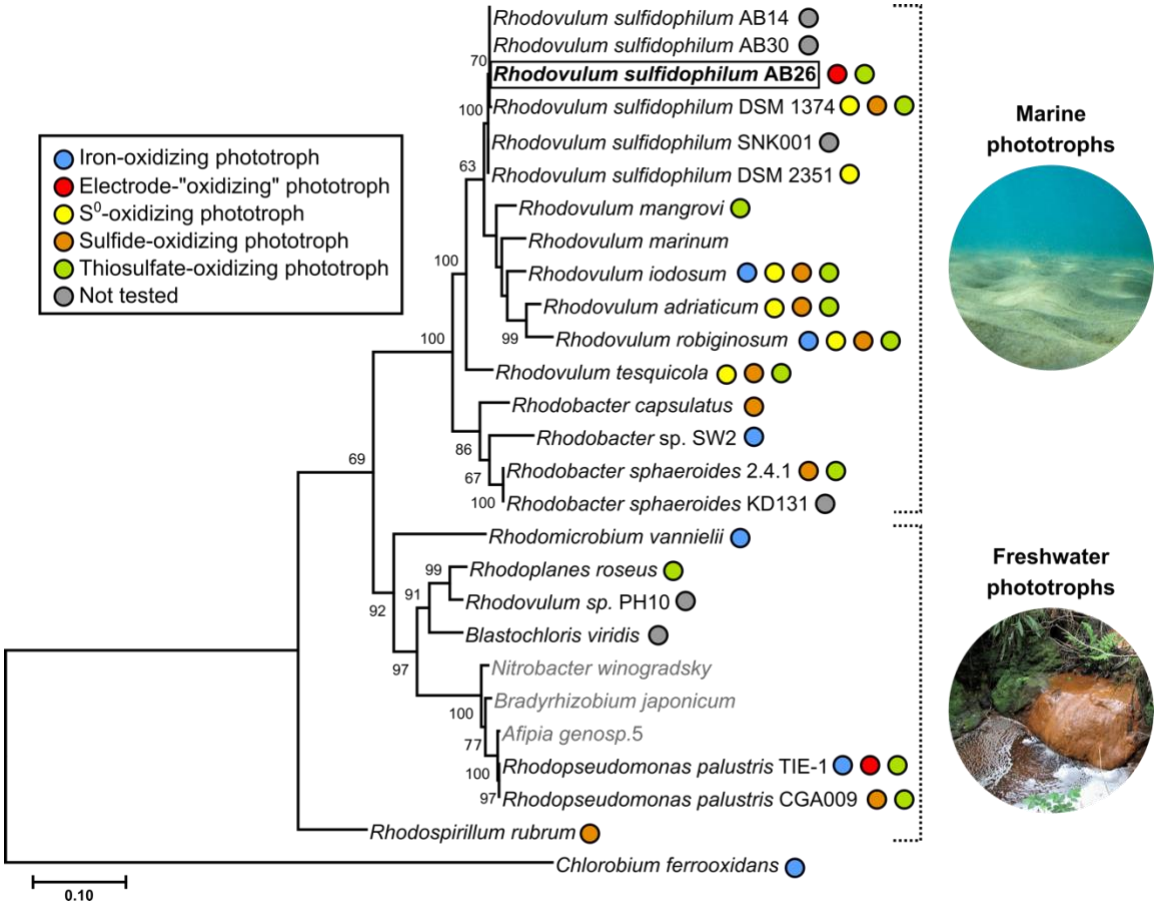

Figure 3.6. Phylogenetic and metabolic diversity of PNSB related to AB26. Maximum likelihood analysis of the 16S rRNA gene sequences of purple nonsulfur and related bacteria from marine and freshwater environments. *C. ferrooxidans* was used as an outgroup. Non-phototrophic Alphaproteobacteria (included for comparison) are noted in grey. Scale bar represents amino acid substitutions.

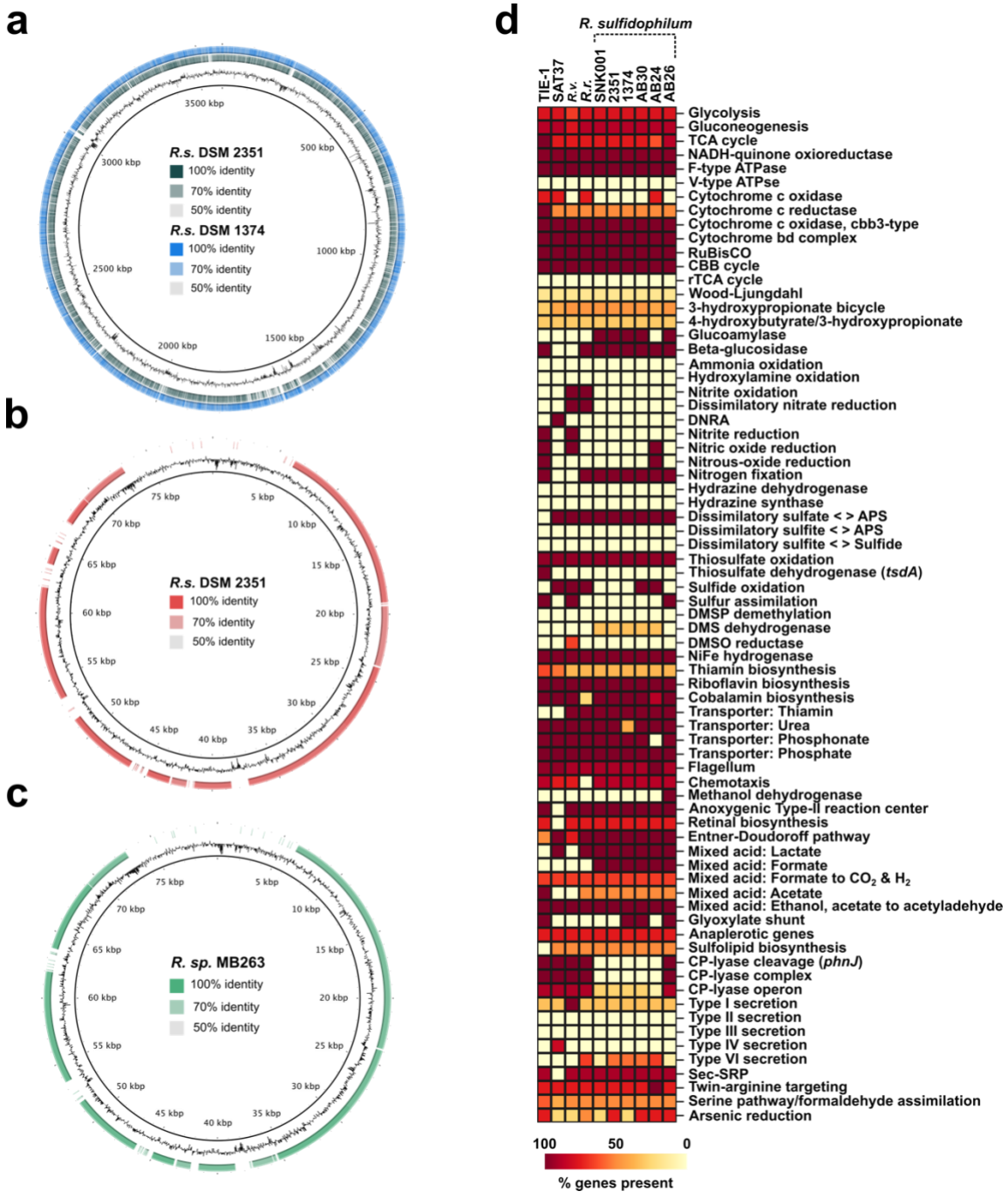
a
R.s. DSM 2351
100% identity
70% identity
50% identity
R.s. DSM 1374
100% identity
70% identity
50% identity
b
R.s. DSM 2351
100% identity
70% identity
50% identity
c
R. sp. MB263
100% identity
70% identity
50% identity
d
R. sulfidophilum
TIE-1
SAT37
R.v.
R.r.
SNK001
2351
1374
AB30
AB24
AB26
Glycolysis
Gluconeogenesis
TCA cycle
NADH-quinone oxioreductase
F-type ATPase
V-type ATPse
Cytochrome c oxidase
Cytochrome c reductase
Cytochrome c oxidase, cbb3-type
Cytochrome bd complex
RuBisCO
CBB cycle
rTCA cycle
Wood-Ljungdahl
3-hydroxypropionate bicycle
4-hydroxybutyrate/3-hydroxypropionate
Glucoamylase
Beta-glucosidase
Ammonia oxidation
Hydroxylamine oxidation
Nitrite oxidation
Dissimilatory nitrate reduction
DNRA
Nitrite reduction
Nitric oxide reduction
Nitrous-oxide reduction
Nitrogen fixation
Hydrazine dehydrogenase
Hydrazine synthase
Dissimilatory sulfate < > APS
Dissimilatory sulfite < > APS
Dissimilatory sulfite < > Sulfide
Thiosulfate oxidation
Thiosulfate dehydrogenase (tsdA)
Sulfide oxidation
Sulfur assimilation
DMSP demethylation
DMS dehydrogenase
DMSO reductase
NiFe hydrogenase
Thiamin biosynthesis
Riboflavin biosynthesis
Cobalamin biosynthesis
Transporter: Thiamin
Transporter: Urea
Transporter: Phosphonate
Transporter: Phosphate
Flagellum
Chemotaxis
Methanol dehydrogenase
Anoxygenic Type-II reaction center
Retinal biosynthesis
Entner-Doudoroff pathway
Mixed acid: Lactate
Mixed acid: Formate
Mixed acid: Formate to CO2 & H2
Mixed acid: Acetate
Mixed acid: Ethanol, acetate to acetyladehyde
Glyoxylate shunt
Anaplerotic genes
Sulfolipid biosynthesis
CP-lyase cleavage (phnJ)
CP-lyase complex
CP-lyase operon
Type I secretion
Type II secretion
Type III secretion
Type IV secretion
Type VI secretion
Sec-SRP
Twin-arginine targeting
Serine pathway/formaldehyde assimilation
Arsenic reduction
100
50
0
% genes present

Figure 3.7. Comparative genomics and metabolic potential of *Rhodovulum* species. (a-c) Genome alignments of species related to AB26. (a) Chromosome I. (b) Plasmid 3. (c) Plasmid 4. The inner-most ring represents the AB26 sequence. (d) Comparative metabolic pathway analysis of AB26 compared to related phototrophic bacteria. A description of the metabolic pathway definitions used in this analysis can be found in the methods. AB26 (*Rhodovulum sulfidophilum* AB26), AB24 (*Rhodovulum sulfidophilum* AB24), AB30 (*Rhodovulum sulfidophilum* AB30), 1374 (*Rhodovulum sulfidophilum* DSM 1372), 2351 (*Rhodovulum sulfidophilum* DSM 2351), SNK001 (*Rhodovulum sulfidophilum* SNK001), *R.r* (*Rhodovulum robiginosum*), *R.v.* (*Rhodomicrobium vannielii*), SAT37 (*Rhodovulum* sp. SAT37), TIE-1 (*Rhodopseudomonas palustris* TIE-1).

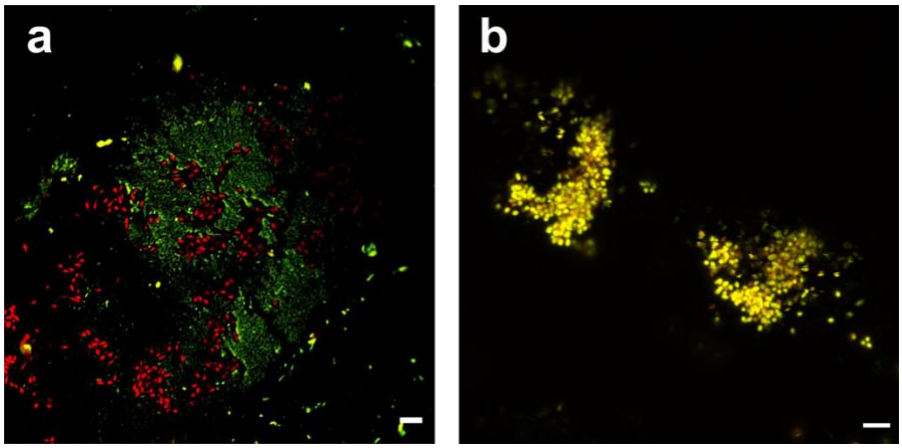

Supplementary Figure 3.1. Fluorescent micrographs of exopolysaccharide and protein staining of AB26 biofilms. (**a**) Biofilms stained with Concanavalin A (green) for labeling exopolysaccharides and RedoxSensor Red to denote cells. (**b**) Biofilms stained with SYPRO (red) for labeling proteins and SYTO9 to denote cells. Scale bars are 5 μm.

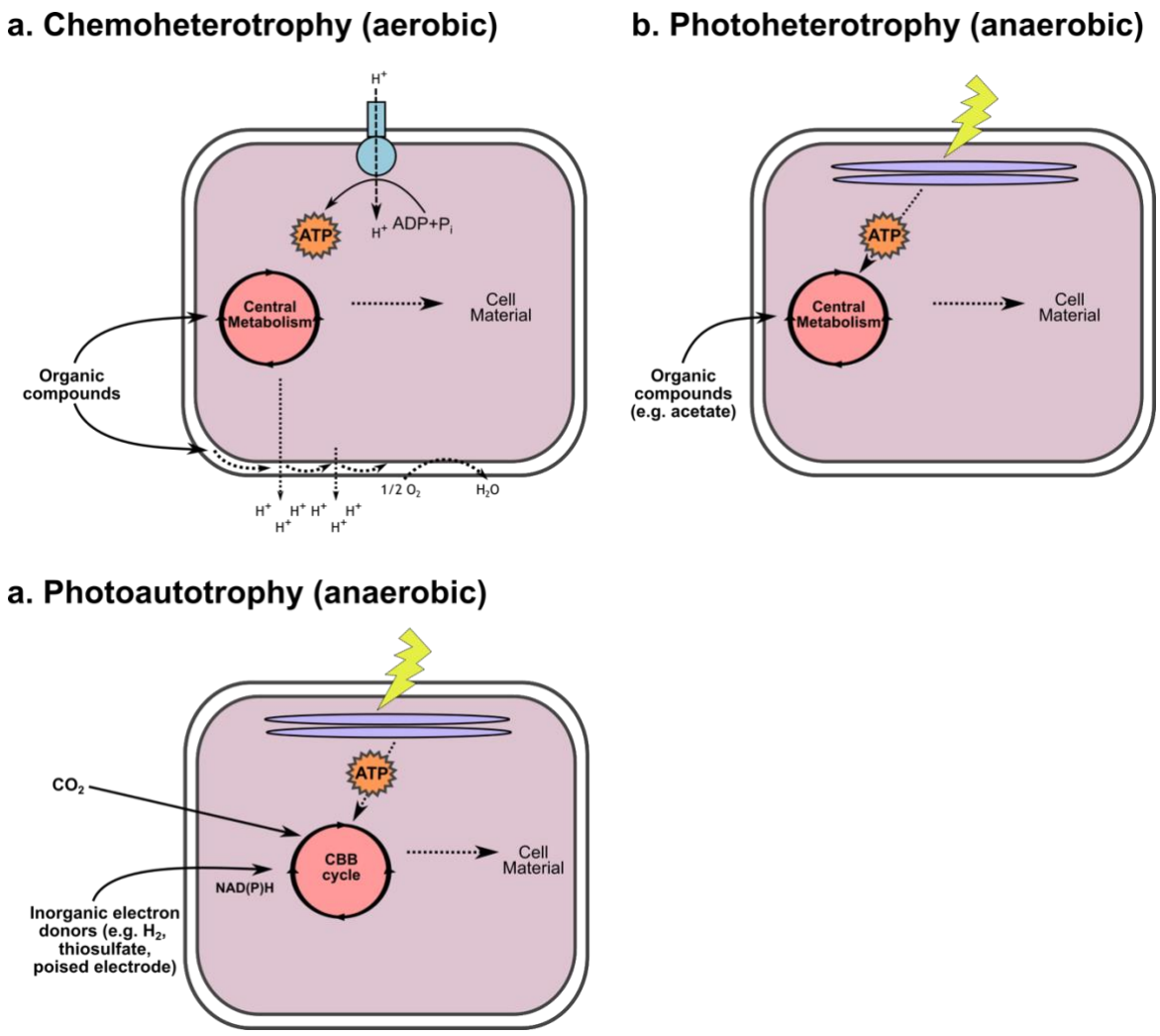

Supplementary Figure 3.2. Metabolic versatility of AB26. (a) aerobic chemoheterotrophic, (b) anaerobic photoheterotrophic, and (c) anaerobic photoautotrophic growth. AB26 can utilize a variety of unconventional electron donors to drive anoxygenic photoautotrophic growth, including H_2 and reduced sulfur compounds (e.g. thiosulfate, sulfide).

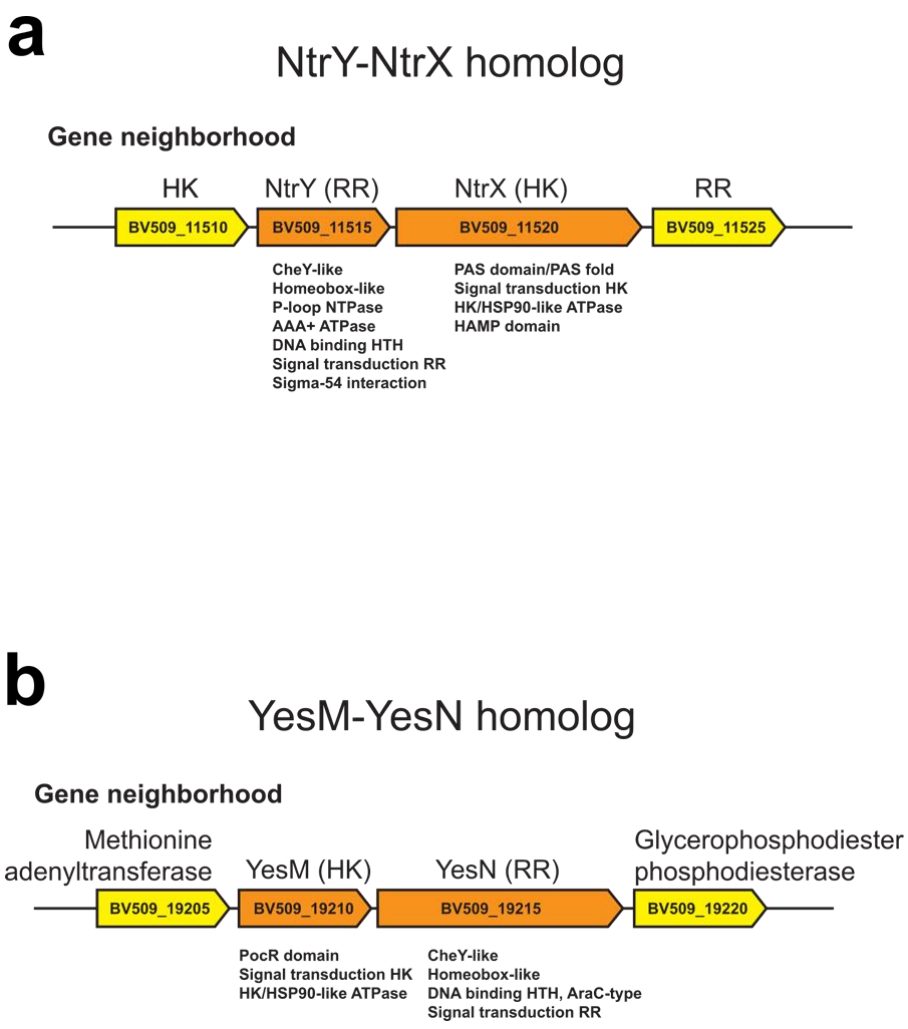

Supplementary Figure 3.3. InterPro domain analysis of two-component systems (TCS). Gene organization and InterPro domain analysis of TCS specifically upregulated during phototrophic extracellular electron uptake (EEU). Locus tags are noted within each open-reading frame (ORF). Names above the ORFs are the top BLAST hits and below each (bold) are the InterPro domains identified.

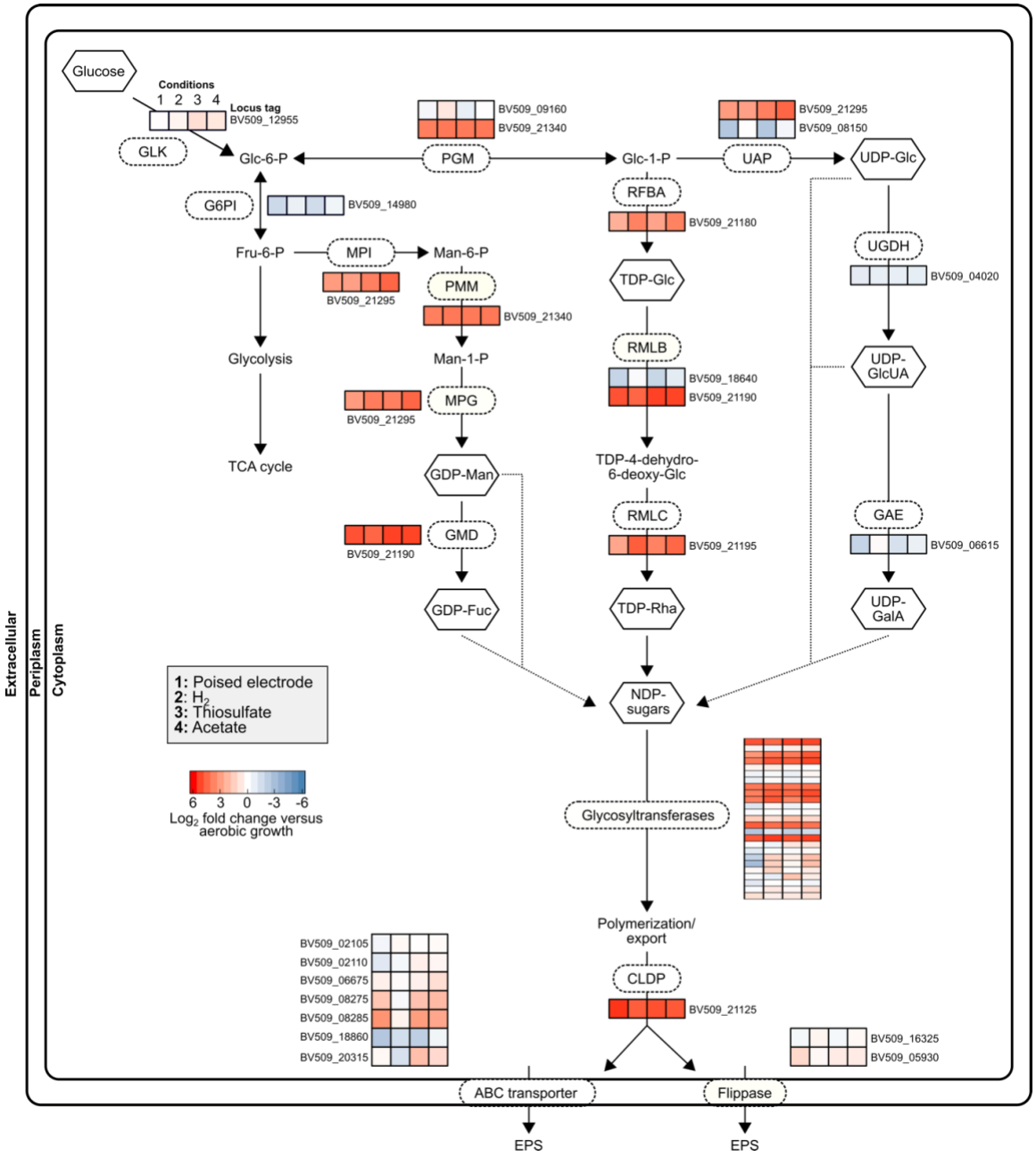

Supplementary Figure 3.4. Putative exopolysaccharide (EPS) biosynthetic pathway. EPS pathway predicted using KEGG, GO, and IPS assignments. Expression data is shown as heatmaps below the enzymes. GLK (glucokinase), G6PI (glucose-6-phosphate isomerase), MPI (mannose-6-phosphate isomerase), PMM (phosphomannomutase), MPG (mannose-1-phosphate guanyltransferase), GMD (GDP-mannose 4,6-dehydratase), CLDP (chain-length determining

protein), PGM (phosphoglycerate mutase), RFBA (glucose-1-phosphate thymidylyltransferase), RMLB (dTDP-D-glucose 4,6- dehydratase), RMLC (dTDP-4-dehydrorhamnose 3,5-epimerase), UAP (UDP-N-acetylglucosamine pyrophosphorylase), UGDH (UDP-glucose 6-dehydrogenase), GAE (UDP-d-glucuronic acid 4-epimerase).

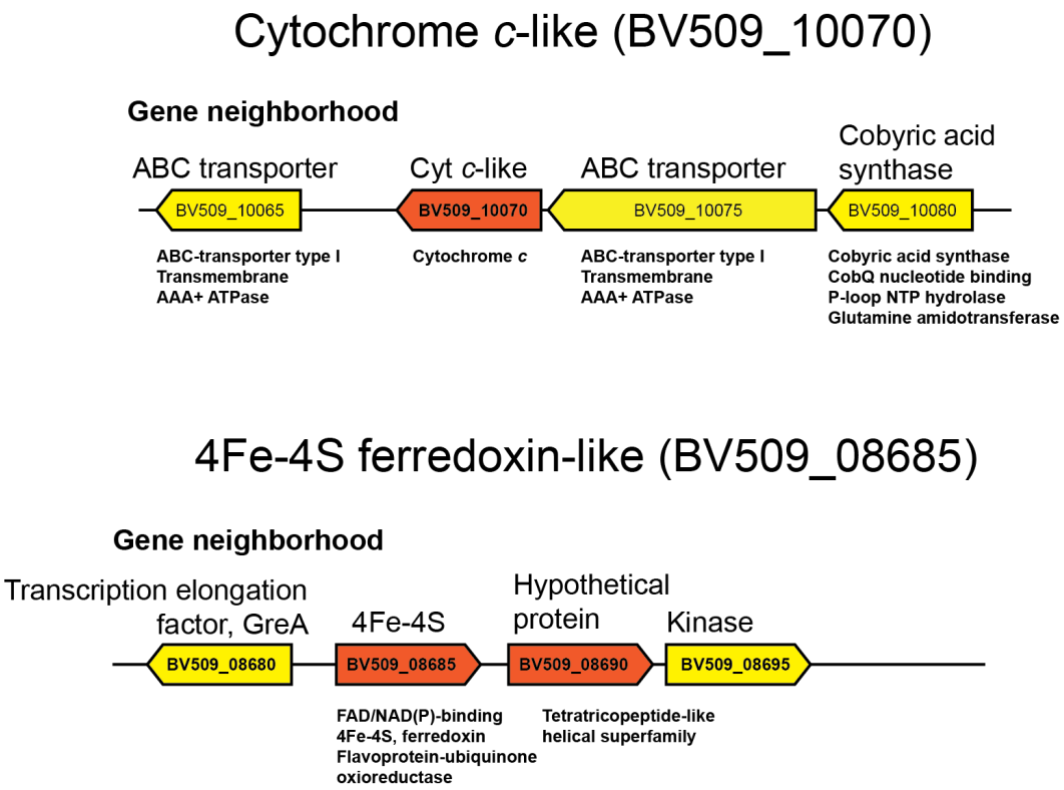

Supplementary Figure 3.5. InterPro domain analysis of top electron transfer proteins identified via mass spectrometry. Gene organization and InterPro domain analysis of electron transfer proteins. Locus tags are noted within each open-reading frame (ORF). Names above the ORFs are the top BLAST hits and below each (bold) are the InterPro domains identified.

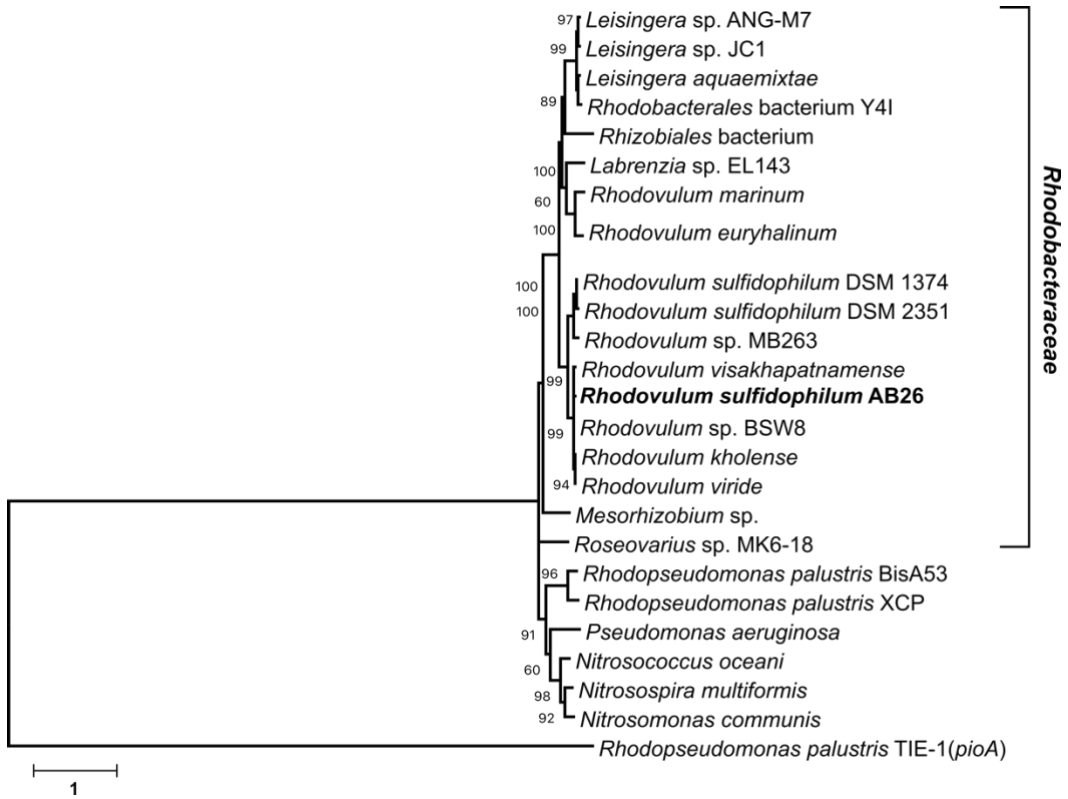

Supplementary Figure 3.6. Phylogenetic analysis of BV509_10070. Maximum likelihood analysis (Whelan And Goldman +G model, (+G, parameter = 0.5384)) of BV509_10070 and related gene sequences. The *pioA* gene from *R. palustris* TIE-1 was used as an outgroup. Scale bar represents amino acid substitutions. The tree with the highest log likelihood (-9413.60) is shown. Tree is representative of 100 replicate trees. Bootstrap values <100 were omitted from the tree. All positions containing gaps and missing data were eliminated (complete deletion option). There is a total of 434 positions in the final dataset. Tree was constructed in MEGA X[82].

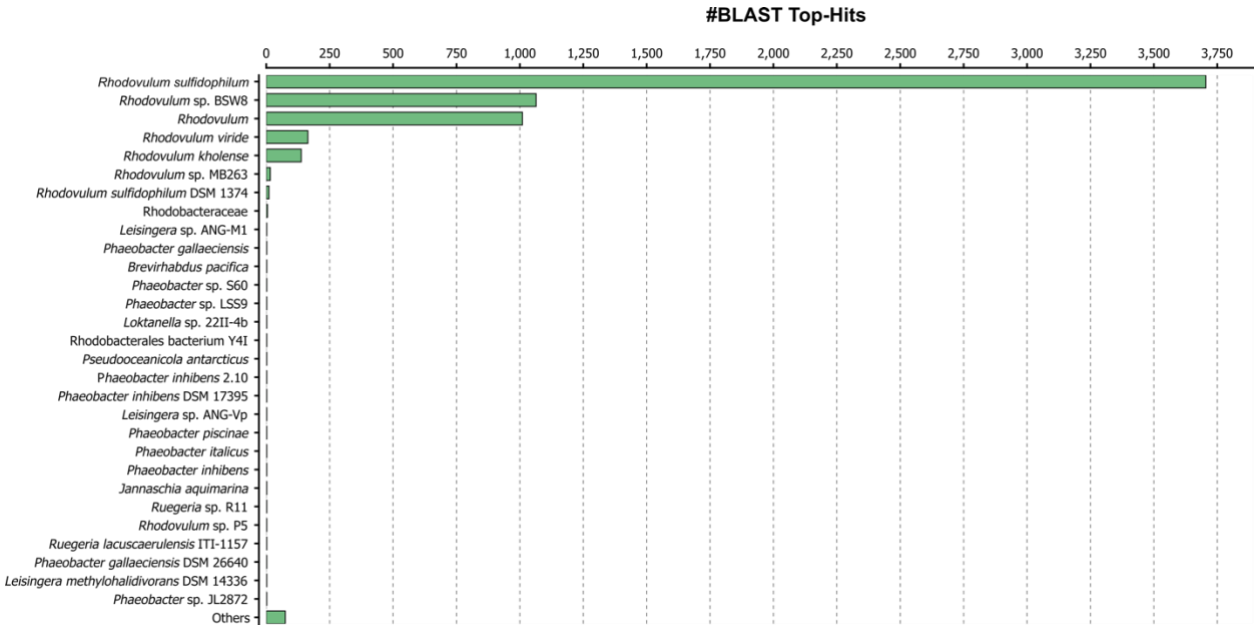

Supplementary Figure 3.7. Species distribution of top BLAST hits. Top NCBI BLAST hits for all proteins in the AB26 genome. Analysis was performed in Blast2GO.

Supplementary Table 3.1. Doubling time (hours) under aerobic and anaerobic growth conditions for AB26. Aerobic chemoheterotrophic (marine broth), photoheterotrophic (acetate), and photoautotrophic (molecular hydrogen (H_2) and thiosulfate) growth. Data are means ± s.e. of three biological replicates.

Growth condition	**Doubling time (h) ± s.e.**
Marine broth	33 ± 0.67
Acetate	3.1 ± 0.11
H_2	21 ± 1.78
Thiosulfate	14 ± 0.21

Supplementary Table 3.2. RNA-Sequencing libraries and NCBI accession numbers.

Library	No. of reads	NCBI accession no.
EEU_1	18,096,180	SRR9335485
EEU_2	25,301,577	SRR9335486
EEU_3	14,402,767	SRR9335487
EEU_4	9,363,447	SRR9335488
EEU_5	7,976,329	SRR9335481
H2_1	19,276,638	SRR9335482
H2_2	15,261,784	SRR9335483
H2_3	15,261,646	SRR9335484
H2_4	21,641,589	SRR9335479
Thiosulfate_1	15,563,689	SRR9335477
Thiosulfate_2	15,928,634	SRR9335478
Thiosulfate_3	19,422,056	SRR9335489
Thiosulfate_4	20,705,340	SRR9335490
Acetate_1	13,481,805	SRR9335493
Acetate_2	24,775,453	SRR9335494
Acetate_3	14,738,639	SRR9335475
Acetate_4	23,880,256	SRR9335476
Marine_broth_1	12,882,332	SRR9335480
Marine_broth_2	16,207,138	SRR9335491
Marine_broth_3	26,980,010	SRR9335492

Supplementary Table 3.3. Predicted CO_2 fixation cycle in the AB26 genome.

Annotation	Locus tag
RuBisCO form I small subunit (CbbS)	BV509_05520
RuBisCO form I large subunit (CbbL)	BV509_05525
RuBisCO activation protein (CbbO)	BV509_05510
RuBisCO activation protein (CbbQ)	BV509_05515
RuBisCO operon transcriptional regulator (CbbR)	BV509_05530
RuBisCO operon transcriptional regulator (CbbR)	BV509_15210
Fructose-bisphosphatase class I (Fbp)	BV509_15215
Phosphoribulokinase (PrK)	BV509_15220
Transketolase (Tkl)	BV509_15225
Glyceraldehyde-3-phosphate dehydrogenase (GAPDH)	BV509_15230
Phosphoglycerate kinase (Pgk)	BV509_15235
Fructose-bisphosphate aldolase class II (Fba)	BV509_15240
RuBisCO form II (CbbM)	BV509_15245
Ribulose-phosphate 3-epimerase (Rpe)	BV509_15250
Ribose-5-phosphate isomerase (Rpi)	BV509_06305
Triosephosphate isomerase (Tpi)	BV509_11205

Supplementary Table 3.4. Predicted multiheme *c*-type cytochromes in the AB26 genome.

Annotation	Locus tag	No. of CXXCH domains	No. of residues	Predicted molecular mass (kDa)
Hypothetical protein	BV509_15885	4	615	63
Cytochrome *c* (PufC)	BV509_00325	3	355	39
Cytochrome *c* family protein	BV509_01335	2	203	21
Cytochrome *c* peroxidase	BV509_02665	2	369	39
Cytochrome *c* family protein (SoxA)	BV509_09630	2	287	31
Cytochrome *c* family protein	BV509_09650	2	238	26
Cytochrome *c*	BV509_10070	2	573	61
Cytochrome *c* family protein	BV509_12985	2	472	49
Cytochrome *c* peroxidase	BV509_14915	2	347	37
Cytochrome *c* oxidase (Cbb3-Cox)	BV509_18680	2	295	32
Cytochrome *c* peroxidase	BV509_20295	2	439	46
Methylamine utilization protein (MauG)	BV509_14805	2	385	41

Supplementary Table 3.5. Predicted iron-sulfur proteins in the AB26 genome.

Annotation	Locus tag	No. of residues	Predicted molecular mass (kDa)
4Fe-4S ferrodoxin-like	BV509_05760	430	46
4Fe-4S ferrodoxin-like	BV509_10890	551	60
4Fe-4S ferrodoxin-like	BV509_13150	447	47
4Fe-4S ferrodoxin-like	BV509_19200	306	33
4Fe-4S ferrodoxin-like	BV509_04265	386	44
4Fe-4S ferrodoxin-like	BV509_08685	550	60
2Fe-2S ferrodoxin-like	BV509_03085	358	39
2Fe-2S ferrodoxin-like	BV509_04200	99	11
2Fe-2S ferrodoxin-like	BV509_05115	124	14
2Fe-2S ferrodoxin-like	BV509_06340	108	12
2Fe-2S ferrodoxin-like	BV509_12075	681	71
2Fe-2S ferrodoxin-like	BV509_13270	100	10
2Fe-2S ferrodoxin-like	BV509_16175	471	50
2Fe-2S ferrodoxin-like	BV509_21040	359	39

Supplementary Table 3.6. Top 20 hits for total protein mass spectrometry of EEU-specific band from the soluble fraction.

				Soluble fraction		Membrane fraction	
Annotation (NCBI)	**Locus tag**	**GenBank accession no.**	**Molecular weight (kDa)**	**Total spectral count**	**Coverage (%)**	**Total spectral count**	**Coverage (%)**
PQQ-dependent dehydrogenase, methanol/ethanol family	BV509_20585	OLS42326.1	70	898	84%	711	94%
ABC transporter substrate-binding protein	BV509_13840	OLS45310.1	64	298	90%	59	66%
Peptide ABC transporter substrate-binding protein	BV509_01545	OLS46536.1	58	173	73%	48	59%
Chaperonin GroL	BV509_18440	OLS46134.1	58	132	89%	420	100%
Peptidoglycan-binding protein	BV509_06420	OLS44012.1	62	96	89%	25	62%
Phosphoenolpyruvate carboxykinase (ATP)	BV509_04720	OLS43704.1	59	82	89%	58	84%
Arginine--tRNA ligase	BV509_14370	OLS45400.1	63	77	76%	23	51%
Translation elongation factor Tu	BV509_04910	OLS43737.1	47	75	90%	34	68%
[NiFe] hydrogenase large subunit	BV509_06125	OLS43955.1	66	71	64%	69	61%
Trigger factor	BV509_15810	OLS46758.1	49	69	67%	84	76%
Xanthine dehydrogenase	BV509_15045	OLS45523.1	81	68	70%	3	5%
X-Pro aminopeptidase	BV509_15660	OLS45638.1	65	66	74%	32	43%
Dihydroxy-acid dehydratase	BV509_11925	OLS44980.1	64	63	66%	27	53%
MaoC family dehydratase	BV509_16470	OLS45789.1	37	56	80%	4	15%
Aspartate--tRNA ligase	BV509_07060	OLS44112.1	67	55	61%	28	39%
4-hydroxy-tetrahydrodipicolinate synthase	BV509_02925	OLS43382.1	31	55	80%	2	10%
Acyl-CoA dehydrogenase	BV509_16055	OLS45708.1	64	53	63%	47	59%
Cytochrome *c*	BV509_10070	OLS44651.1	61	51	59%	66	77%
4Fe-4S ferredoxin-like protein	BV509_08685	OLS44409.1	60	47	66%	40	60%
Methanol dehydrogenase	BV509_20600	OLS42329.1	11	47	72%	4	45%

Supplementary Table 3.7. Top 20 hits for total protein mass spectrometry of EEU-specific band from the membrane fraction.

				Soluble fraction		Membrane fraction	
Annotation (NCBI)	**Locus tag**	**GenBank accession no.**	**Molecular weight (kDa)**	**Total spectral count**	**Coverage (%)**	**Total spectral count**	**Coverage (%)**
PQQ-dependent dehydrogenase, methanol/ethanol family	BV509_20585	OLS42326.1	70	898	84%	711	94%
Chaperonin GroL	BV509_18440	OLS46134.1	58	132	89%	420	100%
30S ribosomal protein S1	BV509_16980	OLS45881.1	62	36	53%	119	82%
F_0F_1 ATP synthase subunit alpha	BV509_06725	OLS44065.1	55	23	43%	106	79%
Trigger factor	BV509_15810	OLS46758.1	49	69	67%	84	76%
[NiFe] hydrogenase large subunit	BV509_06125	OLS43955.1	66	71	64%	69	61%
F_0F_1 ATP synthase subunit beta	BV509_06735	OLS44067.1	51	26	77%	67	96%
Chaperonin GroL	BV509_03350	OLS43452.1	58	No data	No data	67	48%
Cytochrome *c*	BV509_10070	OLS44651.1	61	51	59%	66	77%
Transketolase	BV509_15225	OLS45558.1	70	45	69%	65	78%
MBL fold hydrolase	BV509_15415	OLS45594.1	61	19	43%	65	74%
Chaperonin GroL	BV509_11245	OLS44854.1	57	No data	No data	65	43%
ATP-dependent RNA helicase	BV509_01475	OLS43142.1	107	23	24%	63	35%
PQQ-dependent dehydrogenase, methanol/ethanol family	BV509_04555	OLS43675.1	65	29	51%	61	61%
ABC transporter substrate-binding protein	BV509_13840	OLS45310.1	64	298	90%	59	66%
Phosphoenolpyruvate carboxykinase	BV509_04720	OLS43704.1	59	82	89%	58	84%
Methylmalonyl-CoA carboxyltransferase	BV509_07515	OLS44197.1	56	2	4%	57	62%
Heme peroxidase-domain protein	BV509_18580	OLS46158.1	63	4	9%	55	72%
Dihydroxy-acid dehydratase	BV509_12515	OLS45082.1	64	32	57%	54	68%
Dihydrolipoamide succinyltransferase	BV509_03465	OLS43474.1	53	5	15%	54	64%

Supplementary Table 3.8. Detection of sulfur oxidation (Sox) proteins in the membrane/soluble fraction.

				Soluble fraction		Membrane fraction	
Annotation	**Locus tag**	**GenBank accession no.**	**Molecular weight (kDa)**	**Total spectral count**	**Percent coverage**	**Total spectral count**	**Percent coverage**
Flavocytochrome C	BV509_09655	OLS44573.1	45 kDa	24	51%	5	10%
Flavocytochrome C	BV509_09655	OLS44573.1	45 kDa	24	51%	5	10%
Quinoprotein dehydrogenase-associated SoxYZ-	BV509_04530	OLS43670.1	29 kDa	3	13%	No data	No data
Sulfur oxidation c-type cytochrome SoxA	BV509_09630	OLS44568.1	31 kDa	7	29%	No data	No data
Sulfur oxidation c-type cytochrome SoxA	BV509_09630	OLS44568.1	31 kDa	7	29%	No data	No data
Thiosulfate oxidation carrier complex protein	BV509_09625	OLS44567.1	12 kDa	3	30%	No data	No data
Thiosulfate oxidation carrier protein SoxY	BV509_09620	OLS44566.1	14 kDa	4	24%	No data	No data
Thiosulfohydrolase SoxB	BV509_09635	OLS44569.1	61 kDa	No data	No data	2	3.20%

3.7 References

1. Kirchman, D. L. *Processes in Microbial Ecology* 55-78 (Oxford University Press, 2018).

2. Byrne, J.M., Klueglein, N., Pearce, C., Rosso, K.M., Appel, E. & Kappler, A. Redox cycling of Fe(II) and Fe(III) in magnetite by Fe-metabolizing bacteria. *Science* **347**, 1473-1476 (2015).

3. Byrne, J.M., Van Der Laan, G., Figueroa, A.I., Qafoku, O., Wang, C., Pearce, C.I., Jackson, M., Feinberg, J., Rosso, K.M. & Kappler, A. Size dependent microbial oxidation and reduction of magnetite nano-and micro-particles. *Sci. Rep.* **6**, 30969 (2016).

4. Wu, W., Swanner, E.D., Hao, L., Zeitvogel, F., Obst, M., Pan, Y. & Kappler, A. Characterization of the physiology and cell–mineral interactions of the marine anoxygenic phototrophic Fe(II) oxidizer *Rhodovulum iodosum*–implications for Precambrian Fe (II) oxidation. *FEMS Microbiol. Ecol.* **88**, 503-515 (2014).

5. Hernandez, M. & Newman, D. Extracellular electron transfer. *Cell. Mol. Life Sci.* **58**, 1562-1571 (2001).

6. Kondo, K., Okamoto, A., Hashimoto, K. & Nakamura, R. Sulfur-mediated electron shuttling sustains microbial long-distance extracellular electron transfer with the aid of metallic iron sulfides. *Langmuir* **31**, 7427-7434 (2015).

7. Hunter, C. N., Daldal, F., Thurnauer, M. C. & Beatty, J. T. *The Purple Phototrophic Bacteria*. Vol. 28 (Springer Science & Business Media, 2008).

8. Bose, A., Gardel, E.J., Vidoudez, C., Parra, E.A. & Girguis, P.R. Electron uptake by iron-oxidizing phototrophic bacteria. *Nat. Commun.* **5**, 3391 (2014).

9. Ha, P.T., Lindemann, S.R., Shi, L., Dohnalkova, A.C., Fredrickson, J.K., Madigan, M.T. & Beyenal, H. Syntrophic anaerobic photosynthesis via direct interspecies electron transfer. *Nat. Commun.* **8**, 13924 (2017).

10. Guzman, M.S., Rengasamy, K., Binkley, M.M., Jones, C., Ranaivoarisoa, T.O., Singh, R., Fike, D.A., Meacham, J.M. & Bose, A. Phototrophic extracellular electron uptake is linked to carbon dioxide fixation in the bacterium *Rhodopseudomonas palustris*. *Nat. Commun.* **10**, 1355 (2019).

11. Nealson, K.H. & Saffarini, D. Iron and manganese in anaerobic respiration: environmental significance, physiology, and regulation. *Annu. Rev. of Microbiol.* **48**, 311-343 (1994).

12. Rabaey, K., Rodriguez, J., Blackall, L.L., Keller, J., Gross, P., Batstone, D., Verstraete, W. & Nealson, K.H. Microbial ecology meets electrochemistry: electricity-driven and driving communities. *ISME J.* **1**, 9-18 (2007).

13. Schimmelmann, A. & Kastner, M. Evolutionary changes over the last 1000 years of reduced sulfur phases and organic carbon in varved sediments of the Santa Barbara Basin, California. *Geochim. Cosmochim. Acta* **57**, 67-78 (1993).

14. Chang, R., Bird, L., Barr, C., Osburn, M., Wilbanks, E., Nealson, K. and Rowe, A. *Thioclava electrotropha* sp. nov., a versatile electrode and sulfur-oxidizing bacterium from marine sediments. *Int. J. Syst. Evol. Microbiol.* (2018).

15. Lam, B. R., Rowe, A. R. & Nealson, K. H. Variation in electrode redox potential selects for different microorganisms under cathodic current flow from electrodes in marine sediments. *Environ. Microbiol.* **20**, 2270-2287 (2018).

16. Rowe, A.R., Chellamuthu, P., Lam, B., Okamoto, A. & Nealson, K.H. Marine sediments microbes capable of electrode oxidation as a surrogate for lithotrophic insoluble substrate metabolism. *Front. Microbiol.* **5**, 784 (2014).

17. Rabaey, K. & Rozendal, R.A. Microbial electrosynthesis—revisiting the electrical route for microbial production. *Nat. Rev. Microbiol.* **8**, 706 (2010).

18. Aghababaie, M., Farhadian, M., Jeihanipour, A. & Biria, D. Effective factors on the performance of microbial fuel cells in wastewater treatment–a review. *Environ. Technol. Rev.* **4**, 71-89 (2015).

19. Shi, L., Dong, H., Reguera, G., Beyenal, H., Lu, A., Liu, J., Yu, H.Q. & Fredrickson, J.K. Extracellular electron transfer mechanisms between microorganisms and minerals. *Nat. Rev. Microbiol.* **14**, 651-662 (2016).

20. Friedebold, J. & Bowien, B. Physiological and biochemical characterization of the soluble formate dehydrogenase, a molybdoenzyme from Alcaligenes eutrophus. *J. Bacteriol.* **175**, 4719-4728 (1993).

21. Mota, C.S., Rivas, M.G., Brondino, C.D., Moura, I., Moura, J.J., González, P.J. & Cerqueira, N.M. The mechanism of formate oxidation by metal-dependent formate dehydrogenases. *J. Biol. Inorg. Chem.* **16**, 1255-1268 (2011).

22. Reda, T., Plugge, C. M., Abram, N. J. & Hirst, J. Reversible interconversion of carbon dioxide and formate by an electroactive enzyme. *Proc. Natl. Acad. Sci. USA* **105**, 10654-10658 (2008).

23. Hartmann, T. & Leimkühler, S. The oxygen-tolerant and NAD^+-dependent formate dehydrogenase from *Rhodobacter capsulatus* is able to catalyze the reduction of CO_2 to formate. *FEBS J.* **280**, 6083-6096 (2013).

24. Alissandratos, A., Kim, H.K., Matthews, H., Hennessy, J.E., Philbrook, A. & Easton, C.J. *Clostridium carboxidivorans* strain P7T recombinant formate dehydrogenase catalyzes reduction of CO_2 to formate. *Appl. Environ. Microbiol.* **79**, 741-744 (2013).

25. Rusching, U., Müller, U., Willnow, P. & Höpner, T. CO_2 reduction to formate by NADH catalysed by formate dehydrogenase from *Pseudomonas oxalaticus*. *Eur. J. Biochem.* **70**, 325-330 (1976).

26. Chen, X., Cao, Y., Li, F., Tian, Y. & Song, H. Enzyme-assisted microbial electrosynthesis of poly (3-hydroxybutyrate) via CO_2 bioreduction by engineered *Ralstonia eutropha*. *ACS Catal.* **8**, 4429-4437 (2018).

27. Deutzmann, J.S., Sahin, M. & Spormann, A.M. Extracellular enzymes facilitate electron uptake in biocorrosion and bioelectrosynthesis. *MBio* **6**, e00496-00415 (2015).

28. Zschiedrich, C. P., Keidel, V. & Szurmant, H. Molecular mechanisms of two-component signal transduction. *J. Mol. Biol.* **428**, 3752-3775 (2016).

29. Carrica, M. d. C., Fernandez, I., Martí, M. A., Paris, G. & Goldbaum, F. A. The NtrY/X two-component system of *Brucella* spp. acts as a redox sensor and regulates the expression of nitrogen respiration enzymes. *Mol. Microbiol.* **85**, 39-50 (2012).

30. Drepper, T., Wiethaus, J., Giaourakis, D., Groß, S., Schubert, B., Vogt, M., Wiencek, Y., McEwan, A.G. & Masepohl, B. Cross-talk towards the response regulator NtrC controlling nitrogen metabolism in *Rhodobacter capsulatus*. *FEMS Microbiol. Lett.* **258**, 250-256 (2006).

31. Ishida, M.L., Assumpção, M.C., Machado, H.B., Benelli, E.M., Souza, E.M. and Pedrosa, F.O. Identification and characterization of the two-component NtrY/NtrX regulatory system in *Azospirillum brasilense*. *Braz. J. Med. Biol. Res.* **35**, 651-661 (2002).

32. Pawlowski, K., Klosse, U. & De Bruijn, F. Characterization of a novel *Azorhizobium caulinodans* ORS571 two-component regulatory system, NtrY/NtrX, involved in nitrogen fixation and metabolism. *Mol. Gener. Gen.* **231**, 124-138 (1991).

33. Fabret, C., Feher, V.A. & Hoch, J.A. Two-component signal transduction in Bacillus subtilis: how one organism sees its world. *J. Bacteriol.* **181**, 1975-1983 (1999).

34. Maddocks, S.E. & Oyston, P.C. Structure and function of the LysR-type transcriptional regulator (LTTR) family proteins. *Microbiology* **154**, 3609-3623 (2008).

35. Gibson, J.L. & Tabita, F.R. Nucleotide sequence and functional analysis of *cbbR*, a positive regulator of the Calvin cycle operons of *Rhodobacter sphaeroides*. *J. Bacteriol.* **175**, 5778-5784 (1993).

36. Joshi, G.S., Zianni, M., Bobst, C.E. & Tabita, F.R. Regulatory twist and synergistic role of metabolic coinducer-and response regulator-mediated CbbR-*cbb*$_I$ interactions in *Rhodopseudomonas palustris* CGA010. *J. Bacteriol.* **195**, 1381-1388 (2013).

37. Van Keulen, G., Girbal, L., Van Den Bergh, E., Dijkhuizen, L. & Meijer, W. The LysR-type transcriptional regulator CbbR controlling autotrophic CO_2 fixation by *Xanthobacter flavus* is an NADPH sensor. *J. Bacteriol.* **180**, 1411-1417 (1998).

38. Suriyamongkol, P., Weselake, R., Narine, S., Moloney, M. & Shah, S. Biotechnological approaches for the production of polyhydroxyalkanoates in microorganisms and plants—a review. *Biotechnol. Adv.* **25**, 148-175 (2007).

39. Verlinden, R. A., Hill, D.J., Kenward, M., Williams, C.D. & Radecka, I. Bacterial synthesis of biodegradable polyhydroxyalkanoates. *J. Appl. Microbiol.* **102**, 1437-1449 (2007).

40. Wilson, W.A., Roach, P.J., Montero, M., Baroja-Fernández, E., Muñoz, F.J., Eydallin, G., Viale, A.M. & Pozueta-Romero, J. Regulation of glycogen metabolism in yeast and bacteria. *FEMS Microbiol. Rev.* **34**, 952-985 (2010).

41. Zhang, Z., Chen, Y., Wang, R., Cai, R., Fu, Y. and Jiao, N. The fate of marine bacterial exopolysaccharide in natural marine microbial communities. *PloS ONE* **10**, e0142690 (2015).

42. Pötter, M. & Steinbüchel, A. Poly (3-hydroxybutyrate) granule-associated proteins: impacts on poly (3-hydroxybutyrate) synthesis and degradation. *Biomacromolecules* **6**, 552-560 (2005).

43. Schmid, J., Sieber, V. & Rehm, B. Bacterial exopolysaccharides: biosynthesis pathways and engineering strategies. *Front. Microbiol.* **6**, 496 (2015).

44. Cuthbertson, L., Mainprize, I.L., Naismith, J.H. & Whitfield, C. Pivotal roles of the outer membrane polysaccharide export and polysaccharide copolymerase protein families in export of extracellular polysaccharides in gram-negative bacteria. *Microbiol. Mol. Biol. Rev.* **73**, 155-177 (2009).

45. De Smet, L., Savvides, S.N., Van Horen, E., Pettigrew, G. & Van Beeumen, J.J. Structural and mutagenesis studies on the cytochrome *c* peroxidase from *Rhodobacter*

capsulatus provide new insights into structure-function relationships of bacterial di-heme peroxidases. *J. Biol. Chem.* **281**, 4371-4379 (2006).

46. Hartshorne, R.S., Reardon, C.L., Ross, D., Nuester, J., Clarke, T.A., Gates, A.J., Mills, P.C., Fredrickson, J.K., Zachara, J.M., Shi, L. and Beliaev, A.S. Characterization of an electron conduit between bacteria and the extracellular environment. *Proc. Natl. Acad. Sci. USA* **106**, 22169-22174 (2009).
47. Pirbadian, S., Barchinger, S.E., Leung, K.M., Byun, H.S., Jangir, Y., Bouhenni, R.A., Reed, S.B., Romine, M.F., Saffarini, D.A., Shi, L. and Gorby, Y.A. *Shewanella oneidensis* MR-1 nanowires are outer membrane and periplasmic extensions of the extracellular electron transport components. *Proc. Natl. Acad. Sci. USA* **111**, 12883-12888 (2014).

48. Reguera, G., McCarthy, K.D., Mehta, T., Nicoll, J.S., Tuominen, M.T. & Lovley, D.R. Extracellular electron transfer via microbial nanowires. *Nature* **435**, 1098 (2005).

49. Pfeffer, C., Larsen, S., Song, J., Dong, M., Besenbacher, F., Meyer, R.L., Kjeldsen, K.U., Schreiber, L., Gorby, Y.A., El-Naggar, M.Y. & Leung, K.M. Filamentous bacteria transport electrons over centimetre distances. *Nature* **491**, 218 (2012).

50. Thöny-Meyer, L. Haem-polypeptide interactions during cytochrome *c* maturation. *Biochim. Biophys. Acta Bioenerg.* **1459**, 316-324 (2000).

51. Friedrich, C.G., Bardischewsky, F., Rother, D., Quentmeier, A. & Fischer, J. Prokaryotic sulfur oxidation. *Curr. Opin. Microbiol.* **8**, 253-259 (2005).

52. Borisov, V.B., Gennis, R. B., Hemp, J. & Verkhovsky, M.I. The cytochrome *bd* respiratory oxygen reductases. *Biochim. Biophys. Acta Bioenerg.* **1807**, 1398-1413 (2011).

53. Ekici, S., Pawlik, G., Lohmeyer, E., Koch, H.-G. & Daldal, F. Biogenesis of cbb_3-type cytochrome *c* oxidase in *Rhodobacter capsulatus*. *Biochim. Biophys. Acta Bioenerg.* **1817**, 898-910 (2012).

54. Bird, L.J., Saraiva, I.H., Park, S., Calçada, E.O., Salgueiro, C.A., Nitschke, W., Louro, R.O. & Newman, D.K. Nonredundant roles for cytochrome c_2 and two high-potential iron-sulfur proteins in the photoferrotroph *Rhodopseudomonas palustris* TIE-1. *J. Bacteriol.* **196**, 850-858 (2014).

55. Singer, E., Emerson, D., Webb, E.A., Barco, R.A., Kuenen, J.G., Nelson, W.C., Chan, C.S., Comolli, L.R., Ferriera, S., Johnson, J. & Heidelberg, J.F. *Mariprofundus ferrooxydans* PV-1 the first genome of a marine Fe(II) oxidizing Zetaproteobacterium. *PloS ONE* **6**, e25386 (2011).

56. Wang, Z., Leary, D.H., Malanoski, A.P., Li, R.W., Hervey, W.J., Eddie, B.J., Tender, G.S., Yanosky, S.G., Vora, G.J., Tender, L.M., Lin, B., & Strycharz-Glaven, S.M. A previously uncharacterized, nonphotosynthetic member of the *Chromatiaceae* is the primary CO_2-fixing constituent in a self-regenerating biocathode. *Appl. Environ. Microbiol.* **81**, 699-712 (2015).

57. Kracke, F., Vassilev, I. & Krömer, J.O. Microbial electron transport and energy conservation–the foundation for optimizing bioelectrochemical systems. *Front. Microbiol.* **6**, 575 (2015).

58. Guzman, M. S., McGinley, B., Santiago-Merced, N., Gupta, D. & Bose, A. Draft genome sequences of three closely related isolates of the purple nonsulfur bacterium *Rhodovulum sulfidophilum*. *Genome Announc.* **5**, e00029-00017 (2017).

59. Jiao, Y., Kappler, A., Croal, L.R. & Newman, D.K. Isolation and characterization of a genetically tractable photoautotrophic Fe(II)-Oxidizing bacterium, *Rhodopseudomonas palustris* strain TIE-1. *Appl. Environ. Microbiol.* **71**, 4487-4496 (2005).

60. Straub, K.L., Rainey, F.A. & Widdel, F. *Rhodovulum iodosum* sp. nov. and *Rhodovulum robiginosum* sp. nov., two new marine phototrophic ferrous-iron-oxidizing purple bacteria. *Int. J. Syst. Evol. Microbiol.* **49**, 729-735 (1999).

61. Croal, L.R., Jiao, Y. & Newman, D.K. The fox operon from *Rhodobacter* strain SW2 promotes phototrophic Fe(II) oxidation in *Rhodobacter capsulatus* SB1003. *J. Bacteriol.* **189**, 1774-1782 (2007).

62. Nagao, N., Hirose, Y., Misawa, N., Ohtsubo, Y., Umekage, S. & Kikuchi, Y. Complete genome sequence of Rhodovulum sulfidophilum DSM 2351, an extracellular nucleic acid-producing bacterium. *Genome Announc.* **3**, e00388-00315 (2015).

63. Appia-Ayme, C., Little, P.J., Matsumoto, Y., Leech, A.P. & Berks, B.C. Cytochrome complex essential for photosynthetic oxidation of both thiosulfate and sulfide in *Rhodovulum sulfidophilum*. *J. Bacteriol.* **183**, 6107-6118 (2001).

64. Schedel, M., LeGall, J. & Baldensperger, J. Sulfur metabolism in *Thiobacillus denitrificans*. *Arch. Microbiol.* **105**, 339-341 (1975).

65. Schedel, M., Vanselow, M. & Trüper, H.G. Siroheme sulfite reductase isolated from *Chromatium vinosum*. Purification and investigation of some of its molecular and catalytic properties. *Arch. Microbiol.* **121**, 29-36 (1979).

66. Wagner, M., Roger, A.J., Flax, J.L., Brusseau, G.A. & Stahl, D.A. Phylogeny of dissimilatory sulfite reductases supports an early origin of sulfate respiration. *J. Bacteriol.* **180**, 2975-2982 (1998).

67. Ranaivoarisoa, T.O., Singh, R., Rengasamy, K., Guzman, M.S. & Bose, A. Towards sustainable bioplastic production using the photoautotrophic bacterium *Rhodopseudomonas palustris* TIE-1. *J. Ind. Microbiol. & Biotechnol.* 1-17 (2019).

68. Kotloski, N.J. & Gralnick, J.A. Flavin electron shuttles dominate extracellular electron transfer by *Shewanella oneidensis*. *MBio* **4**, e00553-00512 (2013).

69. Marsili, E., Baron, D.B., Shikhare, I.D., Coursolle, D., Gralnick, J.A. and Bond, D.R. *Shewanella* secretes flavins that mediate extracellular electron transfer. *Proc. Natl. Acad. Sci. USA* **105**, 3968-3973 (2008).

70. Von Canstein, H., Ogawa, J., Shimizu, S. & Lloyd, J.R. Secretion of flavins by Shewanella species and their role in extracellular electron transfer. *Appl. Environ. Microbiol.* **74**, 615-623 (2008).

71. Van der Zee, F.P. & Villaverde, S. Combined anaerobic–aerobic treatment of azo dyes—a short review of bioreactor studies. *Water Res.* **39**, 1425-1440 (2005).

72. Summers, Z. M., Gralnick, J. A. & Bond, D. R. Cultivation of an obligate Fe(II)-oxidizing lithoautotrophic bacterium using electrodes. *mBio* **4**, e00420-00412 (2013).

73. Patel, J. & Gerson, T. Formation and utilisation of carbon reserves by *Rhizobium*. *Arch. Microbiol.* **101**, 211-220 (1974).

74. Harris, H.W., El-Naggar, M.Y., Bretschger, O., Ward, M.J., Romine, M.F., Obraztsova, A.Y. and Nealson, K.H. Electrokinesis is a microbial behavior that requires extracellular electron transport. *Proc. Natl. Acad. Sci. USA* **107**, 326-331 (2010).

75. Oram, J. & Jeuken, L.J. Tactic Response of *Shewanella oneidensis* MR-1 toward Insoluble Electron Acceptors. *mBio* **10**, e02490-02418 (2019).

76. Ishii, S.I., Suzuki, S., Tenney, A., Nealson, K.H. & Bretschger, O. Comparative metatranscriptomics reveals extracellular electron transfer pathways conferring microbial adaptivity to surface redox potential changes. *ISME J.* **12**, 2844 (2018).

77. Hirose, A., Kasai, T., Aoki, M., Umemura, T., Watanabe, K. and Kouzuma, A. Electrochemically active bacteria sense electrode potentials for regulating catabolic pathways. *Nat. Commun.* **9**, 1083 (2018).

78. Smith, S.A. & Tabita, F.R. Up-regulated expression of the *cbb*$_I$ and *cbb*$_{II}$ operons during photoheterotrophic growth of a ribulose 1,5-bisphosphate carboxylase-oxygenase deletion mutant of *Rhodobacter sphaeroides*. *J. Bacteriol.* **184**, 6721-6724 (2002).

79. Maeda, I., Miyasaka, H., Umeda, F., Kawase, M. & Yagi, K. Maximization of hydrogen production ability in high-density suspension of *Rhodovulum sulfidophilum* cells using intracellular poly (3-hydroxybutyrate) as sole substrate. *Biotechnol. Bioeng.* **81**, 474-481 (2003).

80. Alkotaini, B., Abdellaoui, S., Hasan, K., Grattieri, M., Quah, T., Cai, R., Yuan, M. & Minteer, S.D. Sustainable bioelectrosynthesis of the bioplastic polyhydroxybutyrate: overcoming substrate requirement for NADH regeneration. *ACS Sustain. Chem. Eng.* **6**, 4909-4915 (2018).

81. Schindelin, J., Arganda-Carreras, I., Frise, E., Kaynig, V., Longair, M., Pietzsch, T., Preibisch, S., Rueden, C., Saalfeld, S., Schmid, B. & Tinevez, J.Y. Fiji: an open-source platform for biological-image analysis. *Nat. Meth.* **9**, 676 (2012).

82. Kumar, S., Stecher, G., Li, M., Knyaz, C. & Tamura, K. MEGA X: molecular evolutionary genetics analysis across computing platforms. *Mol. Biol. Evol.* **35**, 1547-1549 (2018).

83. Alikhan, N.F., Petty, N.K., Zakour, N. L.B. & Beatson, S.A. BLAST Ring Image Generator (BRIG): simple prokaryote genome comparisons. *BMC Genomics* **12**, 402 (2011).

84. Graham, E., Heidelberg, J. & Tully, B. Potential for primary productivity in a globally-distributed bacterial phototroph. *ISME J.* **12**, 1861 (2018).

Chapter 4: Conclusions and Future Directions

4.1 Summary

Microbe-mineral interactions play an important role in biogeochemical processes on Earth. Bacteria that are capable of utilizing solid-phase electron-donors via extracellular electron transfer (EET) are important for nutrient cycling in soils, marine sediments, and subsurface environments. Microbial EET to minerals and electrodes is well-understood at the mechanistic level. The molecular and physiological underpinnings of the reverse process, extracellular electron uptake (EEU), are poorly understood. In this work, I have shown in the purple nonsulfur bacterium (PNSB) *R. palustris* TIE-1 that EEU is linked to photosynthetic electron transfer, energy generation, and CO_2 fixation. I show that electrons enter the photosynthetic ETC and that cytochrome bc_1 is required for this process. I also demonstrate that NADH dehydrogenase plays an important role in EEU, likely for the generation of cellular reducing equivalents. Lastly, I show that the Calvin-Benson-Bassham (CBB) cycle is the primary electron sink for EEU. Furthermore, I observe that the lack of the CBB cycle gene ribulose-1,5-bisphosphate carboxylase/oxygenase (*ruBisCO*) influences the ability of TIE-1 to accept electrons from other electron donors, including H_2. Overall, this data suggests that carbon metabolism and electron transfer are linked. This may be conserved in other bacteria and important for improving our understanding of nutrient flow in organic-carbon limited ecosystems.

Because phototrophic EEU can be used for microbial CO_2 fixation, my work suggests that EEU may account for primary productivity in nature. To examine the ecological implications of this connection, I tested whether PNSB in marine ecosystems also engage in EEU. I show that the marine phototroph *Rhodovulum sulfidophilum* AB26 (hereafter referred to as AB26) is capable of utilizing electrodes poised over a wide range of potentials as electron donors. The highest rates of current uptake by AB26 occur at -200 mV vs. SHE, which is in the range of geochemically relevant solid-phase and insoluble minerals in marine ecosystems. I also show that AB26 cells attach to electrodes and form biofilms composed of exopolysaccharides and extracellular proteins. Using functional genomics, I interrogate the electron transfer, bioenergetic, and CO_2 fixation pathways in AB26. Using functional genomic approaches (whole-genome and transcriptome sequencing) I show that genes involved in photosynthetic electron transfer, energy generation, and CO_2 fixation are activated during EEU. This analysis also identifies two-component systems (TCS) with EEU-specific expression that may be important for sensing electrodes. Lastly, I also show that an uncharacterized di-heme cytochrome *c*-like protein (BV509_10070) is highly expressed during EEU. This protein is broadly conserved in *Rhodovulum* species and non-photosynthetic bacteria. Because multi-heme *c*-type cytochromes are known to be involved in EET in diverse bacterial genera, BV509_10070 may have a role in electron-transfer from electrodes.

4.2 Outlook

One of the most exciting aspects of my work is that it sets the stage for genetic, physiological, and biochemical studies of AB26. This bacterium does not contain homologs of

genes known to be involved in EEU and/or phototrophic Fe(II)-oxidation, and thus, elucidation of the EEU mechanism(s) in this organism will provide new molecular markers for identifying this process in nature. Another consequential aspect of my work is that it provides a detailed framework for further investigation into the bioenergetic and electron-transfer pathways underlying phototrophic EEU in TIE-1. Significant questions remain related to EEU in TIE-1 and AB26, and the ecological implications of EEU. Future directions are briefly summarized below.

My electrochemical data shows that AB26 is capable of EEU from electrodes poised at -200 mV vs. SHE. There is also a limited capacity for EEU at 0 mV vs. SHE. At this potential, however, there is both limited cell attachment and cell survival on the electrodes. Does AB26 take up electrons from electrodes poised at potentials from 0 to -200 mV vs. SHE, or below -200 mV vs. SHE? The redox potentials with which AB26 can take up electrons likely reflect the redox potential of the electron-transfer protein(s) in the outer membrane that facilitate EEU (in the case of direct EEU), or a redox-soluble molecule that is reduced by the electrode (in the case of indirect EEU). It is also plausible AB26 has multiple extracellular electron pathways. TIE-1 on the other hand accepts electrons at +100 mV vs. SHE[1]. Published data on whether TIE-1 can accept electrons at other redox potentials is not available. Thus, it is plausible TIE-1 could also accept electrons at more electronegative redox potentials. The full range of redox potentials with which TIE-1 and AB26 can accept electrons from poised electrodes should be determined in future electrochemical studies. This will further our understanding of the solid electron donors that PNSB may utilize in the natural environment for photosynthesis.

Interestingly, the redox potentials with which AB26 takes up electrons from electrodes coincide with a recent marine bacterium *Thioclava electrotropha*[2], as well as chemoautotrophic and chemoheterotrophic microbial communities in marine sediments[3,4]. *T. electrotropha* is a sulfur- and H_2-oxidizing chemoautotroph that can use a variety of terminal electron acceptors (e.g. SO_4^{2-}, Fe^{3+}, NO_3^{2-}) for EEU[2]. This microbe was isolated in a recent study of microbial communities in marine sediments from Catalina Harbor, CA, USA in the Pacific Ocean[4]. In this study electrodes were poised between -50 to -400 mV vs. Ag/AgCl (~ +149 to ~ -200 mV vs. SHE) as the sole electron donor with NO^{2-} or Fe^{3+} serving as the terminal electron acceptor. Because these redox potentials are in the range of relevant electron donors in marine sediments (e.g. elemental sulfur, iron oxides, and iron sulfides)[4] these data, along with my studies in AB26, suggest that solid-phase conductive substances (SPCSs) may contribute to biogeochemical cycling in marine ecosystems.

Microscopic data suggests an extracellular polymeric substance (EPS) substance is produced during EEU by AB26. Furthermore, EPS staining suggests that this substance contains exopolysaccharides and extracellular protein. TIE-1 is also known to produce EPS that contains exopolysaccharides and extracellular proteins[1]. AB26 biofilms also appear several cell-layers thick. This is in contrast to TIE-1[1] which forms sparse monolayers on electrodes. Recent studies have shown that EPS has conductive properties and facilitates extracellular electron transfer (EET) from electrodes to a variety of Gram-negative bacteria, including *Shewanella oneidensis* MR-1[5-7]. These studies suggest that soluble proteins in the EPS, such as flavins and extracellular *c*-type cytochromes, contribute to electron transfer to electrodes[6]. This electrical conductivity is hypothesized to allow cells spatially separated from the electrode to exchange electrons. Does

the EPS AB26 produces on electrodes also have conductive properties? Does it contain electron-transfer proteins? If so, this could explain how AB26 cells in biofilms stay viable on the electrodes under the cultivation conditions. Characterizing the structure and composition of EPS phototrophic bacteria produce will improve our understanding of its role in EEU.

My data on TIE-1 shows that genetic mutants of the CBB cycle have a ~90% decrease in EEU, suggesting the CBB cycle is the primary electron sink. Transcriptomic data shows that the CBB cycle enzyme form I *ruBisCO* is highly expressed during EEU in AB26. I also observe that form I *ruBisCO* is highly expressed in TIE-1. This could suggest that the CBB cycle is also an electron sink for EEU in AB26. Direct evidence for CO_2 fixation is lacking, however. In order to test if CO_2 fixation is connected to EEU in AB26, stable isotope studies could be performed to examine carbon uptake under this condition. Connecting this activity to autotrophic CO_2 fixation would require the generation of genetic mutants of the CBB cycle. Lastly, where is the remaining ~10% of current going in TIE-1? Is this current going to other biosynthetic pathways? Future genetic studies could systematically eliminate NADH and/or NAD(P)H consuming pathways to elucidate whether TIE-1 has additional electron sinks. A more exhaustive investigation of the potential electron sinks in TIE-1 would further its biotechnological and bioenergy applications.

A key knowledge gap in EEU research is how EEU-capable bacteria sense electrodes. I identified EEU-specific two-component systems (TCS) in AB26 through transcriptomic analysis. Do these TCS have a role in sensing electrical surfaces? Aside from these uncharacterized TCS, I also observed that the CbbRRS TCS in TIE-1 is highly upregulated during EEU. This TCS is lacking from AB26. The AB26 genome does contain the LysR-homolog CbbR and this gene is upregulated during EEU. CbbR is responsible for activating form I *ruBisCO* expression in

related bacteria, such as *R. palustris* CGA009/10 and *R. sphaeroides*[8-11]. Because TIE-1 and AB26 differ in their regulation of the CBB cycle, it is challenging to draw conclusions about the role of CbbR. It is likely this system has a role in regulating carbon metabolism in AB26. Whether this gene has an EEU-specific role is unlikely, but this question should be investigated in future studies.

Very little is known about the extracellular electron transfer pathways involved in microbial EEU. In TIE-1, the *pioABC* system likely has a role in this process[1] but the precise molecular mechanism of the *pioABC* system and whether other EET pathways exist in this organism is unclear. My studies on TIE-1 in bulk bioreactors suggest that planktonic electron uptake contributes to ~70% of current uptake in the system. How are these cells accessing electrons from the electrode? Does TIE-1 have an indirect mechanism (e.g. secretion of extracellular flavins) similar to *S. oneidensis* MR-1? A previous study on TIE-1 did not detect a redox-active molecule in the spent media, so the presence of an indirect pathway is unlikely[1]. It is also plausible TIE-1 cells have a dynamic biofilm-plankton lifecycle during EEU. This could explain why TIE-1 bioreactors without planktonic cells exhibit less current uptake. In AB26, the extracellular electron conduit that transports electrons from the electrode into the cell is unknown. AB26 also lacks homologs of known EET pathways. I identified a multiheme c-type cytochrome (BV509_10070) that is upregulated at the transcriptional level. This protein also has EEU-specific upregulation at the protein level. Does BV509_10070 have a role in EEU? If so, what is the extracellular component? Interestingly, I observed a subtle redox peak in the AB26 cyclic voltammograms of the spent media. Does this peak represent a redox-active molecule? If

so, this could explain how AB26 cells access electrons from the electrode without an obvious outer membrane protein complex.

What is the electron transfer pathway post-EEU in AB26 and TIE-1? My studies in TIE-1 show that electrons from the cathode enter the photosynthetic electron transport chain (pETC) and pass through the cytochrome bc_1 complex and NADH dehydrogenase. Because the pETC is highly conserved in PNSB, antimycin A and rotenone-based electrochemical studies could also be applied to AB26. This could reveal whether electrons are also entering the pETC and whether electrons are utilized for NADH production. But which electron-transfer components deliver electrons to the pETC in the first place? This is unknown for both TIE-1 and AB26. In most anoxygenic phototrophs, this is accomplished by cytochrome c_2 and/or high-potential iron-sulfur proteins (HiPIPs)[12]. This is thought to be the case for phototrophic Fe(II)-oxidation in TIE-1[12]. The *pioABC* operon (which is essential for phototrophic Fe(II)-oxidation in this organism) encodes an HiPIP (*pioC*) that is thought to transfer electrons to the photosystem[12,13]. Whether PioC is also involved in electron transfer during EEU has not been determined. It is also plausible, however, that the redox potential of the electron donor dictates the periplasmic electron acceptor, and thus the entry point of electrons into the pETC. For the case of EEU by TIE-1 at +100 mV vs. SHE, my data shows that a proton motive force (PMF) is required for EEU. This could suggest that reverse electron flow is required to transfer electrons from electron donors sufficiently lower than the NAD^+/NADH redox couple. Reverse electron flow has been shown to be an active pathway in chemoautotrophic Fe(II)-oxidizing bacteria[14-17]. In these microbe's cytochrome bc_1 pushes electron uphill to NADH dehydrogenase to reduce NAD^+. Reverse electron flow has also been suggested for phototrophic Fe(II)-oxidizing bacteria[12].

Because reverse electron flow requires the activity of cytochrome bc_1, which is an essential pETC component, uncoupling its roles in these two processes would be challenging.

Before this work, the scientific community had only two phototrophic bacterial isolates capable of EEU (i.e. TIE-1[1,18] and *Prosthecochloris aestuarii*[19]). The microbial isolation, whole-genome[20] and transcriptome-sequencing, and electrochemical characterization of AB26 will improve our understanding of the microbial and mechanistic diversity of EEU. Furthermore, AB26 fills a key knowledge gap in our understanding of the ecological diversity of EEU since this is the only marine organism known to carry out this process. What is still unknown is whether EEU is conserved among other PNSB. For example, are *R. sulfidophilum* or *R. palustris* strains other than AB26 and TIE-1, respectively, capable of phototrophic EEU? Are PNSB outside of these genera capable of EEU? And, how prevalent is phototrophic EEU among anoxygenic phototrophs? Understanding these questions would help us determine the quantitative contribution of phototrophic EEU to carbon cycling in anoxic environments. To aid in addressing these questions, I isolated and whole-genome sequenced an additional 18 marine phototrophic bacteria from Woods Hole, MA (Figure A1). These isolates are primarily PNSB (*Rhodovulum sulfidophilum* (n = 15) and *Rhodobacter sphaeroides* (n = 4)) but also purple sulfur bacteria (PSB) (*Marichromatium* spp. (n = 2))[20-22]. These genomes have been deposited in public databases and will serve as a resource for genetic and comparative genomic studies of marine PSB and PNSB[20-22]. Overall the work in this thesis, and the questions outlined above, will contribute to detailed understanding of how photoautotrophic bacteria oxidize SPCSs and how this microbial metabolism influences global biogeochemical cycles.

4.3 References

1. Bose, A., Gardel, E.J., Vidoudez, C., Parra, E.A. & Girguis, P.R. Electron uptake by iron-oxidizing phototrophic bacteria. *Nat. Commun.* **5**, 3391 (2014).

2. Chang, R., Bird, L., Barr, C., Osburn, M., Wilbanks, E., Nealson, K. and Rowe, A. *Thioclava electrotropha* sp. nov., a versatile electrode and sulfur-oxidizing bacterium from marine sediments. *Int. J. Syst. Evol. Microbiol.* (2018).

3. Lam, B. R., Rowe, A. R. & Nealson, K. H. Variation in electrode redox potential selects for different microorganisms under cathodic current flow from electrodes in marine sediments. *Environ. Microbiol.* **20**, 2270-2287 (2018).

4. Rowe, A.R., Chellamuthu, P., Lam, B., Okamoto, A. & Nealson, K.H. Marine sediments microbes capable of electrode oxidation as a surrogate for lithotrophic insoluble substrate metabolism. *Front. Microbiol.* **5**, 784 (2014).

5. Kitayama, M., Koga, R., Kasai, T., Kouzuma, A. & Watanabe, K. Structures, compositions, and activities of live *Shewanella* biofilms formed on graphite electrodes in electrochemical flow cells. *Appl. Environ. Microbiol.* **83**, e00903-00917 (2017).

6. Xiao, Y., Zhang, E., Zhang, J., Dai, Y., Yang, Z., Christensen, H.E., Ulstrup, J. and Zhao, F. Extracellular polymeric substances are transient media for microbial extracellular electron transfer. *Sci. Adv.* **3**, e1700623 (2017).

7. Xiao, Y. & Zhao, F. Electrochemical roles of extracellular polymeric substances in biofilms. *Curr. Opin. Electrochem.* **4**, 206-211 (2017).

8. Gibson, J.L. & Tabita, F.R. Nucleotide sequence and functional analysis of *cbbR*, a positive regulator of the Calvin cycle operons of *Rhodobacter sphaeroides*. *J. Bacteriol.* **175**, 5778-5784 (1993).

9. Joshi, G.S., Zianni, M., Bobst, C.E. & Tabita, F.R. Further unraveling the regulatory twist by elucidating metabolic coinducer-mediated CbbR-cbb_I promoter interactions in *Rhodopseudomonas palustris* CGA010. *J. Bacteriol.* **194**, 1350-1360 (2012).

10. Joshi, G.S., Zianni, M., Bobst, C.E. & Tabita, F.R. Regulatory twist and synergistic role of metabolic coinducer-and response regulator-mediated CbbR-cbb_I interactions in *Rhodopseudomonas palustris* CGA010. *J. Bacteriol.* **195**, 1381-1388 (2013).

11. Romagnoli, S. & Tabita, F.R. A novel three-protein two-component system provides a regulatory twist on an established circuit to modulate expression of the *cbbI* region of *Rhodopseudomonas palustris* CGA010. *J. Bacteriol.* **188**, 2780-2791 (2006).

12. Bird, L.J., Bonnefoy, V. & Newman, D.K. Bioenergetic challenges of microbial iron metabolisms. *Trends Microbiol.* **19**, 330-340 (2011).

13. Bird, L.J., Saraiva, I.H., Park, S., Calçada, E.O., Salgueiro, C.A., Nitschke, W., Louro, R.O. & Newman, D.K. Nonredundant roles for cytochrome c_2 and two high-potential iron-sulfur proteins in the photoferrotroph *Rhodopseudomonas palustris* TIE-1. *J. Bacteriol.* **196**, 850-858 (2014).

14. Dupuis, A. Genetic disruption of the respiratory NADH-ubiquinone reductase of *Rhodobacter capsulatus* leads to an unexpected photosynthesis-negative phenotype. *FEMS Microbiol. Lett.* **148**, 107-113 (1997).

15. Dupuis, A., Darrouzet, E., Duborjal, H., Pierrard, B., Chevallet, M., Van Belzen, R., Albracht, S.P. & Lunardi, J. Distal genes of the *nuo* operon of *Rhodobacter capsulatus* equivalent to the mitochondrial ND subunits are all essential for the biogenesis of the respiratory NADH-ubiquinone oxidoreductase. *Mol. Microbiol.* **28**, 531-541 (1998).

16. Herter, S.M., Kortlüke, C. M. & Drews, G. Complex I of *Rhodobacter capsulatus* and its role in reverted electron transport. *Arch. Microbiol.* **169**, 98-105 (1998).

17. Marrs, B., Stahl, C.L., Lien, S. & Gest, H. Biochemical physiology of a respiration-deficient mutant of the photosynthetic bacterium *Rhodopseudomonas capsulata*. *Proc. Natl. Acad. Sci. USA* **69**, 916-920 (1972).

18. Jiao, Y., Kappler, A., Croal, L.R. & Newman, D.K. Isolation and characterization of a genetically tractable photoautotrophic Fe(II)-Oxidizing bacterium, *Rhodopseudomonas palustris* strain TIE-1. *Appl. Environ. Microbiol.* **71**, 4487-4496 (2005).

19. Ha, P.T., Lindemann, S.R., Shi, L., Dohnalkova, A.C., Fredrickson, J.K., Madigan, M.T. & Beyenal, H. Syntrophic anaerobic photosynthesis via direct interspecies electron transfer. *Nat. Commun.* **8**, 13924 (2017).

20. Guzman, M. S., McGinley, B., Santiago-Merced, N., Gupta, D. & Bose, A. Draft genome sequences of three closely related isolates of the purple nonsulfur bacterium *Rhodovulum sulfidophilum*. *Genome Announc.* **5**, e00029-00017 (2017).

21. Guzman, M. S. & Bose, A. Draft Genome Sequences of Four *Rhodobacter sphaeroides* Strains Isolated from a Marine Ecosystem. *Microbiol*. *Resour. Announc*. **8**, e01648-01618 (2019).

22. Guzman, M. S., Kuse, J. C., Santiago-Merced, N. & Bose, A. Draft Genome Sequences of Two Closely Related *Marichromatium* Isolates, Photosynthetic Gammaproteobacteria from Marine Ecosystems. *Microbiol. Resour. Announc.* **8**, e01510-01518 (2019).

Appendix

Figure A1. Maximum likelihood phylogenetic tree of photosynthetic reaction center gene *pufM* from assembled genomes of bacteria isolated from Trunk River, Woods Hole, MA. Tree was constructed as described in Chapter 3, section 3.5.5 ("Molecular phylogenetic analysis"). Scale bar represents amino acid substitutions.

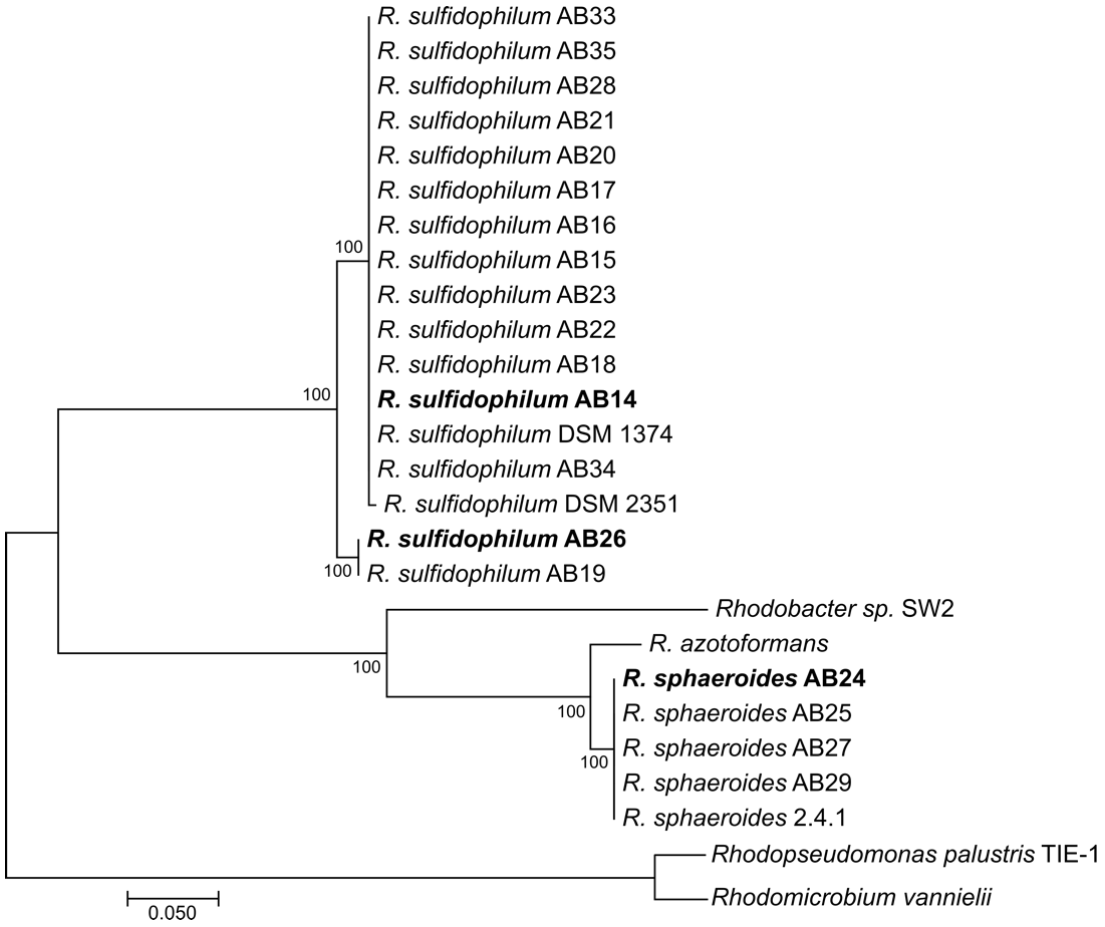

Figure A2. Heme-staining to identify proteins upregulated during phototrophic Fe(II)-oxidation in *Rhodovulum sulfidophilum* AB26 (MB#26) and AB14 (MB#14_Pellet), and *Rhodobacter sphaeroides* AB24 (MB#24_Pellet). Cells were pre-grown photoautotrophically on 80% hydrogen-20% carbon dioxide (H_2-CO_2) in freshwater (FW) media. Cells were transferred 1:100 into 50 mL anaerobic serum bottles containing FW media supplemented with 5 mM Fe(II) and 10 mM nitrilotriacetic acid (NTA). Cells were harvested once half of Fe(II) was oxidized. Preparation of membrane fractions (pellet) was performed as described in Chapter 3, section 3.5.10 ("Preparation of soluble and membrane fractions for mass spectrometry"). The ~56-72 kDa band in the coomassie stain for AB26 was used for mass spectrometry analysis in Table A2.

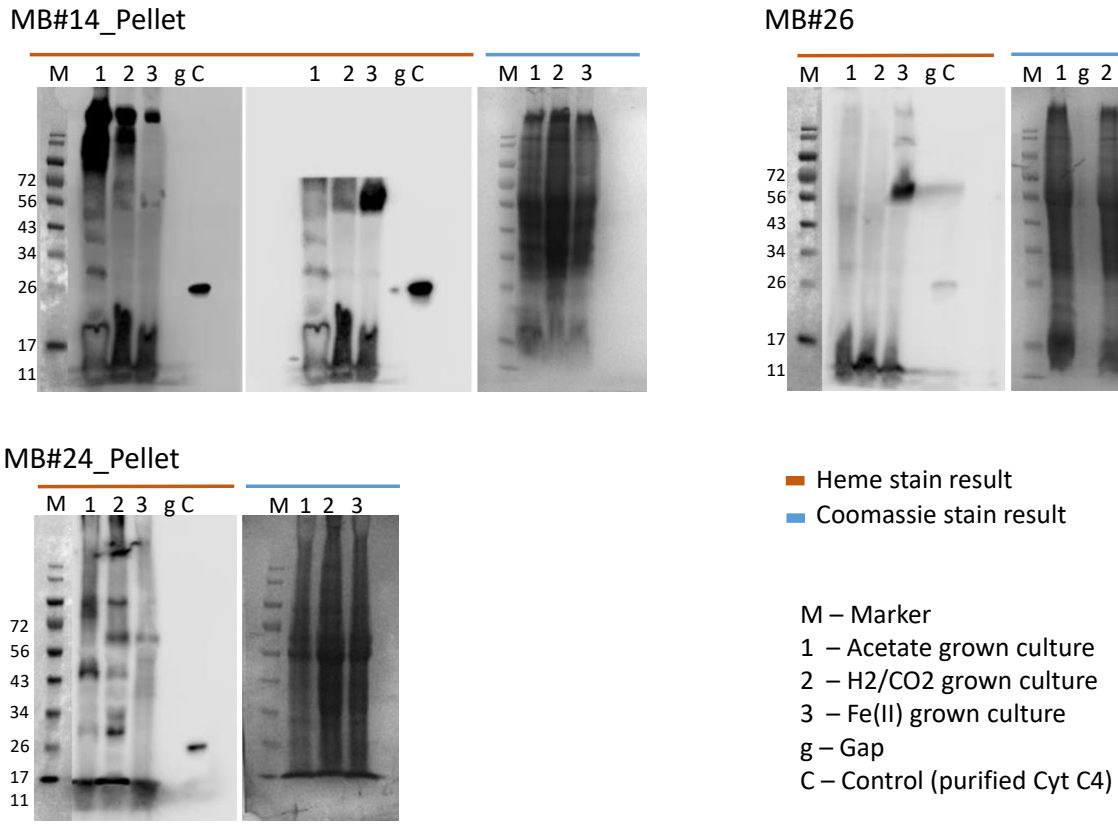

Figure A3. Polymerase chain reaction (PCR) of the 16S rRNA gene from select bacterial isolates from Trunk River, Woods Hole, MA to determine optimal buffer conditions.

Letters (A-L) denote the different FailSafe™ 2X PreMix Buffers tested for six different strains. *Rhodovulum sulfidophilum* AB29 (#29 – G1A); *Rhodovulum sulfidophilum* AB30 (#30 – G1T); *Marichromatium* sp. AB31 (#31 – G2A); *Marichromatium* sp. AB32 (#32 – G3A); *Rhodovulum sulfidophilum* AB33 (#33 – G3T); *Rhodovulum sulfidophilum* AB35 (#35 – G4T)

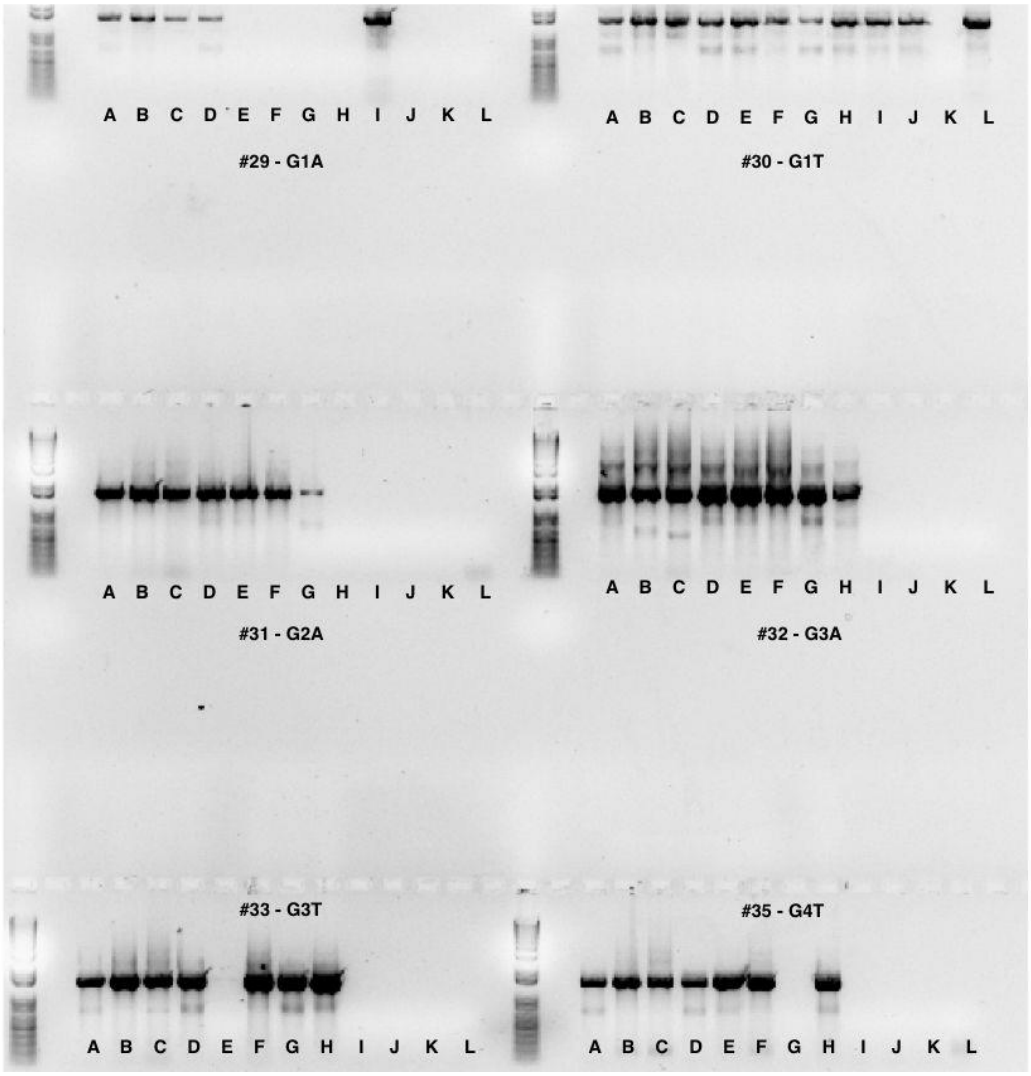

Table A1. Iron oxidation rates under anoxygenic phototrophic conditions as measured by the ferrozine assay. Cells were pre-grown photoautotrophically on 80% hydrogen-20% carbon dioxide (H_2-CO_2) in freshwater (FW) media. Cells were transferred 1:100 into 50 mL anaerobic serum bottles containing FW media supplemented with 5 mM Fe(II) and 10 mM nitrilotriacetic acid (NTA). Iron-oxidation rates were determined using the ferrozine assay.

Strain	Average rate (mM/day) ± S.E. (*n* = 3)	Organism
AB14	2.11 ± 0.167	*Rhodovulum sulfidophilum*
AB15	2.18 ± 0.227	*Rhodovulum sulfidophilum*
AB16	2.00 ± 0.129	*Rhodovulum sulfidophilum*
AB17	2.09 ± 0.197	*Rhodovulum sulfidophilum*
AB18	2.12 ± 0.151	*Rhodovulum sulfidophilum*
AB19	1.37 ± 0.278	*Rhodovulum sulfidophilum*
AB20	1.48 ± 0.165	*Rhodovulum sulfidophilum*
AB21	1.41 ± 0.296	*Rhodovulum sulfidophilum*
AB22	1.62 ± 0.233	*Rhodovulum sulfidophilum*
AB23	1.76 ± 0.405	*Rhodovulum sulfidophilum*
AB24	0.422 ± 0.259	*Rhodobacter sphaeroides*
AB25	0.594 ± 0.283	*Rhodobacter sphaeroides*
AB26	1.39 ± 0.195	*Rhodovulum sulfidophilum*
AB27	0.589 ± 0.269	*Rhodobacter sphaeroides*
AB28	1.71 ± 0.199	*Rhodovulum sulfidophilum*
AB29	0.425 ± 0.344	*Rhodobacter sphaeroides*
AB30	1.82 ± 0.255	*Rhodovulum sulfidophilum*
AB32	No data	*Marichromatium* spp.
AB33	1.85 ± 0.235	*Rhodovulum sulfidophilum*
AB34	1.47 ± 0.172	*Rhodovulum sulfidophilum*
AB35	1.94 ± 0.534	*Rhodovulum sulfidophilum*

Table A2. Heme-containing proteins identified in mass spectrometry analysis of *Rhodovulum sulfidophilum* AB26 cells cultivated during phototrophic Fe(II)-oxidation. Cells were pre-grown photoautotrophically on 80% hydrogen-20% carbon dioxide (H_2-CO_2) in freshwater (FW) media. Cells were transferred 1:100 into 50 mL anaerobic serum bottles containing FW media supplemented with 5 mM Fe(II) and 10 mM nitrilotriacetic acid (NTA). Preparation of soluble and membrane fractions for mass spectrometry was performed as described in Chapter 3, section 3.5.10 ("Preparation of soluble and membrane fractions for mass spectrometry"). Mass spectrometry was performed at the Proteomics and Mass Spectrometry facility at Donald Danforth Plant Science Center.

Locus tag	Coverage (%)	No. CXXCH motifs	Signal peptide	MW (kDa)	BLAST
BV509_10070	83	2	Sec	61	Hypothetical protein
BV509_18570	68	3	Sec	67	Hypothetical protein
BV509_09615	54	1	Sec	16	Sulfur oxidation *c*-type cytochrome SoxX
BV509_00835	48	1	Tat	20	Ubiquinol-cytochrome c reductase iron-sulfur
BV509_15055	46	1	None	75	Threonine--tRNA ligase
BV509_00825	40	1	Sec	29	Cytochrome c_1
BV509_14485	26	1	None	50	Dihydrolipoyl dehydrogenase
BV509_00325	23	3	TM	39	Photosynthetic reaction center cytochrome *c* subunit
BV509_09630	16	2	Sec	30	Sulfur oxidation *c*-type cytochrome SoxA
BV509_16080	11	1	None	60	Acyl-CoA synthetase
BV509_21435	11	1	Sec	54	Membrane-bound cytochrome *c*
BV509_10485	7.8	1	None	107	Ribonuclease

Table A3. Characterization of gentamicin sensitivity for *Rhodovulum sulfidophilum* AB26 and *Rhodobacter sphaeroides* AB24. Cells were cultivated on Bacto agar with Difco marine broth 2216 (BD Diagnostic Systems, Sparks, MD, USA) for 7 days in the dark under oxic conditions.

	Gentamicin (μg mL^{-1})									
Strain	0	5	10	25	50	75	100	150	200	300
R. sphaeroides AB24	*	#	#	#	#	NG	NG	NG	NG	NG
R. sulfidophilum AB26	*	*	NG	NG	NG	NG	NG	NG	NG	NG
R. sphaeroides strain HR	ND	NG[1]	ND	ND	ND	ND	ND	ND	ND	ND
R. sulfidophilum DSM 1374^T	ND	NG[2]	ND	ND	ND	ND	ND	ND	ND	ND

* = No growth defect compared to untreated (no antibiotic) controls

= intermediate growth (10 colonies or less)

NG = No growth

ND = No data available

[1]Qian & Tabita (1996) J. Bacteriol. **178**: 12-18

[2]Appia-Ayme *et al.* (2001) J. Bacteriol. **183**: 6107-6118

Table A4. Extracellular electron uptake (EEU)-specific upregulated genes in *Rhodovulum sulfidophilum* AB26. Complete list of genes upregulated during phototrophic EEU but not upregulated under all other phototrophic growth conditions. Only those genes with $\log_2$ fold change (FC) ≥ 2 and an adjusted p-value (P-value) ≤ 0.05. EEU (poised electrode), H_2 (photoautotrophic growth with H_2 as an electron donor), Thiosulfate (photoautotrophic growth with thiosulfate as an electron donor), Acetate (photoheterotrophic growth with 10 mM acetate). Methods can be found in Chapter 3, section 3.5.9 ("RNA sequencing (RNA-Seq) and differential expression analysis").

Locus tag	EEU FC	P-value	H_2	P-value	Thiosulfate FC	P-value	Acetate FC	P-value
BV509_09760	6.11	1.05E-27	-2.33	0.37	-0.91	0.82	-2.47	0.29
BV509_07330	4.90	3.59E-12	-0.26	0.90	2.67	0.05	1.61	0.32
BV509_15805	4.76	2.41E-28	0.69	0.63	1.76	0.15	1.17	0.49
BV509_18335	4.59	2.78E-20	1.56	0.20	1.99	0.06	1.14	0.43
BV509_20215	4.50	1.22E-13	1.29	0.34	1.94	0.08	0.68	0.71
BV509_07495	4.45	6.76E-33	0.78	0.58	1.57	0.13	1.22	0.42
BV509_14220	4.19	2.11E-15	0.12	0.92	1.55	0.21	0.41	0.86
BV509_09195	4.06	3.08E-12	2.02	0.07	1.76	0.06	1.33	0.31
BV509_08245	3.90	5.74E-10	0.76	0.62	1.62	0.19	-0.66	0.56
BV509_16075	3.85	8.63E-20	0.24	0.89	0.69	0.46	-0.28	0.80
BV509_17685	3.79	1.44E-26	0.83	0.48	1.48	0.12	1.21	0.34
BV509_05655	3.58	7.85E-12	1.16	0.29	1.81	0.07	0.84	0.53
BV509_10545	3.54	2.85E-14	0.14	0.90	1.45	0.16	0.73	0.62
BV509_06910	3.48	1.22E-37	0.19	0.92	0.15	0.76	-0.17	0.87
BV509_09220	3.48	2.98E-39	1.60	0.09	1.25	0.07	1.45	0.14

BV509_10785	3.48	7.43E-13	0.84	0.53	1.11	0.23	0.09	0.99
BV509_19205	3.31	5.98E-33	0.95	0.43	0.91	0.22	0.72	0.61
BV509_20210	3.30	1.61E-37	0.26	0.87	0.09	0.76	-0.19	0.84
BV509_06550	3.25	3.07E-26	1.57	0.10	0.90	0.16	1.21	0.25
BV509_10555	3.21	8.00E-30	1.08	0.37	0.75	0.29	0.66	0.64
BV509_19540	3.20	1.17E-09	0.63	0.56	1.50	0.09	0.64	0.67
BV509_14225	3.16	7.69E-14	0.13	0.92	1.11	0.25	0.23	0.93
BV509_16865	3.13	5.32E-24	-1.47	0.35	-1.24	0.57	-0.48	0.78
BV509_03570	3.13	2.74E-12	0.09	0.91	1.48	0.09	0.79	0.57
BV509_07050	3.12	1.36E-21	0.66	0.59	0.43	0.51	0.25	0.92
BV509_19300	3.08	4.61E-14	1.34	0.16	1.26	0.08	0.97	0.38
BV509_19360	3.01	4.54E-03	2.63	0.06	2.00	0.08	2.34	0.14
BV509_06360	3.00	1.66E-17	-0.44	0.86	-0.20	0.94	-0.29	0.82
BV509_10550	2.95	1.09E-39	0.75	0.51	0.57	0.35	0.57	0.68
BV509_09670	2.94	4.51E-09	0.54	0.69	1.33	0.12	0.67	0.65
BV509_14235	2.93	7.79E-22	0.71	0.57	0.77	0.29	0.47	0.77
BV509_09560	2.91	3.72E-19	0.99	0.47	-0.07	0.82	0.35	0.85
BV509_11125	2.90	8.66E-09	1.68	0.14	0.90	0.22	0.38	0.85
BV509_07045	2.89	8.54E-13	1.65	0.07	1.17	0.07	1.03	0.29
BV509_14210	2.81	5.05E-24	0.42	0.73	0.63	0.34	0.61	0.66
BV509_07055	2.75	5.84E-40	0.11	0.94	-0.14	0.87	0.21	0.94
BV509_11520	2.68	4.87E-71	-0.08	0.97	-0.24	0.95	-0.20	0.82
BV509_15600	2.68	3.31E-08	-0.08	0.97	1.35	0.12	-0.02	0.94
BV509_04835	2.66	6.08E-07	-0.08	0.99	1.28	0.12	0.50	0.76
BV509_06555	2.62	2.21E-24	1.20	0.15	0.90	0.12	0.86	0.37

BV509_15825	2.59	1.50E-05	-2.02	0.06	0.48	0.57	-0.32	0.81
BV509_02610	2.59	7.30E-21	0.69	0.52	0.58	0.32	0.61	0.66
BV509_19700	2.52	9.31E-08	0.71	0.43	1.20	0.10	0.56	0.67
BV509_08525	2.45	1.59E-13	-0.42	0.74	0.58	0.40	0.15	0.96
BV509_15935	2.38	9.81E-07	1.28	0.23	0.93	0.18	-0.49	0.45
BV509_19640	2.37	1.41E-27	1.40	0.06	0.49	0.20	1.11	0.18
BV509_20075	2.37	1.51E-10	0.64	0.48	1.04	0.10	0.66	0.56
BV509_18700	2.32	4.40E-16	0.02	0.94	0.53	0.38	0.37	0.81
BV509_02800	2.31	1.00E-08	0.33	0.74	1.19	0.09	-0.02	0.89
BV509_15940	2.31	2.53E-07	0.97	0.40	0.62	0.34	-0.63	0.37
BV509_18710	2.28	6.49E-32	0.48	0.61	0.17	0.56	0.72	0.54
BV509_04840	2.27	1.79E-06	-0.15	0.95	1.26	0.08	0.69	0.59
BV509_06560	2.26	2.59E-31	0.90	0.27	0.64	0.20	0.64	0.51
BV509_13605	2.26	6.21E-26	0.19	0.90	-0.53	0.85	0.16	0.97
BV509_14915	2.23	4.11E-03	-4.25	0.00	-0.92	0.78	-2.85	0.07
BV509_02695	2.23	5.09E-06	-1.16	0.43	-0.17	0.92	-1.62	0.14
BV509_10570	2.20	2.16E-19	0.63	0.54	-0.02	0.74	0.15	0.99
BV509_01550	2.19	7.28E-18	-0.10	0.95	0.20	0.57	0.55	0.68
BV509_06885	2.17	6.26E-09	1.36	0.09	1.11	0.05	0.18	0.93
BV509_05320	2.16	4.66E-18	0.49	0.47	0.96	0.06	1.25	0.11
BV509_15160	2.15	6.91E-03	-2.09	0.02	1.57	0.16	-0.23	0.85
BV509_19775	2.15	1.70E-07	-0.04	1.00	1.14	0.07	0.83	0.45
BV509_10560	2.12	6.79E-09	1.03	0.25	0.80	0.14	1.00	0.32
BV509_13255	2.11	2.09E-06	-0.16	0.93	0.01	0.75	1.41	0.21
BV509_03220	2.10	1.37E-17	0.20	0.88	-0.82	0.59	0.05	0.95

BV509_06900	2.09	3.35E-10	0.35	0.75	0.85	0.17	0.30	0.84
BV509_15165	2.08	1.00E-02	-2.24	0.01	1.48	0.19	-0.35	0.80
BV509_18695	2.07	2.08E-03	-1.36	0.17	1.24	0.18	-0.22	0.84
BV509_18685	2.07	1.53E-03	-1.43	0.17	1.07	0.28	-0.63	0.57
BV509_05430	2.06	7.24E-08	-0.33	0.72	0.92	0.14	1.03	0.32
BV509_04780	2.06	4.24E-29	0.29	0.79	0.19	0.56	0.25	0.89
BV509_10580	2.06	2.60E-19	0.75	0.48	-0.07	0.76	0.20	0.94
BV509_10575	2.05	9.75E-11	0.66	0.57	-0.04	0.78	0.22	0.96
BV509_21655	2.05	5.94E-04	1.34	0.27	-1.28	0.20	0.85	0.57
BV509_15200	2.03	7.30E-17	-1.13	0.36	-0.66	0.80	-0.60	0.63
BV509_15155	2.03	1.68E-02	-2.09	0.02	1.84	0.08	-0.31	0.81
BV509_15815	2.03	2.46E-06	-1.70	0.09	-0.06	0.85	-0.38	0.74
BV509_12130	2.02	3.08E-08	1.12	0.24	0.42	0.37	0.18	0.97
BV509_18690	2.01	1.21E-03	-1.15	0.24	1.23	0.16	-0.26	0.80